WEATHER AND TOPOGRAPHICAL INFLUENCES ON SPATIAL AND TEMPORAL VARIABILITY OF WINTER WHEAT YIELD IN OKLAHOMA

BY

XIAOXUE LI

Bachelor of Engineering
Gansu Agricultural University
Lanzhou, Gansu, China
1993

Master of Engineering
Irrigation and Drainage Engineering
Postgraduate School of North China
Water Conservancy and Hydropower Institute
Beijing, China
1996

Submitted to the Faculty of the
Graduate College of the
Oklahoma State University
partial fulfillment of
requirement for
the Degree of
DOCTOR OF PHILOSOPHY
May 2011

WEATHER AND TOPOGRAPHICAL INFLUENCES ON

SPATIAL AND TEMPORAL VARIABILITY OF

WINTER WHEAT YIELD IN OKLAHOMA

Thesis Approved:

Dr. John Solie
Dissertation Adviser

Dr. Glenn Brown

Dr. Paul Weckler

Dr. William R. Raun

Dr. Mark Payton
Dean of the Graduate College

ACKNOWLEDGEMENTS

I would like to thank my adviser Dr. John Solie for his guidance and support through my completion of this research. His profound knowledge of the issue involved and critical analyses were very important factors in successful completion of this research. Dr. Solie's contribution to my completion of this research is acknowledged with a great sense of gratitude. I would like to thank Dr. Ronald L. Elliott for his guidance, support and encouragement throughout my study at OSU. I also extend my appreciation to my other committee members, Dr. Glenn Brown, Dr. Paul Weckler and Dr. William Raun for their advice and encouragement. Their professional and personal frameworks have had a very positive impact in carrying me forward successfully.

I would like to acknowledge Oklahoma Mesonet for providing weather data for this research.

Appreciation is extended to Dr. Mark Gregory for his GPS field work training and field data processing. I thank Ronald Tejral and Carly Washingman for their assistances in the field works. I thank Jim Kent for providing his wheat field as a research field. I thank Tom Underwood for his lab work in analyzing soil samples.

Finally I thank my family, without their support this would not have been possible.

TABLE OF CONTENTS

LIST OF TABLES

Table Page

LIST OF FIGURES

Figure Page

CHAPTER 1

INTRODUCTION

Background

Variability of wheat yield across a field confounds not only farmers, but also scientists. From yield maps, some trends of variability have been identified. For instance, in dry years, yields are lower on hilltops and are high in low areas where overland flow from rainstorms tends to converge, while in wet years, the trend may be reversed. Because of temporal variations in weather conditions and consequently, in soil moisture regime, the effect of topography on plant development may differ in different growing seasons. Research conducted by Michelle et al. (1988) showed that total above-ground mass of wheat increased from knolls to the swales, while the harvest index increased in the reverse direction. Grain yields varied from year to year at a specific site as well as from site to site in a given year (Hairston et al., 1988). The yield-limiting factors were dynamic: in a year with adequate rainfall and subsequently adequate soil moisture, soil fertility (mainly nitrogen availability) is usually the limiting factor. In a dry year, wheat yield at a specific site in a field may be limited by available soil moisture at the site, which in turn was determined mainly by the characteristics of rainfall events, topography at the site, and soil depth and water holding capacity of the soil at the site.

There are many factors influencing the spatial and temporal variability of wheat yield across a field. The major factors include soil physical properties, such as soil texture, soil organic matter content, soil depth, and water holding capacity of the soil; soil chemical properties, such as soil pH and concentrations of nitrogen, phosphorus, potassium and other nutrients; crop cultivars; topography, such as slope, aspect and relief; weather, such as rainfall and temperature. Most of these factors interact with each other to influence the yield across a field. It is very challenging to distinguish the variability caused by the various factors.

Non-irrigated wheat such as that grown in much of Oklahoma generally uses most of the water that is available from precipitation during the growing season. With adequate fertility and a high level of management, the potential of a soil to produce wheat largely depends on the soil's capacity to store and supply water. In dryland farming, sub-field-scale topography and weather conditions work together to influence the soil moisture regimes at different sites across a field. The amount of water retained by a soil for crop use at a specific site is, therefore, determined not only by the soil's physical properties such as depth and volumetric water holding capacity, but also by the topography such as landscape position, slope, and aspect. The effect of topography on soil moisture the regime is more prominent in fine textured soils that have low intake rates and high runoff potential (Hanna et al., 1982). The study conducted by Hanna et al. (1982) in southern Nebraska indicated that most of the differences in soil moisture levels among the sites studied were better correlated to topographic differences among the sites than to the differences in soil physical properties. They found that soils on footslopes and backslopes contained an average of 4 cm more available water than soils on summits and shoulders.

The study of Sinai et al. (1981) in Israel demonstrated moisture content measured in the soil correlated strongly with the curvature of the soil surface. At concave locations of the landscape, the moisture was as high as 14 percent. At convex locations, the moisture content was as low as 5 percent.

Moulin et al. (1994) recognized that an interaction between elevation and surface curvature affects the spatial and statistical distribution of soil properties and wheat yield in the landscape. Sinai (1981) found that there was a strong linear correlation between wheat grain yield and the soil surface curvature. Ciha (1984) demonstrated that the slope position had a strong influence on grain yield of winter wheat. The relationship was attributed to soil properties such as surface soil thickness and available water as well as differences in environmental conditions along the slope.

Rainfall pattern and temporal distribution may influence the crop available water stored in surface soil. Because of lateral surface and subsurface flow during rainfall, water is not evenly distributed in the landscape (Halvorson and Doll, 1991). High runoff may increase the spatial relationship between surface soil moisture content and landscape position. Campbell et al. (1988) concluded that the amount and distribution of growing season precipitation that control cereal grain yields on level landscapes should be modified for variable landscapes by considering moisture redistribution and storage capacities with the landscape as factors controlling productivity in undulating topography. However, developing clear relationships between slope position and crop productivity or soil water regime has been difficult because of the confounding influences of three-dimensional slope curvature (Sinai et al., 1981; Simmons et al., 1989; Halvorson and Doll, 1991) or of differing slope aspect (Jones et al., 1989).

Because of the large spatial and temporal variability in yield observed across a field, new techniques of precision agriculture based on optical sensors and GIS technology were developed for variable application of N fertilizers. The variable-rate fertilizer applicator, Green Seeker^{TM} (Trimble Inc. Sunnyvale, CA), developed at Oklahoma State University, can apply different rate of N fertilizer to different sites in a field with an accuracy of sub-meter scale (Raun et al., 2004; Solie et al., 1996; Stone et al., 1996a, b). The rate of N application at a specific site is determined based on the potential yield at the site. The potential yield is estimated from NDVI reading at the site (Girma et al., 2005; Lukina et al., 2001; Raun et al., 2001, 2005). The potential yield estimated from NDVI reading at a specific site did not directly determine the effect of soil moisture regime or the amount of water available for crop use at the site. It implicitly assumed that soil moisture condition at the site was reflected by the measurement of reflectance incorporated in to NDVI (Normalized Difference Vegetative Index) and subsequent growth after the NDVI measurement was dependent on available N fertilizer and available soil moisture remained constant. Because of the high temporal variability in weather conditions after optical measurements sensing and high spatial variability in soil moisture conditions in an undulating field, potential yields estimated from NDVI readings alone may not reflect the temporal and spatial variations of grain yield. To more fully capitalize on the potential benefits of site-specific management, it is important to be able to quantify the influence of soil moisture on wheat yield variability, using methodologies, such as remote sensing, that can be applied over large areas coupled with expected rainfall during the growing period after optical sensing. In a non-irrigated setting, soil physical properties, topography, and weather are plausibly the

dominant factors influencing variability in soil moisture (and hence variability in evapotranspiration). The research reported here focuses on those factors in the context of a field and modeling study.

Objectives

The overall objective of this research is to study weather and topographical influences on spatial and temporal variability in winter wheat yield by estimating spatial distribution and temporal changes of soil moisture and evapotranspiration over heterogeneous wheat fields. To support this objective, there are three specific tasks:

1. To collect topographical, soil properties, and satellite data of the field and fine-tune the DEMs (Digital Elevation Models) with the field topographical data collected, simulate soil moisture regime and evapotranspiration with MESONET (Mesoscale Network) data and soil properties measured, and analyze yield variability with the satellite data.
2. To examine the topographical factors affecting wheat yield variance within a field and to develop a soil moisture index by combining topography and soil information.
3. To determine the degree to which modeled differences in evapotranspiration and soil moisture can explain temporal and spatial variability in winter wheat yield.

Scope of the study

In this research, a privately owned, 160-acre field in Grant County of north-central Oklahoma was selected as the study site to take advantages of the existing data of (1) natural variability of topography; (2) soil variability; and (3) time series satellite

images for the field. The research focuses on the effect of soil physical properties, field topography, and weather conditions on the temporal and spatial variability of wheat yield. Detailed topography measurements of the field were conducted to fine-tune the DEMs to meet the scale and accuracy required by this research. Soil samples were taken across the field to measure soil physical properties. MESONET data and soil physical properties were used in a computer program to simulate soil moisture regime and daily evapotranspiration. Satellite data were used to analyze yield variability in the field.

CHAPTER 2

FIELD DATA COLLECTION

Introduction

Good quality topography, soil, and weather data are necessary to study the effects of weather and topography on wheat yield variability on a field scale. In Oklahoma, wheat farming is dry land farming. Wheat extracts all available water stored in the soil from precipitation. Besides weather factors, both the topography and the soil itself have great influences on soil water storage and distribution across a field. The accuracy and precision of the Digital Elevation Models (DEMs) from the US Geographical Survey (USGS) and soil maps from the Natural Resources Conservation Service (NRCS) are questionable for a precise study of topography and soil variance on a field scale. Their low accuracy and coarse resolution may cover up the real variability within the field. For this research, West field in Grant County, Oklahoma was selected as the study site. A Global Positioning System (GPS) was used to gather highly accurate elevation data at fine resolution in this field. A stratified random sampling method was used to collect soil samples at two different soil depths, one depth was 0-9 inches, and the other depth was 9-18 inches, throughout the field. Wheat yield data were obtained using a prediction equation derived from the relationship between NDVI and grain yield by Itenfisu et al.

(1999). Oklahoma has well developed and advanced Mesonet weather stations throughout the state. Daily weather data were obtained from the Medford, Grant County, Oklahoma Mesonet station, which is the closest station to the study field. This chapter addresses the procedures used in the field data collection and presents the data gathered in the field.

Topographical Data

DEMs Review

Digital elevation models (DEMs) are now standard tools to represent terrain surface. In the United States, the US Geological Survey (USGS) supplies the most widely available DEMs. DEMs provided by the USGS use elevation data derived from existing contour maps, digitized elevations, and photogrammetric stereo-modes based on aerial photographs and satellite images. All USGS DEMs provide elevation values in integer feet or meters and are classified into three levels of increasing quality. For a Level 1 classification, the targeted accuracy standard is a vertical Root Mean Square Error (RMSE) of 7 meters; the maximum permitted is an RMSE of 15 meters. For a Level 2 classification, the maximum permitted is an RMSE of one-half of the original contour interval; no errors greater than one contour interval in magnitude exist. For a Level 3 classification, the maximum permitted is an RMSE of one-third of the contour interval, and no errors greater than two-thirds of the contour interval in magnitude exist. Most DEMs fall into the Level 2 classification. The availability of Level 3 DEMs is very limited (Garbrecht and Martz, 2001). Since elevation has a great impact on drainage patterns in hydrology modeling, a one or two meter elevation difference might change the

drainage pattern entirely in the field. So the accuracy of available DEMs provided by the USGS is very questionable in estimating topographical and geomorphologic parameters in order to study the topographical effects on soil water distribution of non-uniform runoff due to topography changes within the field.

Description of the terrain surface through digital elevation models (DEMs) strongly depends on the method used to collect data and DEM data structures (Rieger, 1998). Normally three methods are used to model the terrain surface: a regular spaced grid of elevations, a triangulated irregular network (or TIN), or a set of landform elements based on the intersection of contours and flowlines. The second and third methods are in many ways superior to the first, in that both are made more representative of the actual terrain surface (Mark, 1979). The use of contours and flow lines means that landscape elements are based directly on characteristics that are hydrologically important (Moore et al., 1988), and a TIN also can be constructed such that the triangles match important features in the landscape, such as ridges, valleys, peaks and saddle points (Peucker et al., 1978). However, both the TIN and contour-based methods require complex data structures for their storage in the computer and special purpose software to handle them. In contrast, the gridded DEM simply samples elevation at regular interval, oversampling in low-relief areas, undersampling in high-relief areas, and with little chance that key landscape features will fall on a sample point (Wise, 2000). But the gridded DEM uses the simplest data structure, a two-dimensional array, which can be read and handled by any geographic information system (GIS) software capable of dealing with raster data. So gridded DEMs are becoming increasingly available on all

scales from the global to the national and are likely to remain an important tool for hydrological applications for some time to come (Wise, 2000).

Both quality and resolution must be considered in the selection of a DEM for hydrological modeling. Quality refers to the accuracy of the elevation data while resolution refers to the precision of the data, especially to the horizontal grid spacing and vertical elevation increment. Quality and resolution must be consistent with the scale and model of the physical process under consideration and with the study objectives (Garbrencht and Mart, 2001).

The accuracy of the terrain represented by DEMs is affected by their resolution. The finer the DEM resolution, the more accurately the terrain is represented (Gao, 1997). Finer resolution means that the DEM cell size is smaller and more elevations are sampled (Gao, 1997). Halvorson and Doll (1991) calculated and compared the topographic factors that were determined from measurements made at distances of 3, 6, 15, and 30 m. They found topographic factors measured at 15 m gave the best values qualitatively matching their topographic position. Gao (1997) investigated the effects of DEM resolutions, which are from 10 meters to 60 meters on the accuracy of terrain representation. It was found that the RMSE of a gridded DEM increased linearly with its spatial resolution from 10 meters to 60 meters; the accuracy of gridded DEM decreases significantly at very fine and very coarse resolutions but minimally at an intermediate resolution irrespective of terrain complexity. The accuracy of terrain representation is also inversely correlated with terrain complexity; the representation accuracy is more sensitive to resolution reduction for complex terrain than for simple terrain.

It is necessary to analyze the sensitivity of topographical and geomorphologic parameters to the DEM resolution when they are used in hydrological simulations (Yang et al., 2001). The relationship between DEM grid size, landscape representation, and hydrologic simulations caught the attention of Zhang and Montgomery (1994), Seybert (1996) and Garbrecht and Mart (1996). Zhang and Montgomery (1994) investigated the hydrological process simulation using DEMs with different resolutions at 2 meters, 4 meters, 10 meters, 30 meters, and 90 meters. They concluded that a grid size smaller than the hillslope length is necessary to adequately simulate processes controlled by land form and that the length scale of the primary landscape features provides a natural guide to an appropriate grid size. They also concluded that a grid size of 10 meters would suffice for many DEM-based applications of geomorphic and hydrologic modeling. Seybert (1996) studied the effect of the DEMs resolution ranging from 5 meters to 500 meters on an event-based surface runoff model. His study indicated that runoff volume estimates are less sensitive to spatial resolution change than peak flow estimates and that increasing the number of subcatchments in the watershed representation caused the model to increase estimates of runoff volume and peak flow. He found that a ratio of average subcatchment area to grid cell area of 100 was an acceptable threshold of spatial resolution for reasonable model results. Garbrecht and Mart (2001) investigated the accuracy of drainage features extracted from DEMs as a function of DEM resolution. They suggested that a DEM should have a grid area of less than 5% of the drainage network reference area to reproduce the selected drainage features with an accuracy of about 10%.

The grid size for simulation models is best scaled in reference to the process being modeled (Zhang and Montgomery, 1994). However, the selection of DEM resolution for

simulation application also depends on the numerical approach (grid versus subcatchment models), as well as on the landscape parameters that are to be extracted from the DEM for the simulation (Garbrecht and Mart, 1996). When DEMs produced by a Global Positioning System (GPS) unit are used to estimate topographical parameters and simulate hydrologic processes, the selection of the resolution of the DEMs also depends on cost, data storage capability of the GPS unit, accuracy and precision of the latitudinal, longitudinal and elevation measurements, time consumed in the field data collection and data processing. The data volume of the representation of a terrain with a gridded DEM increases with the square of the resolution. The proper resolution, considering data volume, is a resolution which is as coarse as possible while still meeting the accuracy requirement.

Elevation Data Collection

In this research, a GPS unit, Trimble Model 4000, whose horizontal accuracy is within 0.01 meters, and whose vertical accuracy is within 0.02 meters, was used to collect the elevation data in one 160-acre field. Here after referred to as West Field, in Grant County, Oklahoma. West Field's north west corner's latitude is $36^0$39'31.60"N, longitude is $97^0$59'33.42"W. Its north east corner's latitude is $36^0$39'31.77"N, longitude is $97^0$59'01.08"W. Its south east corner's latitude is $36^0$39'05.54"N, longitude is $97^0$59'01.13"W. Its south west corner's latitude is $36^0$39'05.76"N, longitude is $97^0$59'33.43"W. Its center's latitude is $36^0$39'18.52"N, longitude is $97^0$59'16.19"W. The location of West filed is provided in Figure 2-1. The field data was used to generate grid DEMs. Considering the effects of DEMs' resolution on topography representation, hydrology modeling, capabilities of the GPS unit and characteristics of the study field

itself, the elevation data will be collected at 5 m or less than 5 m grid in areas with high relief, and at about an 8 m or greater than 8 m grid in relatively flat areas.

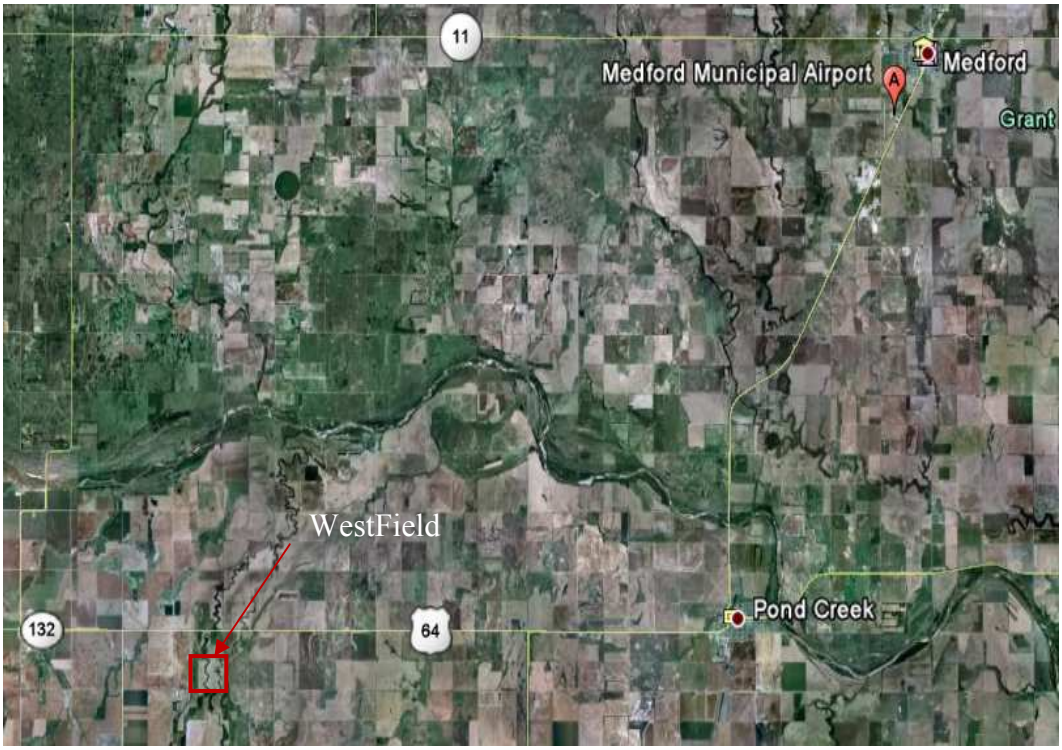

Figure 2-1 West field location

The first step in collecting the GPS data in the field was to locate the benchmark nearest to the study field and to select control points in the study field. These locations are critical for successfully collecting DGPS data. Since a benchmark was used to collect the precise location of control points, the accuracy level of the benchmark itself should meet the HARN station benchmark requirement, which is horizontal order-B or better. For this research, the HARN station benchmark at Medford municipal airport in Grant County, Oklahoma, which is 16.5 miles away from West field, was chosen. The control points were used to set up base units in the study field. The GPS unit works on a line-of-site rule. The roving unit must be able to "see" the base unit to be able to collect data. All roving locations must be within the line-of-site of one of the control points. Seven control

points were established in West field according to the line-of-site rule. All of the control points were established based on a single selected point.

Establishing the control points was a simple, but time consuming process. The stationary unit was set up on the selected benchmark location, the Medford municipal airport benchmark. Setting up this unit involved placing a surveying tripod over the benchmark point and placing the GPS receiver on the tripod. The roving receiver was then transported to the location of a control point in the study field and set up. The same procedure was used to set up the roving unit.

Figure 2-2 Control points set-up

Once the roving receiver was in place, a static survey was started on both units. The two units must collect data simultaneously for about 30 minutes. After collecting data for 30 minutes, the roving unit was dismantled and moved to the location of the next control point. This procedure was repeated until data had been collected for latitude,

longitude and elevation at all control points. Since the distance between the Medford municipal airport benchmark and the study field is about 16 miles, these procedures required at least two people working at the same time to insure both stationary unit and roving unit work simultaneously and reset units if satellite signals are lost. The selection and data collection of control points were completed in two days.

The next step was to process the GPS control point data. The data were downloaded from the data logger, TDC1, also referred to as the data controller, onto a personal computer. The data were corrected and processed using Trimble survey PS software. Once the processing was complete, the data sheets showing the precise locations of the benchmark and all control points that had been surveyed were obtained. Information from these static surveys is necessary to collect GPS data in the roving data collection procedure.

Collection of roving GPS data was the most time consuming part of the GPS data collection process. The first step in this procedure was to set up the stationary, base, GPS unit on one of the control points. With a hand-held data controller, TDC1, the survey was georeferenced by entering the information about the control point. After georeferencing the instrumentation, the base was started using the data controller. The controller was then disconnected from the base unit and connected to the roving GPS unit. After setting up the base station, the unit must be initialized. Initialization tells the roving receiver where it is relative to the location of the base receiver. The data for the roving points were relative to the configured base receiver location. An initialization board was placed on the tripod with the base receiver. The roving receiver was then connected to the

initialization board and the initialization option was selected on the data controller. The initialization took 10 to 15 minutes.

Figure 2-3. Rover initialization.

Once initialization was completed, the roving antenna was attached to a range pole. To speed up the roving data collection, the roving unit was mounted on a four-wheel ATV. The roving data collection model was set to continuous storage mode; the distance between two readings was set as 5 m, 8 m or other numbers, depending on the terrain complexity. The four-wheel ATV was driven across the field from one east-west transect or from west to east following a straight line at a low speed about 5 miles per hour. The distance between two transects of the four-wheel ATV was kept at 5 meters apart.

Figure 2-4. Four-wheel ATV tracks in West field.

Once all the desired points from one control point were surveyed, the survey was ended using the “end survey” command on the data controller. The “end survey” command must be confirmed, so that a survey is not accidentally ended prematurely. The roving receiver was then turned off using the data controller, and the base was turned off using the power button. Then the base unit was moved to another control point and the entire process was repeated. Once all 7 control points in West field were utilized, the data collection process was complete, and the only remaining step was to process the roving data. The data was downloaded from the data controller to a computer using a software package called Trimdata. The output files from the downloading process provided the data labels and the corresponding latitude, longitude, and elevation for each of the surveyed points.

Topography Map

The collected elevation data was processed and the West field topography was processed (Figure 2-5).

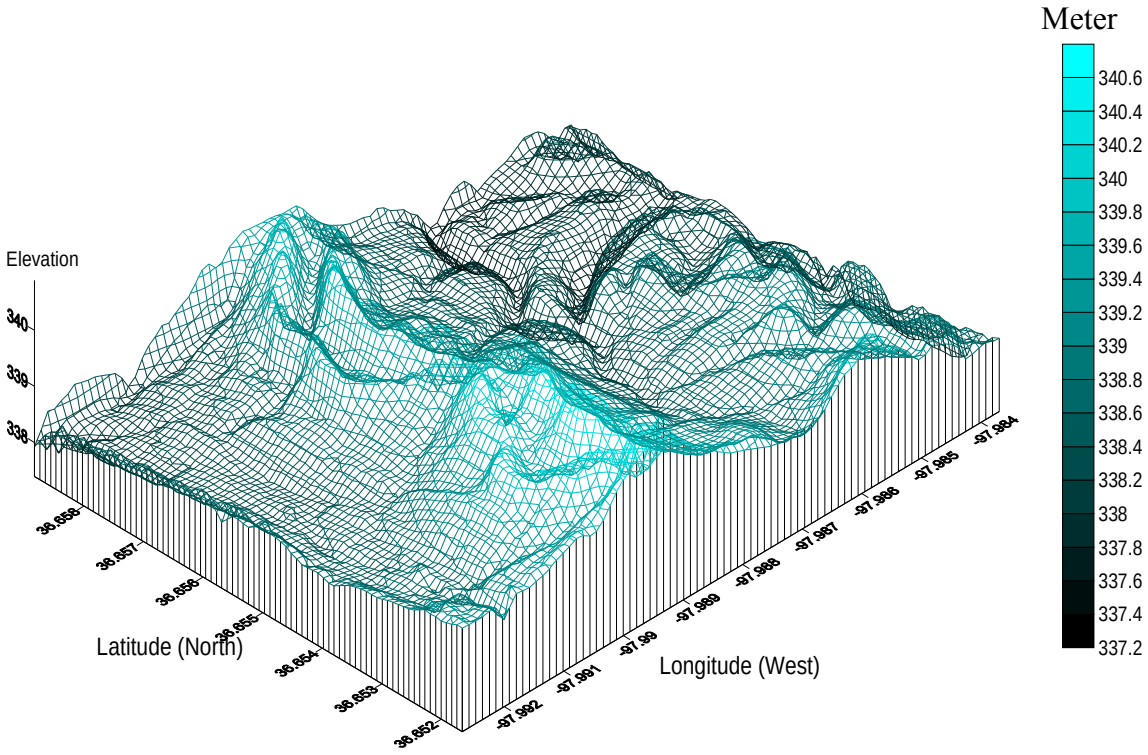

Figure 2-5. West field topography

Soil Data Collection

Soil Sampling Methods Review

Soil properties play important roles in the interaction between weather and topography since soil type dictates how much water can be held in the soil for crop growth. Collecting soil samples and analyzing them in the lab are standard procedures to determine soil information.

To do soil sampling, the first thing is to decide the sampling method and at which resolution soil samples should be collected. The purpose of soil sampling for this research is to measure the variance in soil properties, which interact with weather and topographical factors to affect wheat yield variability within the field. The most widely used soil sampling methods are described below:

Judgment Sampling: The sampler ordinarily knows something about the population and would like to use this information in obtaining a representative sample. The sampler's effort is often directed toward the use of personal judgment in selecting the most "typical" sites from which to draw the sample. Because the sampling units are selected with different but unknown probabilities, samples selected in this manner are biased. They may represent the population very well or not well at all; any confidence in results must rest entirely on faith in the sampler's judgment.

Simple Random Sampling: If **n** units are to be selected from the population, a simple random sample is defined as a sample obtained in such a manner that each possible combination of **n** units has an equal chance of being selected. In practice, the sample is usually drawn by selecting each unit separately, randomly, and independently of any units previously drawn. In soil investigation, the unit to be included in the sample is usually a volume. If the units are listed, a random sample can easily be taken by the use of a table of random numbers. Often, however, it is more convenient to choose one spot in the field and select random distances at which the unit is to be taken.

Stratified Random Sampling: With stratified random sampling, the population is broken into a number of subpopulations, and a simple random sample is taken from each subpopulation, or several random samples are taken from each subpopulation and

composited as one sample. The reasons for sampling soils in this manner include the desire (1) to make statements about each of the subpopulations separately, and (2) to increase the precision of estimates over the entire population. If the stratified random sample is to have greater precision than the simple random sample, stratification must eliminate some of the variation from the sampling error.

Systematic Sample: Systematic sampling covers samples in which the selected units are regular distances away from each other, either in one or two dimensions. If the population is of one dimension, the first unit is assumed to be selected at random from the first k units and subsequent units at each $\mathbf{k^{th}}$ interval. If the population is two dimensional, the surface can be considered to be composed of a number of strata of common size and shape. One of the main problems with the systematic sample has been in estimating sampling error of the sample.

Among these sampling methods, some are more precise than others, and some may be carried out at a much lower cost. So it is difficult to say which method is the best. In general, the best method is one that provides the maximum precision at a given cost or that provides a specified precision at the lower cost.

The variability in soil properties is a fundamental factor in deciding the soil sampling distance or resolution. Normally, the samples are less likely to be similar as the distance between the samples increases. If the distance between the samples is too large, soil variability within a short distance may be missed. But if the distance between soil samples is too small, the number of soil samples may be too large and the sampling process and post lab analyses may be too time-consuming and costly.

Also the properties of the soil itself are important factors for deciding sampling method and resolution. Different soil properties vary with different trends, at different resolutions within the field. Significant differences in surface soil test analyses were found when samples were less than 1 m apart for both mobile and immobile nutrients (Raun et al., 1998). Solie et al. (1999) used semivariance analysis to estimate the range over which samples of the five soil variables (total N, extractable P and K, organic C, and pH) and two plant variables (N concentration and biomass) were related. The range from semivariance analysis was generally between 1.04 and 6.70 m, but was highly dependent upon the variable analyzed (Solie et al., 1999). Soil test P, K and pH generally had smaller ranges, while total N and organic C tended to be larger (Solie et al., 1999). Cassel et al. (2000) studied the spatial variability of soil properties measured for the Ap, E if present, and upper B horizon at each site, including pH, P, Zn, Cu, exchangeable cations, percentage base saturation, cation exchange capacity, bulk density, soil water content at –10, -33, and –1500 Kpa, texture, and humic matter content. He found that the range of spatial dependence or autocorrelation of soil parameters varies from 10 m for Ap horizon depth to 100 m for –1500 Kpa water content of Ap. Base saturation and available water storage capacity were cross-correlated with grain yield to a distance of $\pm$15 and 12.5 m, respectively.

For this research, the purpose of soil sampling is to get soil texture information and to estimate the soil water holding capacity for each soil type. Considering all the factors determining the soil sampling, and observed soil differences in West field, the stratified random sampling method was chosen.

Soil Data Collection

The stratified random sampling method was used to take soil samples in West Field. The whole West field was divided into 17 sub areas based on observed soil differences. Soil samples were collected at two different soil depths: 0-9 in. and 9-18 in.. Two to six soil samples were collected randomly in each sub area, and then composited as one sample. The composite soil samples were analyzed using the soil science society standard hydrometer method to determine soil texture, the percentage of clay, sand, and silt, and therefore to determine the soil types according to the USDA soil classifications. The particle size distribution analysis results of the soil samples are shown in Table 2-1 and Table 2-2. From the particle size distribution analyses of soil samples taken from the two soil depths, we can see that the difference between the two layers is not appreciably different.

Table 2-1 Particle size distribution analyses of soil samples at soil depth 0-23 cm.

Soil sample	Soil texture			Soil type
	Percentage of sand (%)	Percentage of silt (%)	Percentage of clay (%)	
Sample 1	85.77	11.05	3.18	Loamy sand
Sample 2	82.99	13.50	3.51	Loamy sand
Sample 3	80.26	16.56	3.17	Loamy sand
Sample 4	66.71	28.10	5.19	Sandy loam
Sample 5	70.86	24.02	5.12	Sandy loam
Sample 6	67.01	27.45	5.54	Sandy loam
Sample 7	36.69	45.02	18.29	Loam
Sample 8	38.90	50.43	10.67	Silt loam
Sample 9	28.23	58.43	13.34	Silt loam
Sample 10	19.97	59.75	20.28	Silt loam
Sample 11	22.04	58.79	19.17	Silt loam
Sample 12	32.66	54.62	13.72	Sandy loam
Sample 13	56.47	37.18	6.35	Sandy loam
Sample 14	23.79	59.58	16.63	Silt loam
Sample 15	18.24	60.63	21.13	Silt loam
Sample 16	24.29	60.54	15.17	Silt loam
Sample 17	35.38	55.41	9.21	Loam

Table 2-2 Particle size distribution analyses of soil samples in soil depth 23-46 cm.

Soil sample	Soil texture			Soil type
	Percentage of sand (%)	Percentage of silt (%)	Percentage of clay (%)	
Sample 1	84.49	10.93	4.58	Loamy sand
Sample 2	82.07	13.81	4.12	Loamy sand
Sample 3	72.45	22.59	4.96	Sandy loam
Sample 4	76.43	18.87	4.70	Loamy sand
Sample 5	64.20	28.28	7.52	Sandy loam
Sample 6	54.31	37.42	8.27	Sandy loam
Sample 7	14.73	66.04	19.23	Silt loam
Sample 8	34.74	52.73	12.53	Silt loam
Sample 9	19.44	64.57	15.99	Silt loam
Sample 10	22.75	58.72	18.53	Silt loam
Sample 11	17.85	61.70	20.45	Silt loam
Sample 12	24.14	59.21	16.65	Silt loam
Sample 13	56.66	36.82	6.52	Sandy loam
Sample 14	22.81	61.05	16.14	Silt loam
Sample 15	18.36	61.46	20.18	Silt loam
Sample 16	22.29	62.08	15.63	Silt loam
Sample 17	33.74	55.10	11.16	Loam

Wheat Yield Data

Image Processing and NDVI Calculation

Winter wheat has been planted in West field, Grant County, Oklahoma since 1993 and wheat grain yield was monitored from then to 1999 using satellite imagery. A time series of LANDSAT five Thematic Mapper (TM) scenes of north central Oklahoma, with radiometric and geometric corrections, spanning the period 1993 to 1999, was obtained from Earth Observation Satellites, Inc. (EOSAT). Images were georeferenced to US Geological Survey digital 7.5 min orthophoto quadrangle maps and then resampled to a Universal Transverse Mercator grid, with a 25 m pixel size, using a nearest neighbor algorithm. The selected TM scenes were those when the satellite overpasses occurred at or near the heading stage of the winter wheat in the area, from middle April to early May. In some years, due to cloud interference, an image slightly outside of the optimum time window was selected. In the spring of 1995, no acceptable image was available for the whole north central Oklahoma area.

Table 2-3 Dates of the Landsat Thematic Mapper scenes used in the study.

Year	1993	1994	1996	1997	1998	1999
Scene date	April 25	March 27	April 2	April 20	April 23	May 12

The TM data were obtained in the form of brightness values (BV), also referred as to as digital numbers (DN). The utility of BVs lies in the relationship between pixel BVs and surface conditions. However, other factors such as sensor detector calibration and geometry, sun angle, earth-sun distance, and atmosphere affect BVs. Therefore, it is necessary to correct for the non-surface factors and convert pixel BVs to physical values

like reflectance so that data from multiple images data can be properly interpreted (Itenfisu et al., 1999).

In this study, the method described by Markham and Baker (1987) and EOSAT (1993) was applied to correct the BVs. First, the BVs for band 3, red wavelength, and band 4, near infrared (NIR) wavelength, were converted to radiance using the relation shown in Equation (2-1) with the calibration parameters provided by image header files and EOSAT.

$$L_\lambda = LMIN_\lambda + \left(\frac{LMAX_\lambda - LMIN_\lambda}{QCALMAX} \right) QCAL \tag{2-1}$$

Where QCAL is calibrated and quantized scaled radiance in units of DN, digital numbers. $LMIN_\lambda$ is spectral radiance in $mW \cdot cm^{-2} \cdot ster^{-1} \cdot um^{-1}$ at QCAL=0. $LMAX_\lambda$ is spectral radiance in $mW \cdot cm^{-2} \cdot ster^{-1} \cdot um^{-1}$ at QCAL=QCALMAX. QCALMAX is the range of rescaled radiance in DN, 255 for all TM data. L_λ is spectral radiance in $mW \cdot cm^{-2} \cdot um^{-1}$.

Then, the radiance values were converted to exoatmospheric reflectance using Equation (2-2).

$$\rho_p = \frac{\pi \times L_\lambda}{ESUN_\lambda \times \cos\theta_s \times d^2} \tag{2-2}$$

Where ρ_p is unitless effective at-satellite planetary reflectance and d is earth-sun distance in astronomic units from a nautical handbook. $ESUN_\lambda$ is mean solar exoatmospheric irradiances in $mW \cdot cm^{-2} \cdot um^{-1}$. θ_s is solar zenith angle in degrees, provided by the satellite image head file for each scene.

Table 2-4 Landsat TM scene calibration parameters for Band 3 and Band 4

Calibration parameters	Band 3 (Red band)	Band 4 (NIR band)
$LMAX_{\lambda}\,(mW \cdot cm^{-2} \cdot ster^{-1} \cdot um^{-1})$	-0.12	-0.15
$LMAX_{\lambda}\,(mW \cdot cm^{-2} \cdot ster^{-1} \cdot um^{-1}$	20.43	20.62
QCALMAX	255	255
$ESUN_{\lambda}\,(mW \cdot cm^{-2} \cdot um^{-1})$	155.7	104.7

From the reflectance values, the normalized difference vegetation index (NDVI) was calculated on a pixel-by-pixel basis using the following equation:

$$NDVI = \frac{(NIR - \mathrm{Re}\,d)}{(NIR + \mathrm{Re}\,d)} \tag{2-3}$$

In the above correction and converting procedures, no atmospheric correction was applied due to absence of appropriate data.

Wheat Yield Computation and Results

NDVI is a measure of the photosynthetic efficiency of the vegetation; it is indirectly related to the crop yield and thus appears suitable for yield estimation (Itenfisu et al., 1999). Itenfisu et al. (1999) developed and calibrated a winter wheat yield prediction equation, equation (2-4), for north central Oklahoma.

$$Y = 165.9e^{4.0443\,NDVI} \tag{2-4}$$

Where Y is wheat grain yield in Kg/ha. In this research, this prediction equation was applied to compute wheat yield on a pixel-by-pixel basis. The predicted yield results are shown in the predicted yield map for each year in Appendix A.

Weather Data

Weather data is an important part of studying the topography and weather influences on wheat yield variability. Weather data from 1994 to 1999 used in this research were obtained from the Medford Mesonet station, which is the closest Mesonet weather station to the study field. The daily data, precipitation, temperature, wind speed, solar radiation, and station pressure were used to compute evapotranspiration.

CHAPTER 3

SPATIAL DATA INTERPOLATION

Abstract

Spatial data are a fundamental component of a study in the spatial variability of wheat yield across a field. The spatial data required for this research include soil data, elevation data, and actual ET data. Soil data were obtained using the stratified random sampling method. Elevation data were gathered by using a GPS unit at semi regular intervals. Actual ET data were calculated using soil information and weather information, so they have the same spatial distribution as the soil data. Yield data were obtained from satellite images on a pixel-by-pixel basis; the pixel size was 25 m. It is necessary to use interpolation methods to convert soil, elevation, and actual ET data from point observations to continuous surfaces so that the spatial patterns sampled by these measurements can be compared with and correlated to the spatial patterns of yield. The interpolation methods applied in GIS software are inverse distance weighting (IDW), spline, and kriging. These three methods were used to interpolate each data set and interpolation results and errors are compared in this chapter.

Introduction

The goal in studying spatial and temporal variability of wheat yield across a field is to minimize or manage spatial yield variability in order to increase or maximize profitability. Therefore the causes of yield variability must be determined, which requires the acquisition of spatial data sets of information.

Spatial data is a fundamental component in a study of spatial variability of wheat yield across a field. The spatial data sets associated with this research are available soil water content, elevation, actual evapotranspiration (ET) and yield. Available soil water content data were obtained by analyzing soil samples colleted from West Field in Grant County, Oklahoma. Soil samples were taken at two soil depths, 0-23 cm and 23-46 cm. Seventeen composite soil samples were taken at each soil depth. Every composite soil sample was composed of 2 to 6 random soil samples. A total of 92 random soil samples were taken in each soil layer. The 92 random soil samples were distributed across the 160-acre field at irregular intervals. Elevation data were collected every 5 meters in the study field using GPS equipment; for a total 9210 measurements. Wheat grain yield in the study field was monitored from 1993 to 1999 using satellite imagery. Wheat yields were predicted from satellite images using a yield prediction model developed and calibrated by Itenfisu, et al. (1999) for north central Oklahoma. Predicted yields were computed on a pixel-by-pixel basis using a pixel size of 25 m. The actual ET data were calculated using weather data obtained from the Medford Mesonet station, and soil information obtained from soil samples. Therefore the ET data had the same spatial distribution as the soil samples. It is difficult to compare and correlate soil, elevation, and actual ET data with yield data directly because their spatial distributions differ. It is

necessary to use interpolation to convert soil, elevation, and actual ET data from point observations to continuous surfaces so that the spatial patterns sampled by these measurements can be compared with and correlated to the spatial patterns of yield.

Several interpolation methods are available. Some of them generalize to the situation of irregular sampling. The methods may be distinguished according to whether they are conceptually simple or complex, linear or non-linear, direct or iterative, and exact or approximate. Furthermore they may accommodate different statistical weights, respect a potential existing non-negativity constraint, or allow an estimate of the interpolation error. Interpolation methods applied in GIS software can be divided into two main groups, one is a deterministic technique, and the other is a geostatistical technique. The deterministic technique can be divided into two groups too, global and local. Global techniques calculate predicted values using the entire dataset. Local techniques calculate predicted values from the sampled points within the specified neighborhoods, which are smaller spatial areas within the larger study area. A deterministic interpolation can be either exact or inexact, depending on whether the resulting surface is forced to pass through the data values or not. An interpolation method that predicts a value that is identical to the measured values at a sampled location is known as an exact interpolator (Burrough and McDonnell, 1998). An inexact interpolator predicts a value that is different from the measured values (Burrough and McDonnell, 1998). Inexact interpolation can be used to avoid sharp peaks or troughs in the resulting surface. The nearest neighbors, inverse distance weighted (IDW) and spline methods are local deterministic methods used in Arcview. Geostatistical method, known as kriging, is based on statistical models that include autocorrelation.

Since interpolated values are usually less variable than the original data values, they make a smoother surface, which understates the variability and may be misleading from a quantitative point of view. To interpolate data, the spatial features represented by the original data, such as extreme values, the overall trend, the degree of continuity, and information about the physical process or phenomena that may have caused the pattern must be considered. Interpolation accuracy is of great importance for further analysis. Interpolation method, grid size, and the original data set itself affect the accuracy of interpolation. A dense data set requires less interpolation and the resulting surface is more believable, a sparse date set, on the other hand, can result in poor interpolation of spatial variability.

Methods

All the interpolation methods are based on the assumption that spatially distributed objects are spatially correlated; in other words, things that are close together tend to have similar characteristics. The widely used interpolation methods in GIS software are described below:

Inverse Distance Weighted (IDW)

The IDW method combines the ideas of proximity used by the Thiessen polygons with the gradual change surface trends. Thiessen polygons divide a region in a way that is totally determined by the configuration of the data points, with one observation per polygon. If the data lie on a regular square grid, then the Thiessen polygons are all equal, regular cells with sides equal to the grid spacing; if the data are irregularly spaced, then an irregular lattice of polygons results. A common, but implicit use of Thiessen polygons

is the assumption that the meteorological data for any given site can be taken from the nearest weather station. This assumption is not appropriate for gradually varying phenomena (Burrough and McDonnell, 1998).

The assumption of IDW is that each input point has a local influence that diminishes with distance. It weights the points closer to the processing cell greater than those farther away. A specified number of points, or optionally all points within a specified radius, can be used to determine the output value for each location.

$$z(x_o) = \sum_{i=1}^{n} \lambda_i z(x_i) \tag{3-1}$$

$$\sum_{i=1}^{n} \lambda_i = 1 \tag{3-2}$$

Where the weights λ_i are given by $\Phi(d(x, x_i))$. A requirement is that $\Phi(d) \to 0$ as d$\to$ 0, which is given by the commonly used reciprocal exponential function d^{-r}. So the IDW to a power becomes

$$z(x_j) = \sum_{i=1}^{n} z(x_i) d_{ij}^{-r} / \sum_{i=1}^{n} d_{ij}^{-r} \tag{3-3}$$

Where the x_j are the points where the surface is to be interpolated and the x_i are the data points. The power parameter r in the IDW interpolation controls the significance of the surrounding points upon the interpolated value. A higher power results in less influence from distant points.

The resulting surface also depends on the clustering in the data and on the presence of outliers. IDW interpolations commonly have a ‘duck-egg’ pattern around solitary data points with values that differ greatly from their surroundings, though this

can be modified to a certain extent by altering the search criteria for the data points to account for anisotropy (Burrough and McDonnell, 1998).

Splines

Before computers were used to fit curves to sets of data points, draftsmen used flexible rulers to achieve the best locally fitting smooth curves by eye. The flexible rulers were called splines. These rulers were held in place by weights on pegs at data points while the line was drawn (Burrough and McDonnell, 1998). It can be shown that the line drawn along a spline ruler is approximately a piece-wise cubic polynomial that is continuous and has continuous first and second derivatives. Spline functions are mathematical equivalents of the flexible ruler. They are piece-wise functions, which is to say that they are fitted to a small number of data points exactly, while at the same time ensuring that the joints between one part of the curve and another are continuous. This means that with splines, it is possible to modify one part of the curve without having to recompute the whole (Burrough and McDonnell, 1998).

The general definition of a piece-wise polynomial function $p(x)$ is:

$$p(x) = p_i(x) \qquad x_i < x < x_{i+1} \qquad i = 1,2,...,k-1 \tag{3-4}$$

$$p^j(x_i) = p_{i+1}^j(x_i) \qquad j = 0,1,...,r-1; \qquad i = 1,2,...,k-1 \tag{3-5}$$

The points $x_i, ... x_{k-1}$ that divide an interval x_0, x_k into k sub-intervals are called break points and the points of the curve at these values of x are commonly called knots. The functions $p_i(x)$ are polynomials of degree m or less. The term r denotes the constraints on the spline. When r = 0, there are no constraints on the function; when r = 1 the function is continuous without any constraints on its derivatives. If r = m+1, the

interval x_0, x_k can be represented by a single polynomial, so r = m is the maximum number of constraints that leads to a piece-wise solution. For m = 1, 2, or 3, a spline is called linear, quadratic, or cubic. The derivatives are of order1, 2, m-1, so a quadratic spline must have one continuous derivative at each knot, and a cubic spline must have two continuous derivatives at each knot. For a simple spline where r = m there are only k+m degree of freedom. The case of r = m = 3 has particular significance because the term "spline" was first used for cubic piece-wise polynomial functions. The term "bicubic-spline" is used in the three-dimensional situations where surfaces instead of lines need to be interpolated (Burrough and McDonnell, 1998).

The spline methods are best for gently varying surfaces such as elevation, water table heights, or pollution concentrations. It is not appropriate if there are large changes in the surface within a short distance, because it can overshoot estimated values. The regularized spline method yields a smooth surface. The tension spline method tunes the stiffness of the surface according to the character of the modeled phenomenon. When the regularized spline method is chosen, the weigh parameter defines the weight of the third derivatives of the surface in the curvature minimization expression. If the tension spline is chosen, the weight parameter defines the weight of tension. The number of point parameter identifies the number of points per region used for local approximation.

Kriging

Geostatistical methods of interpolation, popularly known as kriging, are used when the variation of an attribute and the density of samples are so irregular that simple methods of interpolation may give unreliable predictions (Burrough and McDonnell, 1998). Kriging methods were developed by Matheron (1963) and named in honor of D.C.

Krige. Kriging methods attempt to optimize interpolation by dividing spatial variation into three components: (a) deterministic variation that can be treated as useful soft information, (b) spatially autocorrelated but physically difficult to explain variations, and finally (c) uncorrelated noise (Burrough and McDonnell, 1998). Kriging works in way similar to how the IDW interpolator in that it weights the surrounding measured values to derive a prediction for each location (Burrough and McDonnell, 1998).

Spatial variation of any variable can be expressed as the sum of three components: (a) a structural component, having a constant mean or trend; (b) a random, but spatially correlated variable, known as the variation of the regionalized variable, and (c) a spatially uncorrelated random noise or residual error term. Then the value of a random variable Z at x is given by

$$Z(x) = m(x) + \varepsilon'(x) + \varepsilon'' \tag{3-6}$$

Where $m(x)$ is a deterministic function describing the structural component of Z at x, $\varepsilon'(x)$ is the term denoting the stochastic, locally varying but spatially dependent residuals from $m(x)$, the regionalized variable, and ε'' is a residual, spatially independent Gaussian noise tern having zero mean and variance σ^2. The first step is to decide on a suitable function for $m(x)$. In the simplest case, where no trend of drift is present, $m(x)$ equals the mean value in the sampling area and the average or expected differences between any and two places x and x+h separated by a distance between sites, h, so that

$$E\left[\{Z(x) - Z(x+h)\}^2\right] = E\left[\{\varepsilon'(x) - \varepsilon(x+h)\}^2\right] = 2\gamma(h) \tag{3-7}$$

Where $\gamma(h)$ is known as the semivariance. Two conditions, stationarity of difference and variance of differences, define the requirements for the intrinsic hypothesis of regionalized variable theory. This means that once structural effects have been accounted

for, the remaining variation is homogeneous so that differences between sites are merely a function of the distance between them. We can rewrite equation 3.7 as:

$$Z(x) = m(x) + \gamma(h) + \varepsilon'' \tag{3-8}$$

In order to show the equivalence between $\varepsilon'(x)$ and $\gamma(h)$. If the conditions specified by the intrinsic hypothesis are fulfilled, the semivariance can be estimated from sample data:

$$\hat{\gamma}(h) = \frac{1}{2n}\sum_{i=1}^{n}\{z(x_i) - z(x_i + h)\}^2 \tag{3-9}$$

Where n is the number of pairs of sample points of observations of the values of attribute z separated by distance h. A plot of $\hat{\gamma}(h)$ against h is known as the experimental variogram. The experimental variogram is the first step towards a quantitative description of the regionalized variation. The variogram provides useful information for interpolation, optimizing sampling, and determining spatial patterns. To interpolate, however, we must first fit a theoretical model to the experimental variogram (Burrough and McDonnell, 1998).

The form of the variogram can be quite revealing about the kind of spatial variation present in an area and can help to decide how to proceed further. When the nugget variation is important but not too large, and there is a clear range and sill, the spherical model can be used to fit the varoigram,

$$\gamma(h) = c_0 + c_1\left\{\frac{3h}{2a} - 1/2(h/a)^3\right\} \qquad \text{for } 0<h<a$$

$$= c_0 + c_1 \qquad \text{for } h \geq a$$

$$\gamma(0) = 0 \tag{3-10}$$

Where a is the range, h is the lag, c_0 is the nugget variance, and $c_0 + c_1$ equals the sill.

If there is a clear nugget and sill, but only a gradual approach to the range, the exponential model is often used to fit the variogram,

$$\gamma(h) = c_0 + c_1\{1 - \exp(-h/a)\} \tag{3-11}$$

If the variation is very smooth and the nugget variance ε'' is very small compared to the spatially dependent random variation $\varepsilon''(x)$, the variogram can be fitted by the Gaussian model,

$$\gamma(h) = c_0 + c_1\{1 - \exp(-h/a)^2\} \tag{3-12}$$

The spherical model, exponential model and Gaussian model are known as transitive variograms because the spatial correlation structure varies with h; non-transitive variograms have no sill within the area sampled and may be modeled by a linear model:

$$\gamma(h) = c_0 + bh \tag{3-13}$$

Where b is the slope of the line. A linear variogram typifies attributes, which vary on all scales.

Results and Comparison

IDW, spline, and kriging methods were applied to interpolate available soil water content, elevation, and actual ET data. Different methods produce different interpolation results from the same data set. The interpolation results from different methods for each data set are compared and discussed below.

Available Soil Water Content Interpolation

To interpolate available soil water content when the IDW method was used, parameters were set as power of 2, searching neighbor 5. When the completely regularized spline method was used to interpolate available soil water content, the parameters were set as searching neighbor 5. When kriging method was used, Gaussian model was chosen as experimental variogram to fit the data because it provided best fit among spherical, exponential and Gaussian models, searching neighbor 5. A summary of these three interpolation methods is shown in Table 3-1.

Table 3-1 Summary of three methods for interpolating spatially variable soil water content

Interpolation error estimate	Interpolation method		
	IDW	Spline	Kriging
Maximal value (%)	8.0000	5.6478	6.7668
Minimal value (%)	15.0000	15.1413	16.0266
Mean absolute error	0.5050	0.3683	0.4604
RMSR	0.8211	0.6956	0.8918
Sample number	92	92	92

Table 3-1 shows that the spline method has less estimated interpolation error among the three methods. The range of the original data was 8% to 15%, and the IDW interpolation kept the same range as the original data. The ranges from the spline and Kriging interpolation methods exceeded the original data range.

The measured vs. interpolated available soil water content from the three methods were plotted in Figure 2-1. In Figure 2-1 a, we can see that the interpolated data were

greater than the measured data when the measured data was at a minimal value; the interpolated data were smaller than the measured data when the measured data was at a maximal value. From Figure 2-1, b and c, we can see that the data points were distributed evenly along the 1:1 line.

(a)

IDW

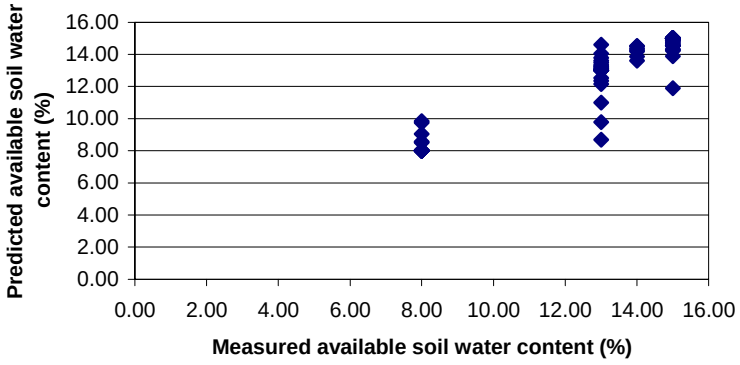

(b)

Spline

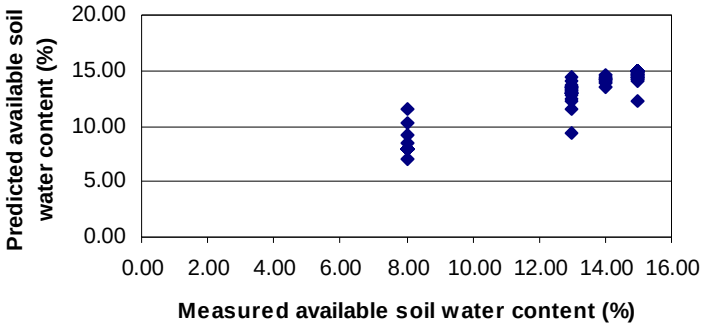

(c)

Kriging

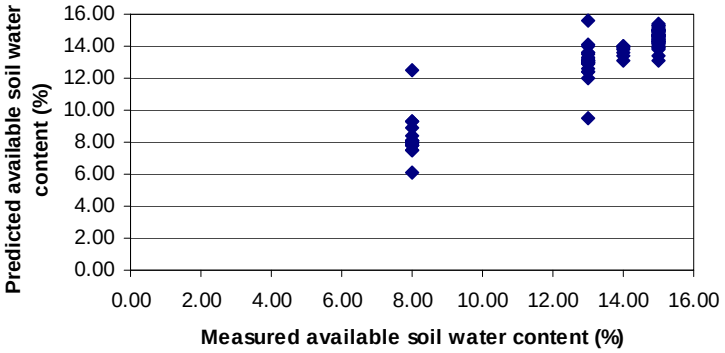

Figure 3-1 Interpolation comparison of available soil water content

The interpolated available soil water content surfaces created by the three methods are compared in Figure C-1 in Appendix C. There are two creeks across the study field. These two creeks divide the field into three parts, the east part, the middle part and the west part. As shown in Figure C-1, a, b, the main pattern of the interpolated available soil water content surfaces are similar in the west and middle parts of the field; differences exist in the east part. The available soil water content surface interpolated by the IDW method was smoother than the surface interpolated by the spline method. The available soil water content interpolated by IDW method gradually increases from the north side to the south side in the east part. The available soil water content interpolated by the spine method gradually increases from the north side to the south side in the east part, too, but with some localized changes in small areas in between. The interpolated available soil water content surfaces in Figure C-1, c was quite different from those in Figure C-1, a and b. The changes in available soil water content in Figure C-1, c is more gradually.

From these comparisons, combining field investigation information, the IDW method was chosen to interpolate available soil water content data for further study in this research.

Elevation Data Interpolation

To interpolate elevation data, when the IDW method was used, parameters were set as power of 2, searching neighbor 5. When completely regularized spline method was used to interpolate available soil water content, the parameters were set as searching neighbor 5. When kriging method was used, exponential model was chosen as

experimental variogram to fit the data, the searching neighbor was 5. The interpolation error estimates for these three methods are shown in Table 3-2.

Table 3-2 Summary of three methods to interpolate spatially variable elevation data.

Interpolation Error Estimate	Interpolation method		
	IDW	Spline	Kriging
Minimum value (m)	337.4087	337.4043	337.4136
Maximum value (m)	340.8573	340.8607	340.8509
Mean absolute error	0.0413	0.0387	0.0327
RMSR	0.0672	0.0688	0.0540
Sample number	9210	9210	9210

The measured elevation range is 337.3723 m to 340.9536 m. From Table 3-2, we can see that the elevation ranges interpolated by the three methods are very close to the measured elevation range. Table 3-2 shows that the estimated interpolated errors from the three methods are close, too, although the kriging method has the least RMSR among the three methods.

The measured vs. interpolated elevations using the three methods are plotted in Figure 3-2. From Figure 3-2, we can see that the data points are distributed evenly along a 1:1 line.

The interpolated elevation surfaces using the three methods are compared in Figure C-2 of Appendix C. From Figure C-2, a, b, and c we can see that the elevation surfaces interpolated by the three methods are quite similar; interpolated differences only exist in very small and localized areas. The reason for the similar interpolated surface is that the original elevation data are dense.

(a)

IDW

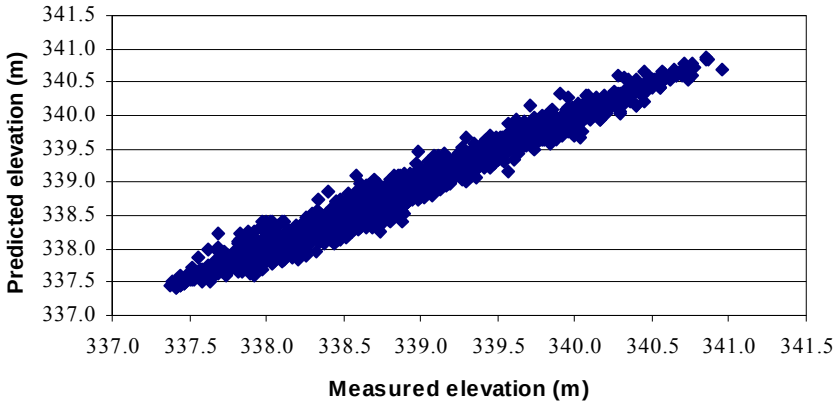

(b)

Spline

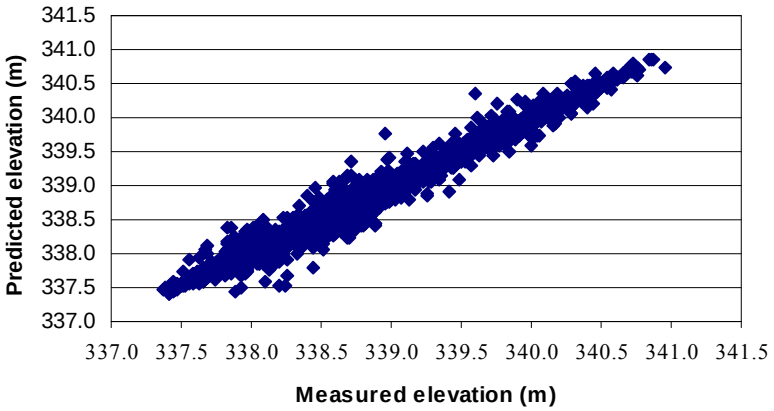

(c)

Kriging

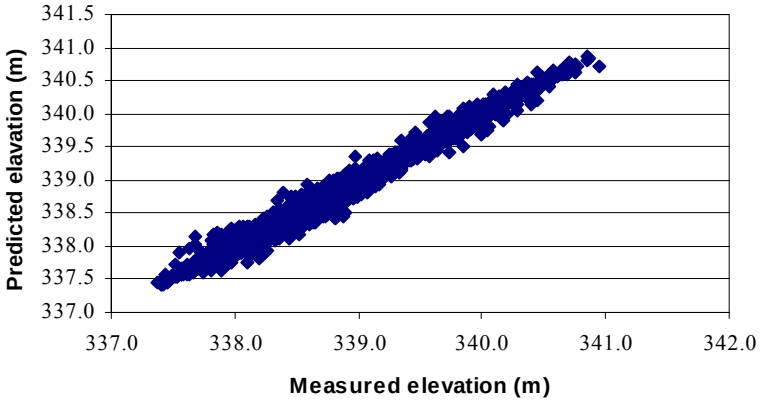

Figure 3-2 Interpolation comparison of elevation

For further studying the correlation between topography and yield, the Kriging method was chosen to interpolate elevation data.

Actual ET data Interpolation

Actual ET data were calculated in the study field for the 1994-1995, 1995-1996, 1996-1997, 1997-1998, and 1998-1999 wheat growth seasons. Since the actual ET for different growth seasons has the same spatial distribution, the actual ET for the 1994-1995 growth season was chosen as an example to conduct interpolation comparisons using the IDW, spline and Kriging methods.

To interpolate actual ET, when the IDW method was used, parameters were set as power of 2, searching neighbor 5. When the completely regularized spline method was used to interpolate soil water holding capacity, the parameters were set as searching neighbor was 5. When the Kriging method was used, the Gaussian model was chosen as the experimental variogram to fit the data, the searching neighbor was 5. The interpolation error estimates for these three methods are shown in Table 3-2.

The range of measured actual ET for the 1998-1999 growth season was 485.53 mm to 494.10 mm. The range of actual ET for the 1998-1999 growth season interpolated by IDW stayed closest to the range of measured actual ET for this season. The range of actual ET for 1998-1999 growth season interpolated by the spline method exceeded the range of the measured data most. Table 3-2 shows that the spline and Kriging methods have less estimated interpolation error than the IDW method did.

Table 3-3 Summary of Three methods to interpolate spatially variable actual ET.

Interpolation Error Estimate	Interpolation method		
	IDW	Spline	Kriging
Maximum value (mm)	485.83	484.40	482.94
Minimum value (mm)	411.10	494.10	497.37
Mean absolute error	0.4107	0.3802	0.7274
RMSR	1.0670	0.9877	1.2620
Sample number	92	92	92

The measured vs. interpolated actual ET using the three methods are plotted in Figure 3-3. From Figure 3-3, a, b, we can see that the interpolated data were greater than the measured data when measured data was at a minimal value; the interpolated data were smaller than the measured data when measured data was at a maximal value. From Figure 3-3, c, we can see that data points were distributed evenly along a 1:1 line.

The interpolated actual ET surfaces using the three methods are compared in Figure C-3 of Appendix C. The spatial pattern of interpolated actual ET surface is very similar to that of available soil water content in Figure C-1 because the original actual ET data were calculated using soil water content data for each soil sample location.

For further study correlation between ET and yield, the IDW method was chosen to interpolate actual ET data.

(a)

IDW

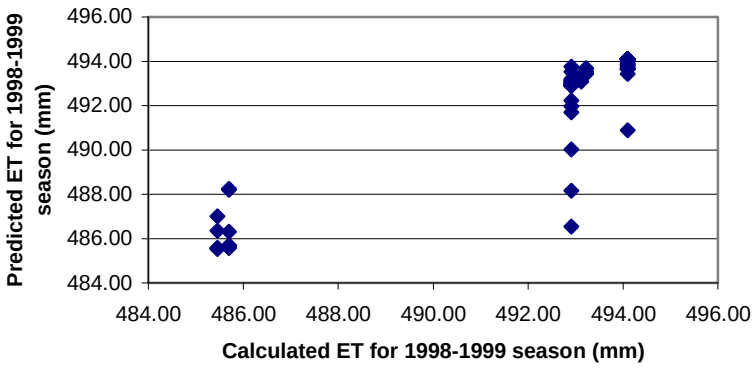

(b)

Spline

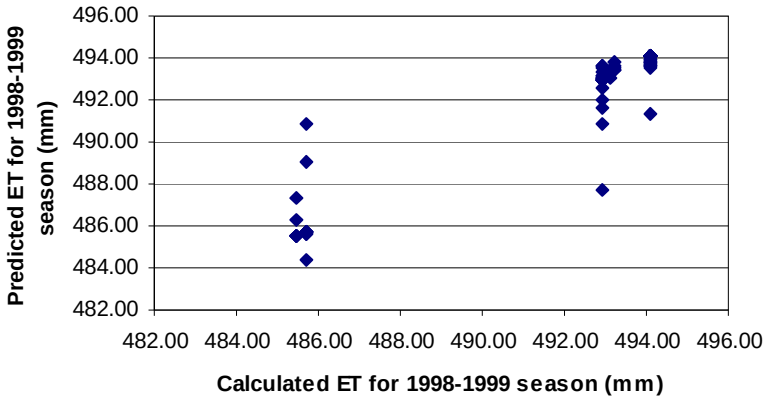

(c)

Kriging

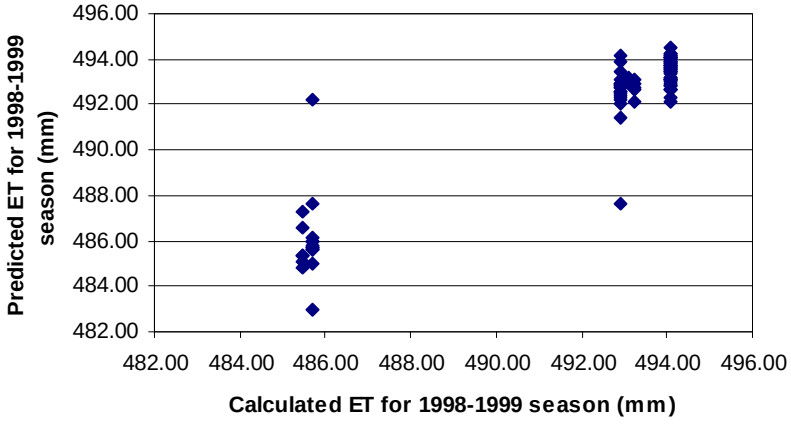

Figure 3-2 Interpolation comparison of 1998-1999 actual ET

CHAPTER 4

EFFECTS OF TOPOGRAPHY ON WHEAT YIELD VARIABLITY

Abstract

Wheat yields vary from year to year for specific sites as well as from site to site within a given year. The precision farming movement began with attempting to explain and treat within field scale yield variability by site-specific fertilizer management, variable rate fertilizer application (Raun et al., 1998; Solie et al., 1999). An increasing body of knowledge suggests that spatial variation in soil-water relations due to topography may be an important factor in causing spatial variation in grain yield (Sadler, 2000). Topography affects yields in a number of ways. First, it influences the redistribution (erosion and/or deposition) of soil particles, organic matter, and soil nutrients, with resulting changes in physical and chemical properties of uphill and downhill soils. Second, it affects water availability due to both vertical and horizontal water redistribution. The amount of plant-available water is an important yield-affecting factor, and water redistribution due to topography can be remarkably significant (Kravchenko and Bullock, 2000). With the development of GIS technology, detailed information on topographical land features can be easily obtained based on dense elevation measurements. Combining this information with the availability of dense yield data via satellite imagery now affords the opportunity to precisely characterize the

correlation between yield variability and topographical changes on a field scale. In this research, the relationship between topographical factors, such as slope, and slope curvature, one soil property, such as available soil water content and wheat yield from 1994 to 1999 were studied. A topography-related soil moisture index was developed by combining topography information and soil information.

Introduction

Spatial patterns of wheat yield differ from year to year because of the interactions among factors that vary spatially and temporally within a field. Attempts to explain within-field spatial yield variability began with fertility limitations and focused primarily on nitrogen, phosphorous, pH, and organic matter content (Raun et al., 1998; Solie et al., 1999; Lukina et al., 2002; Everett and Pierce, 1996). These studies showed that fertility factors could not explain all the yield variability within a field. These conclusions shifted the focus of research toward examining the effect on yield variability of topography or other site-specific soil properties that change with topography and affect patterns in soil moisture or soil drainage (Irmak et al., 2002; Sadler et al., 2000; Yang et al., 1998).

Topography affects yields in a number of ways. First, it influences the redistribution (erosion and/or deposition) of soil particles, organic matter, and soil nutrients, with resulting changes in physical and chemical properties of uphill and downhill soils. Second, it affects water availability due to both vertical and horizontal water redistribution. The amount of plant-available water is an important yield-affecting factor, and water redistribution due to topography can be remarkably significant (Kravchenko and Bullock, 2000).

It is difficult to generalize about the relationships between topography and crop yield (Timlin et al., 1998). Wheat growth is strongly influenced by topographically induced microenvironments. Net radiation, soil water, soil temperature, soil development, and natural erosion vary among topographic features. Moulin et al. (1994) found that wheat yields were lowest on higher elevated knolls where soil erosion losses were greatest. Miller et al. (1988) found no correlations between slope percentage and wheat yields. Yang et al. (1998) found topographic attributes, including elevation, slope, and aspect, have significant effects on wheat yield and could explain 13 to 35% of the variability in the wheat yield. Although yields vary with slope and aspect, these factors alone are not consistent indicators of grain yield; the relative productivity of a given landscape position varies from year to year and from farm to farm (Fiez et al., 1994). Thus, instead of focusing on slope and aspect themselves, we need to determine what factors vary with slope and aspect and how these factors are related to productivity (Fiez et al., 1994). Moulin et al. (1994) reported that the interaction between elevation and surface curvature affects the spatial distribution of soil properties and wheat yield in the landscape. Soil properties and associated crop yield are often spatially correlated; spatial analysis should be used when quantifying their variability (Timlin et al., 1998). The spatial variability of site-specific soil properties related to plant-available soil water has been shown to be a key factor in crop yield (Irmak, 2002). Daniels et al. (1987) suggested that soil water might be the most important yield-controlling factor in hilly topography.

Attempts to characterize site moisture conditions can be segregated into three approaches: direct monitoring, water-balance climatology, and an inferential technique based on topographic factors.

Direct monitoring of soil moisture includes one-time measurement and continuous gauging of site conditions. Soil moisture content and water potential fluctuate irregularly because of precipitation and associated runoff and throughflow events, as well as diurnally and seasonally because of temperature-induced changes in evapotranspiration flux from plants and soil (Parker, 1982). One-time direct measurements, such as gravimetric analysis, or tensiometric determination of soil water potential, hinder the comparison of measurements taken at different times and places. Continuous monitoring of moisture conditions on multiple sites is ideal; however, it is fiscally impractical under most field conditions, particularly given the large number of samples.

The soil water balance model is an often-used method to calculated soil moisture. But modeling soil moisture requires climate data, such as temperature, radiation, wind, pressure, precipitation, from weather stations and complex simulation for a period of time, given a certain soil depth.

The inferential technique based on topographic conditions has been employed to characterize environmental moisture levels while circumventing the difficulties of direct monitoring of soil moisture level. Inferential methods are often designed to provide an index along which individual sites may be ordered based on measurable topographic factors or soil properties.

Parker (1982) described a topographic relative moisture index which combined topographic position, aspect, slope, and slope curvature to characterize the moisture potential for ecologic use. Sinai et al. (1981) calculated a soil surface curvature factor from the elevation of neighboring points on a grid pattern of the field. This factor was

positive in concave position in the landscape and negative in convex position in the landscape. This factor was highly correlated to soil moisture content. Simmons et al. (1989) used a modification of the method developed by Sinai et al. in 1981 to calculate curvature and slope, which were found to be significantly related to crop yields. Halvorson and Doll (1991) measured the slope at the sites in four directions, 90 degrees apart; if the slope was upward from the site, it was designated as positive. The slope measurements from the four directions were then added to give one number, designated as the topographic factor. This topographic factor would then be positive in landscape positions where a net increase in water would be expected from runon water or from lateral subsurface movement within the soil profile from the upslope, and negative in landscape positions where a net loss of water should occur from runoff and downslope subsurface movement of water in the soil profile.

With the development of GIS technology, detailed information on topographical land features can be easily obtained based on dense elevation measurements. Combining this with information with the availability of dense yield data via satellite imagery now affords the opportunity to precisely characterize the correlation between yield variability and topographical changes on a field scale.

The goal of this research is to study the factors which affect yield variability within a field, and develop a topography-related soil moisture index which will indicate the potential soil moisture variability as the topography changes. The initial hypothesis for this study was that topographical data, in combination with soil information, are useful for explaining yield variability on a field scale.

Spatial Data Collection and Interpolation

Soil Data

A 160-acre field, privately owned by Jim Kent in Grant County, Oklahoma (referred as the West Field) was selected as the study field for this research. The stratified random sampling method was used to take soil samples in the study field. After a thorough investigation of the study field, the whole field was divided into 17 sub areas according to the observed soil differences. Sampling was conducted using a 25 mm diameter soil probe at two soil depths, 0-23 cm and 23-46 cm. Seventeen composite soil samples were taken at each soil depth. Every composite soil sample was composed of 2 to 6 random soil samples. A total of 92 random soil samples were taken from each soil layer. Strategic random sampling method was used.

Soil varies greatly in its ability to retain water. This characteristic of a soil is called the characteristic curve. The shape of this curve is largely governed by the soil texture (Jensen et al., 1989). A particle size distribution experiment was conducted to determine the soil texture, and therefore to determine the soil texture classes according to the USDA soil classification. The results are shown in the following tables.

Table 4-1 Particle size distribution analyses of soil samples at soil depth 0-23 cm.

Soil sample	Soil texture			Soil type
	Percentage of sand (%)	Percentage of silt (%)	Percentage of clay (%)	
Sample1	85.77	11.05	3.18	Loamy sand
Sample 2	82.99	13.50	3.51	Loamy sand
Sample 3	80.26	16.56	3.17	Loamy sand
Sample 4	66.71	28.10	5.19	Sandy loam
Sample 5	70.86	24.02	5.12	Sandy loam
Sample 6	67.01	27.45	5.54	Sandy loam
Sample 7	36.69	45.02	18.29	Loam
Sample 8	38.90	50.43	10.67	Silt loam
Sample 9	28.23	58.43	13.34	Silt loam
Sample 10	19.97	59.75	20.28	Silt loam
Sample 11	22.04	58.79	19.17	Silt loam
Sample 12	32.66	54.62	13.72	Sandy loam
Sample 13	56.47	37.18	6.35	Sandy loam
Sample 14	23.79	59.58	16.63	Silt loam
Sample 15	18.24	60.63	21.13	Silt loam
Sample 16	24.29	60.54	15.17	Silt loam
Sample 17	35.38	55.41	9.21	Loam

Table 4-2 Particle size distribution analyses of soil samples in soil depth 23-46cm.

Soil sample	Soil texture			Soil type
	Percentage of sand (%)	Percentage of silt (%)	Percentage of clay (%)	
Sample 1	84.49	10.93	4.58	Loamy sand
Sample 2	82.07	13.81	4.12	Loamy sand
Sample 3	72.45	22.59	4.96	Sandy loam
Sample 4	76.43	18.87	4.70	Loamy sand
Sample 5	64.20	28.28	7.52	Sandy loam
Sample 6	54.31	37.42	8.27	Sandy loam
Sample 7	14.73	66.04	19.23	Silt loam
Sample 8	34.74	52.73	12.53	Silt loam
Sample 9	19.44	64.57	15.99	Silt loam
Sample 10	22.75	58.72	18.53	Silt loam
Sample 11	17.85	61.70	20.45	Silt loam
Sample 12	24.14	59.21	16.65	Silt loam
Sample 13	56.66	36.82	6.52	Sandy loam
Sample 14	22.81	61.05	16.14	Silt loam
Sample 15	18.36	61.46	20.18	Silt loam
Sample 16	22.29	62.08	15.63	Silt loam
Sample 17	33.74	55.10	11.16	Loam

From the particle size distribution analyses of soil samples taken from the two soil depths, we can see that the differences between the two layers are not significant.

Based on soil texture information, soil water classes were summarized by Jensen et al. as shown in Table 4-3.

Table 4-3 General soil-water classes for agricultural soils (from Jensen et al., 1989)

Texture class	Water content, Volume Basis (%)		
	Drained upper limit (field capacity)	Lower limit of extractable water (permanent wilting point)	Available water
Sand	12	4	8
Loamy sand	14	6	8
Sandy loam	23	10	13
Loam	26	12	14
Silt loam	30	15	15
Silt	32	15	17
Silty clay loam	34	19	15
Silty clay	36	21	15
Clay	36	21	15

The drained upper limit, often called field capacity, is a function of soil texture and other parameters that affect the shape of the soil water characteristic curve. The field capacity sets a line for the maximum water that soil can retain. Generally, field capacity occurs at soil water potentials near -10 kPa in coarse textured soils and at potentials near -20 kPa in medium- to fine-textured soils (Jensen et al., 1989). The low limit of available water is also termed the permanent wilting point. Soil water below this limit is considered to be unavailable to plants, with plants experiencing severe water stress with corresponding wilting and eventual plant death (Jensen et al., 1989). Available water is

the difference between the drained upper limit and the low limit of extractable water. This amount of water is stored soil water that can be extracted by plant roots.

Before comparing and correlating soil with topography and yield, it is necessary to use interpolation to convert available soil water data from point observations to continuous surfaces so that the spatial patterns sampled by these measurements can be compared with and correlated to the spatial patterns of yield. The IDW interpolation method was used to interpolate available soil water, with interpolation parameters set as power of 2, and searching neighbor of 5 to a grid-based surface; the grid size is 25 m. The interpolated available soil water surface is shown as Figure 4-1.

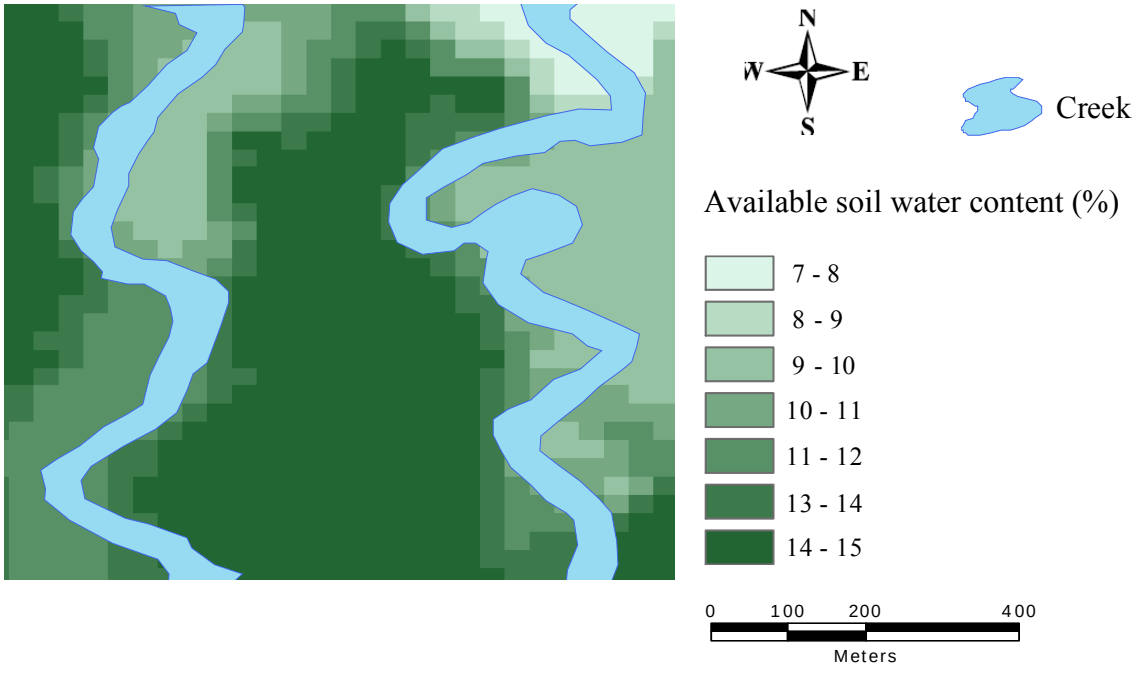

Figure 4-1. Interpolated available soil water content

Elevation Data

A Trimble GPS unit, Model 4000, with a horizontal accuracy within 0.01 meters, and vertical accuracy within 0.02 meters, was used to collect the detailed elevation data

in the study field. Elevation measurements were taken on a semiregular grid at a distance of approximately 2-8 m, depending on the complexity of the terrain. Measurements on level areas in the study field were made at greater distances, while marked depressions and elevations were measured intensely. A total of 9210 elevation measurements were taken in the study field. The measured elevation range is from 337.3723 m to 340.9536 m. From this, we can see that the difference in elevation is not significant.

These 9210 elevation measurements were used to develop DEM for the study field, from which the topographical factors such as aspect, slope, and slope curvature can be derived. An interpolation method is necessary to convert elevation data from point observations to pixel-by-pixel DEM (pixel size 25 m), so that the spatial patterns sampled by these measurements can be compared with and correlated to the spatial patterns of yield. The kriging interpolation method was used to interpolate elevation data, with an exponential model as the experimental variogram to fit the data, and a searching neighbor of 5. The DEM of 0.1 m resolution for the study field is shown after interpolation as Figure 4-2.

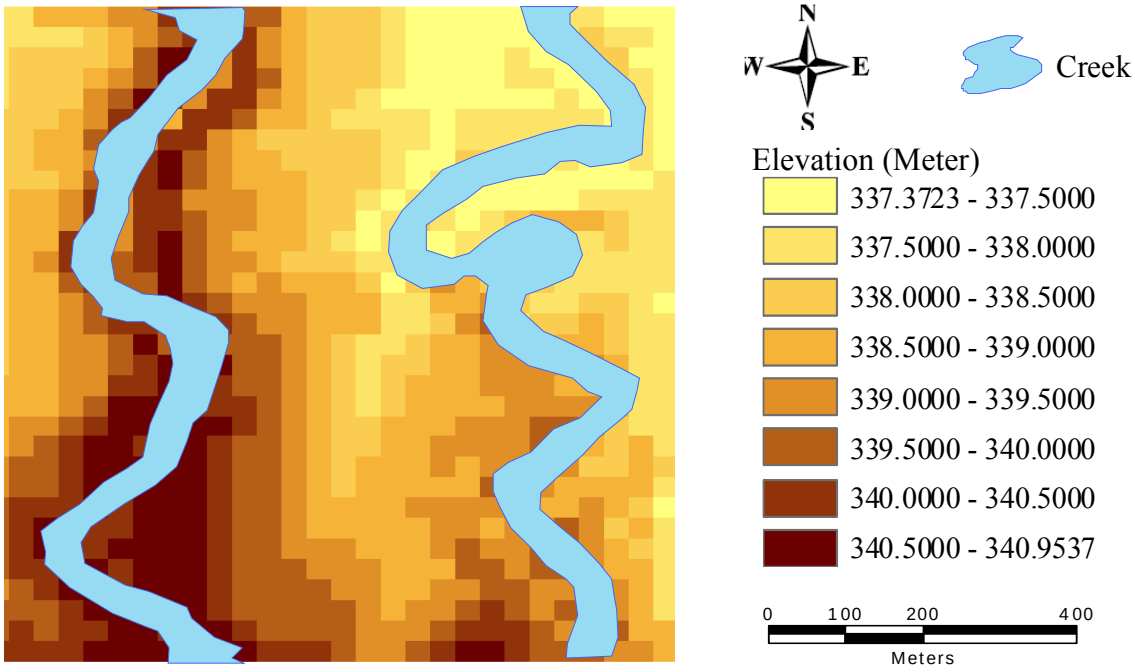

Figure 4-2. DEM for the study field at 25 m resolution

Yield Data

Winter wheat was planted in the study field, in Grant County, Oklahoma from 1994 to 1999 and wheat grain yield was monitored from then to 1999 using satellite imagery. A time series of LANDSAT five Thematic Mapper (TM) scenes of north central Oklahoma, with radiometric and geometric corrections, spaning the period 1993 to 1999, was obtained from Earth Observation Satellites, Inc. (EOSAT). Images were georeferenced to US Geological Survey digital 7.5 min orthophoto quadrangle maps and then resampled to a Universal Transverse Mercator grid, with a 25 m pixel size, using a nearest neighbor algorithm. The TM scenes were chosen when the satellite overpasses occurred at or near the heading stage of winter wheat in the area, middle April to early May. In some years, due to cloud interference, an image that was slightly outside of the

optimum time window was selected. In the spring of 1995, no acceptable image was available for the entire north central Oklahoma area.

Table 4-4 Dates of the Landsat Thematic Mapper scenes used in the study.

Year	1994	1996	1997	1998	1999
Scene date	March 27	April 2	April 20	April 23	May 12

Itenfisu et al. (1999) developed and calibrated a winter wheat yield prediction equation using satellite images for north central Oklahoma.

$$Y = 165.9e^{4.0443\,NDVI} \tag{4-1}$$

Where Y is wheat grain yield in kg/ha. In this research, this prediction equation was applied to compute wheat yield on a pixel-by-pixel basis, with a pixel size of 25 m. Appendix A shows predicted yields results in the predicted yield map for each year.

Topographical Factors Affecting Wheat Yield

After the point measurements for elevation were converted into pixel-by-pixel DEM, with a pixel size of 25 m. The Arcview Spatial Analyst (ESRI, 1996), a GIS tool was used to analyze elevation and to derive the topographical land features, such as slope, aspect, and curvature. The aspect, slope, and curvature were obtained on the same pixel basis as the DEM.

Aspect

Aspect identifies the down-slope direction of the maximum rate of change in value from each pixel to its neighbors. Aspect can be thought of as the slope direction. It is expressed in positive degrees from 0 to 359.9, measured clockwise from the north. An

aspect value of –1 indicates an area of undefined aspect (i.e. flat). A map of the terrain aspect of the study field is shown as Figure 4-3.

Aspect direction is generally associated with the intensity and duration of solar energy input to a site. Sites which face in a southerly direction generally receive greater solar incidence than do more northern-facing sites. Normally the thermal conditions affect wheat growth. Since the elevation difference in the study field is only 3.5813 m, the thermal condition difference due to aspect changes is negligible.

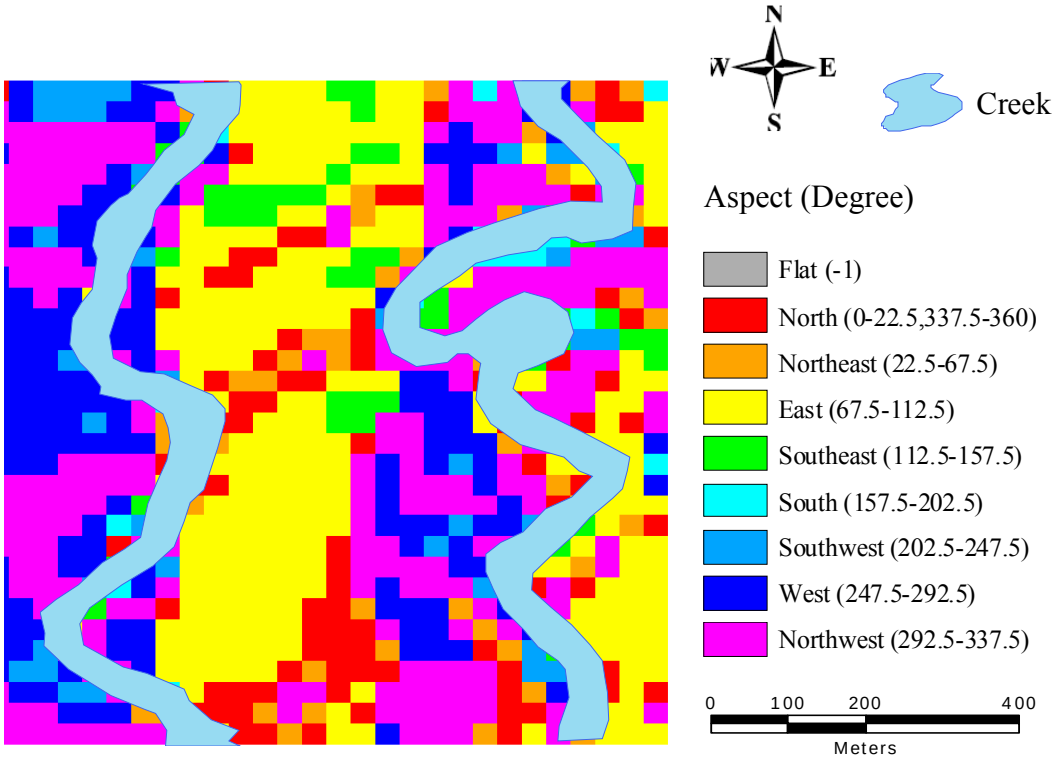

Figure 4-3. Aspect map of the study field.

Slope

Slope identifies the maximum rate of change in value from each cell to its neighbors. It is defined as the first-order derivative of the terrain. An output slope can be

calculated as percent slope or degree slope. The percent slope was calculated as a ratio of the difference in elevation between the centers of adjacent cells and the horizontal distance between them. The degree slope was obtained based on a set of 3×3 neighboring cells using the average maximum technique (Burrough, 1986). A slope map at 25 m resolution is shown as Figure 4-4.

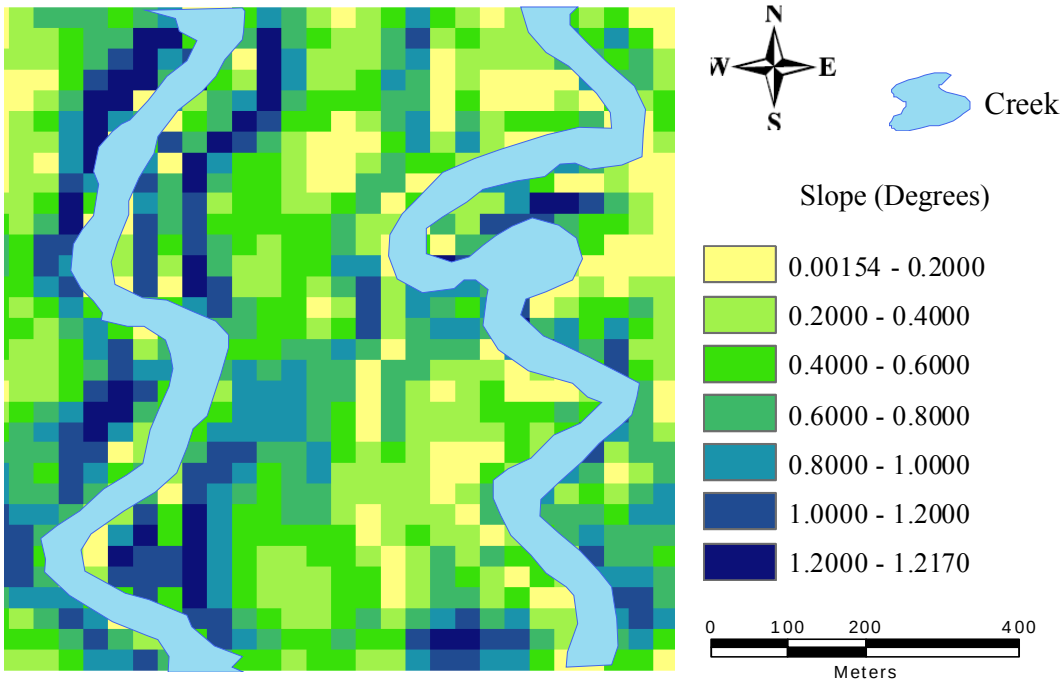

Figure 4-4. Slope map of the study field

Slope strongly affects the flow and residence time of moisture on a landscape. Slope steepness affects the local exposure and erosion at a site. Shallow slope sites retain more moisture and generally retain deeper soils while steep sites generally shed moisture and soil. So slope affects wheat yield through its impact on movement and distribution of soil moisture, and on soil erosion.

Slope Curvature

Slope curvature is defined as the second-order derivative of the terrain surface. A positive curvature indicates that the surface is upwardly convex at that cell. A negative curvature indicates that surface is upwardly concave at that cell. A value of zero indicates that the surface is flat. A curvature map of the study field is shown in Figure 4-5.

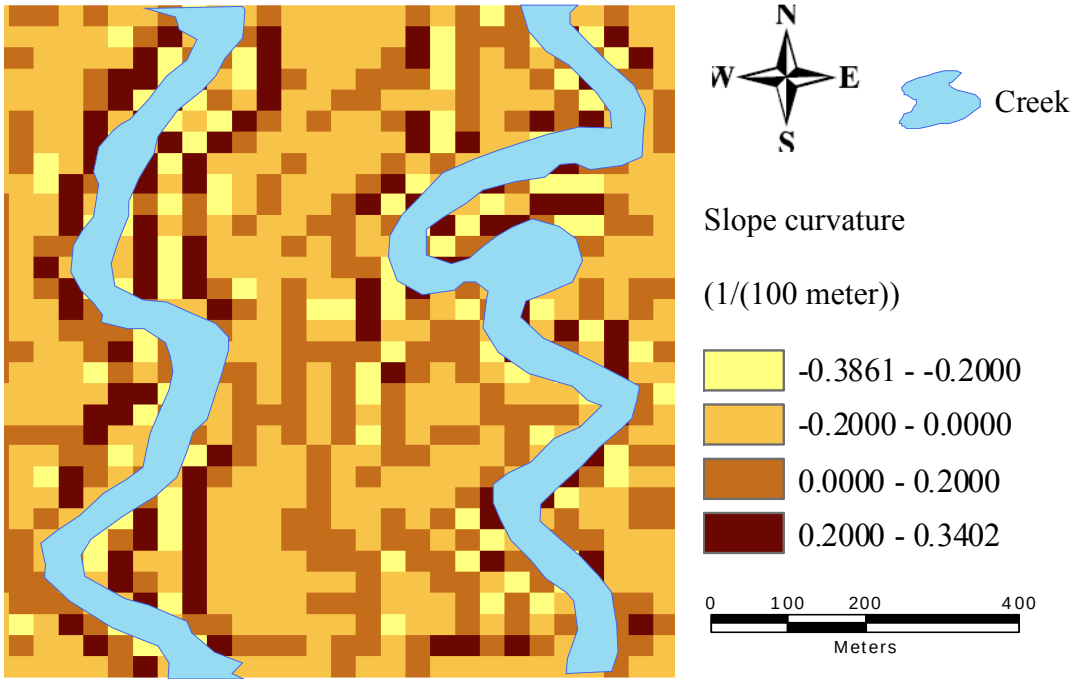

Figure 4-5. Curvature map of the study field.

Curvature can be used to describe the physical characteristics of a drainage terrain. The curvature affects the acceleration and deceleration of flow and the convergence and divergence of flow. During precipitation events, the runoff accumulates and is detained in concave areas while the runoff flows away from the convex and flat areas. The accumulated and detained runoff in concave areas infiltrates to the soil and

evapotranspirates into the air. This later infiltration influences soil moisture redistribution, and therefore influences yields

Topography Related Soil Moisture Index

A topography-related soil moisture index (TRSMI) is constructed from combining two topographic variables, slope and curvature, with one soil variable, available soil water content. A TRSMI is a scalar index determined by summing assigned values for these three variables. TRSMI values may range from 0 to 40. For each stand, the values of slope and curvature are classified into 11 groups; between 0 and 10 units are assigned for each group as shown in Table 4-4. Available soil water content is classified into 21 groups; between 0 and 20 units are assigned to each group as shown in Table 4-5.

Table 4-5 Classification of slope steepness and curvature

Classification of slope		Classification of curvature	
Slope (degrees)	Classified unit	Curvature (m^{-2})	Classified unit
0.0015 to 0.1121	10	-0.3861 to -0.3201	10
0.1121 to 0.2266	9	-0.3201 to -0.2541	9
0.2266 to 0.3331	8	-0.2541 to -0.1881	8
0.3331 to 0.4437	7	-0.1881 to -0.1220	7
0.4437 to 0.5542	6	-0.1220 to -0.0560	6
0.5542 to 0.6647	5	-0.0560 to 0.0100	5
0.6647 to 0.7753	4	0.0100 to 0.0761	4
0.7753 to 0.8858	3	0.0761 to 0.1421	3
0.8858 to 0.9963	2	0.1421 to 0.2081	2
0.9963 to 0.1069	1	0.2081 to 0.2742	1

Classification of slope		Classification of curvature	
Slope (degrees)	Classified unit	Curvature (m^{-2})	Classified unit
0.1069 to 1.2174	0	0.2742 to 0.3402	0

Table 4-6 Classification of available soil water content

Available soil water content (%)	Classified unit	Available soil water content (%)	Classified unit
8.0000 to 8.3333	0	11.6667 to 12.0000	11
8.3333 to 8.6667	1	12.0000 to 12.3333	12
8.6667 to 9.0000	2	12.3333 to 12.6667	13
9.0000 to 9.3333	3	12.6667 to 13.0000	14
9.3333 to 9.6667	4	13.0000 to 13.3333	15
9.6667 to 10.0000	5	13.3333 to 13.6667	16
10.0000 to 10.3333	6	13.6667 to 14.0000	17
10.3333 to 10.6667	7	14.0000 to 14.3333	18
10.6667 to 11.0000	8	14.3333 to 14.6667	19
11.0000 to 11.3333	9	14.6667 to 15.0000	20
11.3333 to 11.6667	10		

Results and Discussions

Wheat yields were correlated with topographical factors, soil, and the TRSMI. When topographical and soil factors were correlated with yield for multiple years, the interpolated available soil water content, slope, and slope curvature derived from the DEM of the study field, directly, without classification, were used to calculate correlation

coefficients. The correlation coefficients calculated for the whole study field are shown in Table 4-7.

Table 4-7 Correlation coefficient (r) between yield and topography factors for the entire study field.

	Slope	Slope curvature	Available soil water content	TRSMI
1994 yield	-0.0291	0.0057	0.3880	0.2948
1996 yield	-0.0414	-0.0168	0.3304	0.2608
1997 yield	0.0437	0.0034	0.3080	0.2195
1998 yield	0.0735	-0.0294	0.3481	0.1517
1999 yield	0.1406	0.0095	0.2398	0.0566
Average yield	0.0735	-0.0132	0.4452	0.2401

From Table 4-7, we can see that among the factors listed above available soil water content has the highest correlation with yield. This demonstrated that the amount of water soils can retain is an important factor causing yield variability on a field scale. In 1996 and 1998, the slope curvatures had a negative correlation with yield. This indicates that the areas with high slope curvature, which are concave areas in the field, had low yields; the areas with low slope curvature values, which are convex areas in the field, had high yields. But in 1994, 1997 and 1999, the correlation between yield and slope curvature was reversed; the areas with high slope curvature, which are concave areas in the field, had high yields; the areas with low slope curvature values, which are convex areas in the field, had low yields.

From the Medford Mesonet station, the total precipitation for growth seasons of 1996, 1997, 1998, and 1999 yields, was obtained as shown in Table 4-8. Since weather

data from Medford Mesonet station was not available for 1993, the precipitation for 1993-1994 can not be calculated.

Table 4-8 Total precipitation for four growth seasons

Yield	Planting date	Harvest date	Total precipitation during growth season (mm)
1994	Sep. 14, 1993	Jun 20, 1994	
1996	Oct. 06, 1995	Jun. 14, 1996	122
1997	Oct. 02, 1996	Jun. 25, 1997	530.35
1998	Oct. 10, 1997	Jun. 09, 1998	510.54
1999	Oct. 14, 1998	Jul. 07, 1999	1049.02

Combining Table 4-8 with Table 4-7, we can see clearer correlations between yields and the slope curvature. In dry growth season, such as 1995-1996, and growth seasons with adequate precipitation, 1997-1998, the concave areas in the field, had high yields, and the convex areas in the field had low yields. In these crop years, the concave areas accumulate runoff during the rainfall events while the convex areas lose runoff. The accumulated runoff in the concave areas infiltrates into the soil later for crop growth. In 1998-1999 crop year, the total precipitation was 1049 mm, which is more than adequate for wheat growth. So in a wet crop year, more than enough water was accumulated in concave areas and yields decreased.

Table 4-7 shows a correlation pattern between the slope and yield, which is similar to, but not as strong as the correlation pattern between yields and the slope curvature.

In Table 4-7, the correlation coefficient between the TRSMI and yields ranges from 0.0566 to 0.2948. This indicates that a positive correlation exists between yield and

TRSM. Although the correlation coefficient between TRSM and yield is not as high as expected, it does show some correlation between yield, topography, and soil.

Wheat yields were correlated to topographical factors, soil, and the TRSMI in 92 sampled locations. When topographical and soil factors were correlated to yield for multiple years, the interpolated available soil water content, slope, and slope curvature derived from the DEM of the study field, directly, without classification, were used to calculate correlation coefficients. The correlation coefficients calculated for these sampled locations are shown in Table 4-9.

Table 4-9 Correlation coefficient (r) between yield and topography factors at sample locations.

	Slope	Slope curvature	Available soil water content	TRSMI
1994 yield	-0.0624	-0.2710	0.7813	0.7205
1996 yield	-0.2077	-0.2834	0.6766	0.6697
1997 yield	-0.0460	-0.1491	0.4852	0.4455
1998 yield	-0.0380	-0.3174	0.5988	0.5773
1999 yield	0.0475	-0.0924	0.3643	0.3532
Average yield	-0.0765	-0.2707	0.7104	0.6755

We can see that the patterns of correlation between yields and the slope, curvature, available soil water content and TRSMI, are similar to those in Table 4-7, but the correlation Table 4-9 is much stronger than that in Table 4-7. The possible reasons for this are that the interpolation values in the areas without measured data partially reflect the variability of these factors. From the above comparison, we can see that it is possible

to improve the correlations between yields, topography and soil properties by having soil sampled in more locations in the study field.

Although the precision agriculture movement began with fertilizer management, an increasing body of knowledge suggests that spatial variation in soil water relation may be an important factor in causing spatial variation in grain yield. Developing a topography-related soil moisture index using a one-time measurement of elevation and soil data is important for (1) quickly and simply identifying yield losses due to water stress and predicting yield patterns earlier in the season, (2) estimating soil water interaction with other stresses such as weeds, pests, and nutrients, (3) forecasting spatial yield patterns in similar years, and (4) supplying support and refinement for mid-season yield estimated for optical sensor based variable rate fertilizer application to improve site-specific management.

CHAPTER 5

EFFECTS OF WEATHER ON WHEAT YIELD VARIBILITY

Abstract

The weather conditions in Oklahoma, with high evaporative demand and limited precipitation, restrict yields of winter wheat. Although the weather conditions are always considered uniform in one field, soil water, the thermal condition of the soil, soil development, and natural erosion vary across a field, as do the yields. Since seasonal Evapotranspiration (ET) is strongly related to grain yield. ET reflects both crop growth and weather. This research studies the relationship between the variability in seasonal ET and yield across a field in order to explain the weather influence on spatial and temporal yield variability. This research shows that correlation coefficients between average seasonal ET and average yield calculated from Landsat NDVI data for 4 years were 0.4500 for the entire field, and 0.6991 for the soil sample locations in the field.

Introduction

Wheat growth is strongly influenced by weather condition. Incident radiation, precipitation, and temperature are the main weather factors influencing wheat yield. Even though the weather condition is always considered uniform in one field, soil water, soil temperature, soil development, and natural erosion vary across a field. So does the yield. The reason is that weather interacts in a complex way with topography to affect crop

yield because of the relationship among soil relief, root growth, and hydrologic regime (Timlin et al., 1998).

Evapotranspiration (ET) represents the loss of water from a crop canopy surface through the combined processes of surface evaporation (soil and plant surfaces) and plant transpiration. Crop growth, weather and environment determine the ET rate of the crop. Crops adjust their growth to respond to changes in the environment and weather. When precipitation is little and soil water in the upper soil layer is depleted, roots of the wheat grow into the deeper soil to extract water for growth. The distribution of soil water content at the rooting depth affects on root development while the canopy development and ET are determined by the amount of soil water that crops can extract from the soil. When the temperature is high, the wheat transpiration rate increases to decrease plant temperature. A climate with high evaporative demand and limited precipitation restricts the yields of winter wheat grown in the semiarid southern high plains, such as in Oklahoma. ET is a comprehensive weather indicator. It does not only reflect the weather conditions, but also reflects the crop growth situation.

Scientists have reported the relationship between ET and yield. Musick et al. (1994) developed relationships that define the grain yield and water-use efficiency response to a wide range in season ET associated with water deficit. They found that the ET-yield relationship was linear, with a regression slope of 1.22 kg grain per m^3 ET above the ET threshold of 208 mm required to initiate grain yield, and maximum yields (greater than 7.0 Mg ha^{-1}) required 650 to 800 mm seasonal ET. The relationship of yield to seasonal ET for wheat has been reported as linear also by Hunsaker and Bucks (1987), Steiner et al. (1985), and Musicj and Porter (1990). Since ET has a strong relationship

with wheat grain yield, this research studied the relationship between the variable, seasonal ET and yield across a field.

Spatial Data Collection

The Description of the Study Field

For this research, a 160-acre wheat field, privately owned by Jim Kent to the east of Nash, Grant County, Oklahoma, was selected as the study field. The legal description of this study field is T 25 N, R7W, Sec.7, and SE/4. There are two creeks across the study field. The creek in the east part of the study field is called Sand Creek; the other one in the west part of the field is called Coldwater Creek. These two creeks divide the study field into three parts, east, middle and west.

Soil Data

The stratified random sampling method was used to take soil samples in the study field. After thorough investigation of the study field, the whole study field was divided into 17 sub areas according to the observed soil differences. Sampling was conducted using a 25-mm diameter soil probe at two soil depths, 23cm and 23-46cm. In each sub area, at each soil depth, 2-6 random soil samples were taken and composited.

Soil varies greatly in its ability to retain water. This characteristic of a soil is called the characteristic curve. The shape of this curve is largely governed by the soil texture (Jensen et al., 1989). Particle size distribution experiments were conducted to determine the soil texture, and therefore to determine the soil texture classes according to the USDA soil classification. The results are shown in the following tables.

Table 5-1 Particle size distribution analyses of soil samples at soil depth 0-23cm.

Soil sample	Soil texture			Soil type
	Percentage of sand (%)	Percentage of silt (%)	Percentage of clay (%)	
Sample1	85.77	11.05	3.18	Loamy sand
Sample 2	82.99	13.50	3.51	Loamy sand
Sample 3	80.26	16.56	3.17	Loamy sand
Sample 4	66.71	28.10	5.19	Sandy loam
Sample 5	70.86	24.02	5.12	Sandy loam
Sample 6	67.01	27.45	5.54	Sandy loam
Sample 7	36.69	45.02	18.29	Loam
Sample 8	38.90	50.43	10.67	Silt loam
Sample 9	28.23	58.43	13.34	Silt loam
Sample 10	19.97	59.75	20.28	Silt loam
Sample 11	22.04	58.79	19.17	Silt loam
Sample 12	32.66	54.62	13.72	Sandy loam
Sample 13	56.47	37.18	6.35	Sandy loam
Sample 14	23.79	59.58	16.63	Silt loam
Sample 15	18.24	60.63	21.13	Silt loam
Sample 16	24.29	60.54	15.17	Silt loam
Sample 17	35.38	55.41	9.21	Loam

Table 5-2 Particle size distribution analyses of soil samples in soil depth 23-46cm

Soil sample	Soil texture			Soil type
	Percentage of sand (%)	Percentage of silt (%)	Percentage of clay (%)	
Sample 1	84.49	10.93	4.58	Loamy sand
Sample 2	82.07	13.81	4.12	Loamy sand
Sample 3	72.45	22.59	4.96	Sandy loam
Sample 4	76.43	18.87	4.70	Loamy sand
Sample 5	64.20	28.28	7.52	Sandy loam
Sample 6	54.31	37.42	8.27	Sandy loam
Sample 7	14.73	66.04	19.23	Silt loam
Sample 8	34.74	52.73	12.53	Silt loam
Sample 9	19.44	64.57	15.99	Silt loam
Sample 10	22.75	58.72	18.53	Silt loam
Sample 11	17.85	61.70	20.45	Silt loam
Sample 12	24.14	59.21	16.65	Silt loam
Sample 13	56.66	36.82	6.52	Sandy loam
Sample 14	22.81	61.05	16.14	Silt loam
Sample 15	18.36	61.46	20.18	Silt loam
Sample 16	22.29	62.08	15.63	Silt loam
Sample 17	33.74	55.10	11.16	Loam

From the particle size distribution analyses of soil samples taken from the two soil depths, we can see that the difference between the two layers is not significant.

Based on soil texture information, soil water classes were summarized by Jensen et al. as shown in Table 5-3.

Table 5-3 General soil-water classes for agricultural soils (from Jensen et al., 1989)

Texture class	Water content, Volume Basis (%)		
	Drained upper limit (field capacity)	Lower limit of extractable water (permanent wilting point)	Available water
Sand	12	4	8
Loamy sand	14	6	8
Sandy loam	23	10	13
Loam	26	12	14
Silt loam	30	15	15
Silt	32	15	17
Silty clay loam	34	19	15
Silty clay	36	21	15
Clay	36	21	15

The drained upper limit, often called field capacity, is a function of soil texture and other parameters that affect the shape of the soil water characteristic curve. The field capacity sets a line for the maximum water that soil can retain. Generally, field capacity occurs at soil water potentials near -10 kPa in coarse-textured soils and at potentials near -20 kPa in medium- to fine-textured soils (Jensen et al., 1989). The low limit of available water is also termed the permanent wilting point. Soil water below this limit is considered to be unavailable to plants, with plants experiencing severe water stress with corresponding wilting and eventual plant death (Jensen et al., 1989). Available water is

the difference between the drained upper limit and the low limit of extractable water. This amount of water is stored soil water that can be extracted by plant roots. The field capacity, permanent point, and available soil water content were used to estimate actual ET, combined with the weather data.

Weather Data

The Oklahoma Mesonet, an automated network of 114 stations (Elliott et al., 1994; Brock et al., 1995) provided meteorological data. The Mesonet station used for this research is the Medford Mesonet Station (lat: 36^{o} 47' 31"N, long: 97^{o} 44' 44" W, elev: 330m), which is 25.49 km from the study field. The variables used, on a daily basis, were maximum air temperature (C), minimum air temperature (C), Mean air temperature (C), dew point temperature (C), pressure (Pa), precipitation (mm), solar radiation (W m^{-2}), and wind speed at a height of 2 m above ground (ms^{-1}). It should be noted that units of these variables were derived quantities using the original Mesonet variable units. The weather data for the study field were obtained for the growth seasons listed in Table 5-4.

Table 5-4 Winter wheat growth seasons in the study field.

Growth season	Planting date	Harvest date
1995-1996	Oct. 06, 1995	Jun. 14, 1996
1996-1997	Oct. 02, 1996	Jun. 25, 1997
1997-1998	Oct. 10, 1997	Jun. 09, 1998
1998-1999	Oct. 14, 1998	Jul. 07, 1999

Yield data

Winter wheat was planted and wheat grain yield was monitored in the study field, in Grant County, Oklahoma from September 1993 to 1999 using satellite imagery. A time series of LANDSAT five Thematic Mapper (TM) scenes of north central Oklahoma, with radiometric and geometric corrections, spanning the period 1993 to 1999, were obtained from Earth Observation Satellites, Inc. (EOSAT). Images were georeferenced to US Geological Survey digital 7.5 min orthophoto quadrangle maps and then resampled to a Universal Transverse Mercator grid, with a 25 m pixel size, using the nearest neighbor algorithm. The TM scenes were chosen from the time when the satellite overpasses occurred at or near the heading stage of winter wheat in the area, middle April to early May. In some years, due to cloud interference, the selection of an image was slightly outside of the optimum time window. In the spring of 1995, no acceptable image was available for the whole north central Oklahoma area.

Table 5-5 Dates of the Landsat Thematic Mapper scenes used in the study.

Year	1993	1994	1996	1997	1998	1999
Scene date	April 25	March 27	April 2	April 20	April 23	May 12

Itenfisu et al. (1999) developed and calibrated a winter wheat yield prediction equation using satellite images for north central Oklahoma.

$$Y = 165.9e^{4.0443\,NDVI} \tag{5-1}$$

Where Y is wheat grain yield in kg/ha. In this research, this prediction equation was applied to compute wheat yield on a pixel-by-pixel basis, with a pixel size of 25 m. The predicted yield results are shown in the predicted yield map for each year in Appendix A.

ASCE Standardized Reference Evapotranspiration

Evapotranspiration (ET) represents the loss of water from a vegetated surface through the combined processes of surface evaporation (soil and plant surfaces) and plant transpiration (i.e., internal evaporation). Reference evapotranspiration (ET_{ref}) is the rate at which readily available soil water is vaporized from specified vegetated surfaces (Jensen et al., 1990). The rate of evapotranspiration (ET) from soil and vegetated surfaces is dependent upon the atmospheric demand for water and the surface characteristics. In the commonly applied two-step approach to estimating ET, the atmospheric demand is quantified through the calculation of a "reference ET," and the surface characteristics are incorporated into a "crop coefficient." The product of these two parameters provides an estimate of the actual crop ET. Ideally, crop coefficients (K_c) can be transferred from one location to another, with the calculated reference ET reflecting the local climate and weather.

There are many different equations for calculating reference ET, such as FAO-56 Penman-Monteith, 1963 Penman, Kimberly Penman, CIMIS Penman, and ASCE Standardized Penman-Monteith. For this research, ASCE Standardized Reference Evapotranspiration was used to calculated reference ET on a daily time step for the study field. The following calculated procedures and equations are extracted from ASCE's Standardized Reference Evapotranspiration Equation (Walter, et al., 2000).

The Form of ASCE Standardized Reference Evapotranspiration

The Standardized reference evapotranspiration equation is intended to simplify and clarify the presentation and application of the method. The form of the standardized reference evapotranspiration equation is represented in Equation 5-1.

$$ET_{sz} = \frac{0.408\Delta(R_n - G) + \gamma \frac{C_n}{T+273} u_2 (e_s - e_a)}{\Delta + \gamma(1 + C_d u_2)} \quad (5\text{-}1)$$

Where ET_{SZ} is the standardized reference crop evapotranspiration representing ET_{OS} for the short reference (i.e. clipped grass) and representing ET_{RS} for the tall reference (i.e. alfalfa) where units are mm d^{-1} for daily time steps; R_n is net radiation at the reference crop surface (MJ m^{-2} $d^{-1}$for daily time steps); G is soil heat flux density at the soil surface (MJ m^{-2} d^{-1} for daily time steps); T is mean daily or hourly air temperature at 1.5 to 2.5-m height (°C); u_2 is mean daily wind speed at 2 m height (m s^{-1}); e_s is mean saturation vapor pressure at a 1.5 to 2.5-m height above the surface (kPa); computated daily, e_s is the average of e_s at maximum and minimum air temperature; e_a is mean actual vapor pressure at a 1.5 to 2.5-m height above the surface (kPa); Δ is the slope of the vapor pressure-temperature curve (kPa $°C^{-1}$); γ is the psychrometric constant (kPa $°C^{-1}$); C_n is the numerator constant representing the reference type and calculation time step; and C_d is the denominator constant representing the reference type and calculation time step. Table5-2. provides values for C_n and C_d.

Table 5-6 Values for C_n and C_d in Equation. 5-1(From Walter, et al., 2000)

Calculation Time Step	Short reference ET_{os}		Tall reference ET_{rs}	
	C_n	C_d	C_n	C_d
Daily	900	0.34	1600	0.38

Table5-7 ASCE Penman-Monteith terms standardized for application of the standardized reference evapotranspiration equation (From Walter, et al., 2000)

Term	ET_{os}	ET_{rs}
Reference vegetation height, h	0.12 m	0.50 m
Height of air temperature and humidity measurements, z_h	1.5 – 2.5 m	1.5 – 2.5 m
Height corresponding to wind speed, z_w	2.0 m	2.0 m
Zero plane displacement height	0.08 m	0.08 m [a]
Latent heat of vaporization	2.45 MJ kg^{-1}	2.45 MJ kg^{-1}
Surface resistance, r_s, daily	70 s m^{-1}	45 s m^{-1}

The zero plane displacement height for ET_{rs} assumes that the wind speed measurement is over clipped grass.

The calculation process for ET_{sz} for daily time steps is presented in this chapter.

Psychrometric and Atmospheric Variables

Latent Heat of Vaporization (λ): The value of the latent heat of vaporization, λ, varies only slightly over the ranges of air temperature that occur in agricultural or hydrologic systems. For ET_{sz}, a constant value of λ = 2.45 MJ kg^{-1} is recommended. The inverse of λ is approximately 0.408 kg MJ^{-1}.

Mean Air Temperature (T): For the standardized method, the mean air temperature, T, for a daily time step is preferred to be the mean of the daily maximum and daily minimum air temperatures rather than the average of hourly temperature measurements to provide for consistency across all data sets.

$$T = \frac{T_{max} + T_{min}}{2} \tag{5-2}$$

Where T is daily mean air temperature in ^{o}C; T_{max} is daily maximum air temperature in ^{o}C; and T_{min} is daily minimum air temperature in ^{o}C.

Atmospheric Pressure (P): the mean atmospheric pressure at the weather site is predicted from site elevation using a simplified formulation of the Universal Gas Law.

$$P = 101.3\left(\frac{293 - 0.0065z}{293}\right)^{5.26} \tag{5-3}$$

Where P is mean atmospheric pressure at station elevation z in kPa; z is weather site elevation above mean sea level in m.

Psychrometric Constant (γ): the standardized application using λ = 2.45 MJ kg^{-1} results in a value for the psychrometric constant, γ, that is proportional to the mean atmospheric pressure:

$$\gamma = 0.000665\ P \tag{5-4}$$

Where P has units of kPa and γ has units of kPa $^{\circ}$C^{-1}.

Slope of the Saturation Vapor Pressure-Temperature Curve (Δ): the slope of the saturation vapor pressure-temperature curve, Δ, is computed as:

$$\Delta = \frac{2504 \exp\left(\frac{17.27T}{T + 237.3}\right)}{(T + 237.3)^2} \quad (5\text{-}5)$$

Where Δ the slope of the saturation vapor pressure-temperature curve in the units of kPa^oC^{-1}, and T is daily mean air temperature in ^oC.

Saturation Vapor Pressure (e_S): The saturation vapor pressure (e_S) represents the capacity of the air to hold water vapor. For calculation of daily ET_{sz} , e_s is given by:

$$e_s = \frac{e^o(T_{\min}) + e^o(T_{\max})}{2} \quad (5\text{-}6)$$

Where $e^o(T)$ is the saturation vapor pressure function presented in Equation 5-7.

$$e^o(T) = 0.6108 \exp\left(\frac{17.27\,T}{T + 237.3}\right) \quad (5\text{-}7)$$

Where vapor pressure is in units of kPa and temperature is in $^\circ C$.

Actual Vapor Pressure (e_a): Actual vapor pressure (e_a) represents the water content (humidity) of the air at the weather site. e_a can be calculated from the measured dew point temperature by:

$$e_a = e^o(T_{dew}) = 0.6108 \exp\left[\frac{17.27\ T_{dew}}{T_{dew} + 237.3}\right] \quad (5\text{-}8)$$

Net Radiation (R_n)

Net radiation (R_n) is the net amount of radiant energy available at the surface for evaporating water, heating the air, or heating the surface. R_n includes both short and long wave radiation components

$$R_n = R_{ns} - R_{nl} \quad (5\text{-}9)$$

Where R_{ns} is net short-wave radiation in MJ m^{-2} d^{-1}, defined as being positive downwards and negative upwards; R_{nl} is net long-wave radiation, [MJ m^{-2} d^{-1}], defined as being positive upwards and negative downwards.

Net radiation is difficult to measure because net radiometers are problematic to maintain and calibrate. There is good likelihood of systematic biases in R_n measurements. Therefore, R_n is often predicted from observed short wave (solar) radiation, vapor pressure, and air temperature. This prediction is routine and generally highly accurate.

Net Solar or Net Short-Wave Radiation (R_{ns}): net short-wave radiation resulting from the balance between incoming and reflected solar radiation is given by:

$$R_{ns} = R_s - \alpha R_s = (1-\alpha) R_s \qquad (5\text{-}10)$$

Where R_{ns} is net solar or short-wave radiation in MJ m^{-2} d^{-1}; α is the albedo or canopy reflection coefficient, is fixed at 0.23 the standardized short and tall reference surfaces, α is dimensionless; and R_s is incoming solar radiation in MJ m^{-2} d^{-1}.

Net Long-Wave Radiation (R_{nl}): R_{nl} is the difference between upward long-wave radiation from the surface (R_{lu}) and downward long-wave radiation from the sky (R_{ld}):

$$R_{nl} = R_{lu} - R_{ld} \qquad (5\text{-}11)$$

The daily net long-wave radiation can be calculated using the method of Brunt (1932, 1952) that uses vapor pressure from a weather station to predict net surface emissivity:

$$R_{nl} = \sigma \left[\frac{T_{K\,\max}^4 + T_{K\,\min}^4}{2} \right] \left(0.34 - 0.14\sqrt{e_a}\right) \left(1.35 \frac{R_s}{R_{so}} - 0.35\right) \qquad (5\text{-}12)$$

Where R_{nl} is net long-wave radiation in MJ m^{-2} d^{-1}; σ is Stefan-Boltzmann constant, with a value of 4.901 x 10^{-9} MJ K^{-4} m^{-2} d^{-1}; $T_{K\ max}$ is the maximum absolute temperature during the 24-hour period in K (K = °C + 273.16); $T_{K\ min}$ is the minimum absolute temperature during the 24-hour period in K (K = °C + 273.16); e_a is the actual vapor pressure in kPa; R_s/R_{so} is the relative solar radiation (limited to $0.25 < R_s/R_{so} \leq 1.0$); R_s is measured or calculated solar radiation in MJ m^{-2} d^{-1}; and R_{so} is calculated clear-sky radiation in MJ m^{-2} d^{-1} .

Clear-Sky Solar Radiation (R_{so}): Clear-sky solar radiation is defined as the amount of solar radiation (R_s) that would be received at the weather measurement site under conditions of a clear sky (i.e., cloud-free). The ratio of R_s to R_{so} in the equation for R_n characterizes the impact of cloud-cover on the downward emission of thermal radiation to the earth's surface. Daily R_{so} is a function of the time of year and latitude. These parameters affect the potential incoming solar radiation from the sun. Clear-sky solar radiation is also affected by the station elevation (affecting atmospheric thickness and transmissivity), the amount of precipitable water in the atmosphere (affecting the absorption of some short-wave radiation), and the amount of dust or aerosols in the air.

$$R_{so} = R_a \exp\left(\frac{-0.0021P}{Kt \sin\phi}\right) \tag{5-12}$$

Where R_a is extraterrestrial radiation in MJ m^{-2} d^{-1}; P is atmospheric pressure in kPa; K_t is the turbudity coefficient, $0<K_t<1.0$ where Kt = 1.0 for clean air and K_t = 0.5 for extremely turbid, dusty, or polluted air; and ϕ is the angle of the sun above the horizon in radians.

For 24-hour periods, the mean daily sumn angle, weighted according to R_a, can be approximated as:

$$\sin\phi_{24} = \sin\left[0.85 + 0.3\varphi\sin\left(\frac{2\pi}{365}J - 1.39\right) - 0.42\varphi^2\right] \quad (5\text{-}13)$$

Where ϕ_{24} is average ϕ during the daylight period, weighted according to R_a; φ is latitude in rad; and J is day in the year.

For daily (24-hour) periods, R_a can be estimated from the solar constant, the solar declination, and the day of the year:

$$R_a = \frac{24}{\pi} G_{sc}\, d_r\, [\omega_s \sin(\varphi)\sin(\delta) + \cos(\varphi)\cos(\delta)\sin(\omega_s)] \quad (5\text{-}14)$$

Where R_a is extraterrestrial radiation in MJ m^{-2} d^{-1}; G_{sc} is the solar constant, with a value of 4.92 MJ m^{-2} h^{-1}; d_r is the inverse relative earth-sun distance factor (squared) and is unitless; ω_s is sunset hour angle in radians; φ is latitude in radians; and δ is solar declination in radians.

The latitude, φ, is positive for the Northern Hemisphere and negative for the Southern Hemisphere. The conversion from decimal degrees to radians is given by:

$$Radians = \frac{\pi}{180}\,[\text{decimal degrees}] \quad (5\text{-}14)$$

and d_r and δ are calculated as:

$$d_r = 1 + 0.033\cos\left(\frac{2\pi}{365}J\right) \quad (5\text{-}15)$$

$$\delta = 0.409\sin\left(\frac{2\pi}{365}J - 1.39\right) \quad (5\text{-}16)$$

Where J is the number of the day in the year between 1 (1 January) and 365 or 366 (31 December). J can be calculated as:

$$J = D_M - 32 + \text{Int}\left(275\frac{M}{9} \right) + 2\ \text{Int}\left(\frac{3}{M+1} \right) + \text{Int}\left(\frac{M}{100} - \frac{\text{Mod}(Y,4)}{4} + 0.975 \right) \quad (5\text{-}17)$$

Where D_M is the day of the month (1-31), M is the number of the month (1-12), and Y is the number of the year (for example 1996 or 96). The "Int" function in Eq. 25 finds the integer number of the argument in parentheses by rounding downward. The "Mod (Y,4)" function finds the modulus (remainder) of the quotient Y/4.

The sunset hour angle, ω_s, is given by:

$$\omega_s = \arccos\left[-\tan(\varphi)\tan(\delta) \right] \quad (5\text{-}18)$$

The "arccos" function is the arc-cosine function and represents the inverse of the cosine. This function is not available in all computer languages, so that ω_s can alternatively be computed using the arc-tangent (inverse tangent) function:

$$\omega_s = \frac{\pi}{2} - \arctan\left[\frac{-\tan(\varphi)\tan(\delta)}{X^{0.5}} \right] \quad (5\text{-}19)$$

Where:

$$X = 1 - [\tan(\varphi)]^2\,[\tan(\delta)]^2 \quad (5\text{-}20)$$

$$\textit{and}\quad X = 0.00001\ \textit{if}\quad X \le 0 \quad (5\text{-}21)$$

Soil Heat Flux Density (G): Soil heat flux density is the thermal energy that is utilized to heat the soil. G is positive when the soil is warming and negative when the soil is cooling. For Daily Periods, the magnitude of the daily, weekly, or ten-day soil heat flux density, G, beneath a fully vegetated grass or alfalfa reference surface is relatively small in comparison with R_n. Therefore, it is ignored so that:

$$G_{day} = 0 \quad (5\text{-}22)$$

Where G_{day} is daily soil heat flux density in MJ m^{-2} d^{-1}.

Application of Crop Coefficient(Kc)

Calculation of crop evapotranspiration ($ET_{c)}$ requires the selection of the correct crop coefficient (K_c) for use with the standardized reference evapotranspiration (ET_{os} or ET_{rs}). The abbreviation for crop coefficients developed for use with ET_{os} is denoted as K_{co} and the abbreviation for crop coefficients developed for use with ET_{rs} is denoted as K_{cr}. ET_c is to be calculated as shown in Equation 5-23:

$$ET_c = K_{co} * ET_{os} \text{ or } \quad ET_c = K_{cr} * Et_{rs} \quad (5\text{-}23)$$

Crop coefficients (K_c) are referenced to either clipped grass or full-cover alfalfa. In ASCE Standardized Reference Evapotranspiration Equation, a grass reference crop is defined as an extensive, uniform surface of dense, actively growing, cool-season grass with a height of 0.12 m, and not short of soil water; a alfalfa reference crop is defined as an extensive, uniform surface of dense, actively growing alfalfa with a height of 0.50 m, and not short of soil water. Grass-based crop coefficients should be used with $Et_{os.,}$ and alfalfa-based coefficients should be used with ET_{rs}.

For this research, grass-based mean crop coefficients using the ASCE short crop developed at USDA-ARS lab in Bushland, TX, based on growth stage and growing degree days (GDD) for winter wheat was used to calculate crop evapotranspiration.

Table 5-8 Mean crop coefficients for winter wheat (USDA_ARS, Bushland TX)

Wheat growth Stages	K_{cm}	Accumulative GDD from sowing date			
		Aug 15	Sep. 10	Oct. 1	Oct. 15
Seeded	0.35	347	324	272	274
Emerged	0.55	1088	766	1023	1032
Tiller 1	0.50	2073	946	1510	1247
Tiller 2	0.35	2655	1901	1832	1483
Tiller 3	0.45	2863	2256	1981	1604
Tiller 4	0.80	3097	2537	2134	1750
Stem elongation	0.80	3619	3052	2549	2115
1^{st} node	0.95	4014	3395	2846	2406
2cd node	0.95	4334	3672	3123	2682
Flag	1.10	4629	3919	3390	2910
Heading 1	1.05	4732	3972	3454	3003
Heading 2	1.00	4823	4064	3539	3091
Heading 3	1.00	4899	4128	3636	3150
Flower 1	1.00	4983	4214	3703	3217
Flower 2	1.00	5108	4275	3807	3319
Flower 3	1.00	5193	4344	3876	3422
Grain development	0.95	5461	4550	4140	3687
Milk	0.90	5729	4781	4439	4020
S dought	0.65	6027	4984	4793	4484
H dought	0.50	6410	5252	5253	4649
Physical maturity	0.20	6986	5651	5339	4923

Wheat growth Stages	K_{cm}	Accumulative GDD from sowing date			
		Aug 15	Sep. 10	Oct. 1	Oct. 15
Harvest	0.00	9000	9000	9000	9000

Growth degree days for winter wheat is calculated by:

$$GDD = (T_{\min} + T_{\max})/2 - T_{base} \quad (5\text{-}24)$$

where GDD is growing degree days in ^{o}C; T_{min} is the minimum daily temperature in ^{o}C and limited to T_{min}=0^{o}C when the daily T_{min} is less than 0^{o}C ; T_{max} is the maximum daily temperature in ^{o}C and limited to T_{max}=26.1^{o}C if the daily T_{max} is greater than 26.1^{o}C; and T_{base} is the base temperature for calculating GDD, and T_{base} is limited to 0 ^{o}C.

The sowing date of winter wheat for each year in the study field for this research was different from the sowing date listed in Table 5-8. So the interpolated K_{cm} based on the K_{cm} listed in Table 5-8 were used to calculate crop evepotranspiration. The interpolated K_{cm} are shown in Table 5-9 for the study field based on GDD and sowing date.

Table 5-9 Interpolated crop coefficient (K_{cm}) for the study field.

Wheat growth Stages	K_{cm}	Accumulative GDD from sowing date			
		Oct. 2	Oct. 6	Oct. 10	Oct.14
Seeded	0.35	272	273	273	274
Emerged	0.55	1024	1027	1029	1031
Tiller 1	0.50	1475	1405	1346	1265
Tiller 2	0.35	1785	1692	1614	1506
Tiller 3	0.45	1931	1830	1745	1629
Tiller 4	0.80	2083	1980	1894	1776

Wheat growth Stages	K_{cm}	Accumulative GDD from sowing date			
		Oct. 2	Oct. 6	Oct. 10	Oct.14
Stem elongation	0.80	2491	2375	2278	2144
1st node	0.95	2787	2670	2571	2435
2cd node	0.95	3064	2947	2847	2711
Flag	1.10	3326	3198	3090	2942
Heading 1	1.05	3394	3274	3172	3033
Heading 2	1.00	3479	3360	3259	3121
Heading 3	1.00	3571	3442	3332	3182
Flower 1	1.00	3638	3509	3399	3249
Flower 2	1.00	3742	3612	3502	3352
Flower 3	1.00	3815	3694	3592	3452
Grain development	0.95	4080	3959	3857	3717
Milk	0.90	4383	4271	4177	4048
S dought	0.65	4752	4669	4600	4505
H dought	0.50	5172	5011	4876	4689
Physical maturity	0.20	5284	5173	5079	4951
Harvest	0.00	9000	9000	9000	9000

In estimating actual daily crop ET, the use of the crop coefficient representing primarily the transpiration component of ET with adjustment for wet soil effects after rain permits a finer resolution than that obtained using K_{cm} (Jensen et al., 1989).

$$K_c = K_{cm} K_a \tag{5-25}$$

Where Ka is a dimensionless coefficient dependent on available soil water. The value of Ka is 1 unless available soil water limits transpiration, in which case it has a value less than 1. The functional relationship between K_a and available soil water depends on soil properties and crop rooting patterns (Jensen et al., 1989), represented as:

$$K_a = \ln(A_w + 1) / \ln(101) \tag{5-26}$$

Where A_w is the percentage of available soil water (A_w = 100 when the soil is at field capacity). Aw can be calculated by the following equation:

$$A_w = \frac{\theta - \theta_{wt}}{\theta_{Fc} - \theta_{wt}} \tag{5-27}$$

Where θ is daily soil water content, θ_{wt} is the permanent wilting point of the each soil type as shown in Table 5-3, and θ_{Fc} is the field capacity of each soil type also as shown in Table 5-3. To estimate daily soil water content, θ, for the root zone, the soil water balance model needs to be used to simulate daily soil water changes.

Soil Water Balance

In order to estimate the soil water in the study field during each growth season, a daily soil water balance model was used. The objective of deriving these estimates is to obtain the estimate of soil water changes for daily steps, and therefore to adjust the mean crop coefficient to calculate actual ET. Following is the description of the model and procedures used to estimate soil water.

Model Description

The soil water balance model was developed based on the continuity equation, which states that over any time intervals and for any hydrological systems the difference

in the volume of water entering the system, I, and leaving the system, O, must equal the change in the volume of water stored in the system, S (Haan et al., 1994);

$$I - O = \Delta S \tag{5-28}$$

For this research, the hydrological system is the rooting depth of winter wheat. The inflow to the rooting depth would be precipitation. The outflow from the rooting depth would be deep seepage, ET, and lateral flow. The amount of precipitation really infiltrated into the rooting depth is not the total precipitation because of canopy surface interception and runoff. The surface interception was ignored due to its small amount. The total precipitation deducted after runoff is effective rainfall. So the total inflow to the rooting depth is the effective rainfall. Since the soil water balance model used for this research is one dimensional, vertical, and for one soil layer, the lateral flow was ignored. After the effective rainfall infiltrates into the root zone, if the effective rainfall is greater than the soil water field capacity, the extra infiltrated water becomes deep seepage, flowing into the soil layer below the rooting depth. After the above simplifications, the soil water balance equation used for this research became:

$$\theta_i = \theta_{i-1} + I - ET_i \tag{5-28}$$

Where θ_i is soil water content in the rooting depth in mm; I is total daily inflow, equals to effective rainfall in mm; ET is actual daily evapotranspiration in mm; and i is an index of the day of interest.

Rooting Depth

The typical maximum effective rooting depth from literature (Jensen et al., 1989) for winter wheat is 1.5 m to 1.8 m; this represents rooting depth for healthy plants in soil under typical irrigated conditions with no soil- or water-induced restrictions such as hard

layers or nearly saturated profile. Annual crops typically attain maximum rooting depths shortly after developing a complete crop canopy. The increase in rooting depth from planting to effective cover can be approximated by linear interpolation with time as (Jensen et al., 1989):

$$R_z = R_{z_i} + \frac{D - D_p}{D_c - D_p}(R_{z_{\max}} - R_{z_i}), \quad D < D_c$$
$$R_z = R_{z_{\max}}, \quad \mathrm{D} \geq \mathrm{D_c} \tag{5-29}$$

where R_{z_i} is the initial effective rooting depth at planting (or plant emergence), $R_{z_{\max}}$ is the maximum effective rooting depth for a mature crop, D is the current calendar day of the year, D_p is the planting time, and D_c is the data of effective full cover. For this research, the value of R_{z_i} was assumed to be 15 cm because of the upward flow of soil water and the rapid expansion of the root system following germination; the date of D_c was assumed to be the date that winter wheat grows into the flowering stage. $R_{z_{\max}}$ was assumed to be 1.0 m considering the activity and affectivity of the root involved with soil water transportation and ET.

Effective Rainfall

The Soil Conservation Services (SCS) of the USDA combines infiltration losses with initial abstractions and estimates effective rainfall or equivalent runoff volume by the relationship (Haan et al., 1994):

$$Q = \frac{(P - 0.2S)^2}{P + 0.8S}, \quad P > 0.2S \tag{5-30}$$

Where Q is the runoff volume in mm, P is total precipitation in mm, and S is a parameter, called a maximum soil water retention parameter, given by:

$$S = \frac{25400}{CN} - 254 \tag{5-31}$$

Where CN is known as the curve number. The curve number of an area indicates the runoff potential of the area. Curve number tables are available from a number of sources. The curve number table used for this research was from Haan et al. (1994). Before looking up a curve number from the table, it is necessary to decide the hydrology soil groups (HGS) of the soils of interest and land use characteristics. An estimate of HSG can be made based on the texture of soil as shown in Table 5-10.

Table 5-10 Hydrology soil group (Haan et al., 1994)

HSG	Soil texture
A	Sand, loamy sand, or sandy loam
B	Silt loam or loam
C	Sandy clay loam
D	Clay loam, silt clay loam. Sandy clay, silty clay, or clay

Wheat is a small grain. For this research, based on the hydrology soil group and land surface cover situation of wheat, the curve number was decided as listed in Table 5-11.

Table 5-11 Curve number for the soils in the study field.

HSG	Soil texture	Curve number
A	Loamy sand, or sandy loam	64
B	Silt loam or loam	75

The effective rainfall, used as the total inflow for this research was calculated by:

$$I = P - Q \tag{5-32}$$

Where I is the total inflow to the assumed rooting depth in mm.

Actual ET data Interpolation

The actual ET for each growth season was calculated for each soil sample location on a daily basis using the method and procedures described above. After actual daily ET was calculated, the cumulative ET for each growth season was calculated by summing up the daily ET. Seasonal ET data were calculated in the study field for the 1995-1996, 1996-1997, 1997-1998, and 1998-1999 wheat growth seasons. The seasonal ET for each growth season was used to study the spatial correlation between ET and yields. Before comparing and correlating ET with yields, it is necessary to use interpolation to convert ET data from-point calculated data to continuous surfaces so that the spatial patterns sampled by these estimates can be compared with and correlated to the spatial patterns of yield. Since the actual ET for different growth seasons has the same spatial distribution, the actual ET for the 1998-1999 growth season was chosen as an example to conduct interpolation comparisons using the IDW, spline and kriging methods.

To interpolate actual ET, when the IDW method was used, parameters were set as power of 2, searching neighbor 5. When the completely regularized spline method was used to interpolate soil water holding capacity, the parameters were set as searching neighbor was 5. When the kriging method was used, the Gaussian model was chosen as the experimental variogram to fit the data, the searching neighbor was 5. The interpolation error estimates for these three methods are shown in Table 5-12.

Table 5-12 Summary of actual ET interpolation

Interpolation Error Estimate	Interpolation method		
	IDW	Spline	Kriging
Minimum value (mm)	485.53	484.40	482.94
Maximum value (mm)	494.10	494.10	497.37
Mean error	0.4107	0.3802	0.7274
RMSR	1.067	0.9877	1.262
Sample number	92	92	92

The range of measured actual ET for the 1998-1999 growth season was 485.46 mm to 494.10 mm. The range of actual ET for the 1998-1999 growth season interpolated by IDW stayed closest to the range of measured actual ET for this season. The range of actual ET for 1998-1999 growth season interpolated by the kriging method exceeded the range of the measured data most. Table 5-12 shows that the estimated interpolation errors of these three methods do not differ significantly.

The measured vs. interpolated actual ET using the three methods are plotted in Figure 5-1. From Figure 5-1, a, b, we can see that the interpolated data were greater than the measured data when measured data was at a minimal value; the interpolated data were smaller than the measured data when measured data was at a maximal value. From Figure 5-1, c, we can see that data points were distributed evenly along a 1:1 line.

The interpolated actual ET surfaces using the three methods are compared in Figure 5-2. The spatial pattern of interpolated actual ET surface is very similar to that of available soil water content in Figure 5-2 because the original actual ET data were calculated using soil water content data for each soil sample location.

(a)

IDW

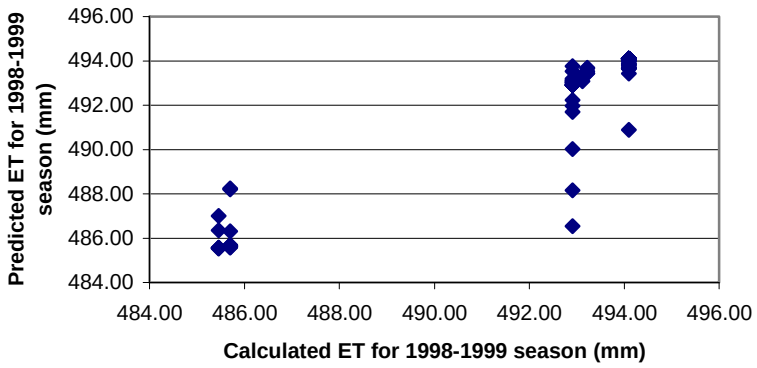

(b)

Spline

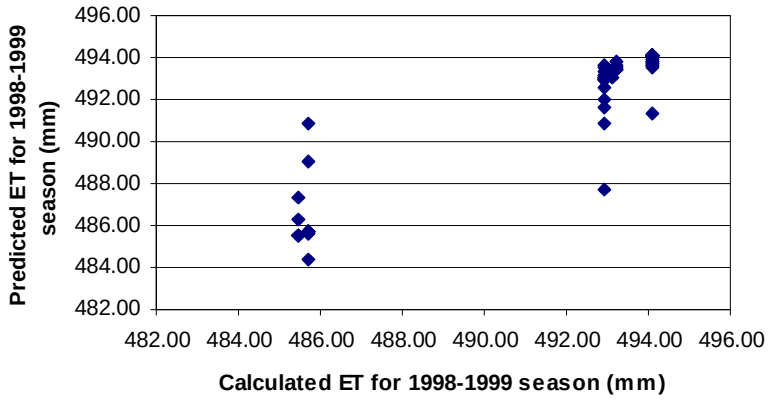

(c)

Kriging

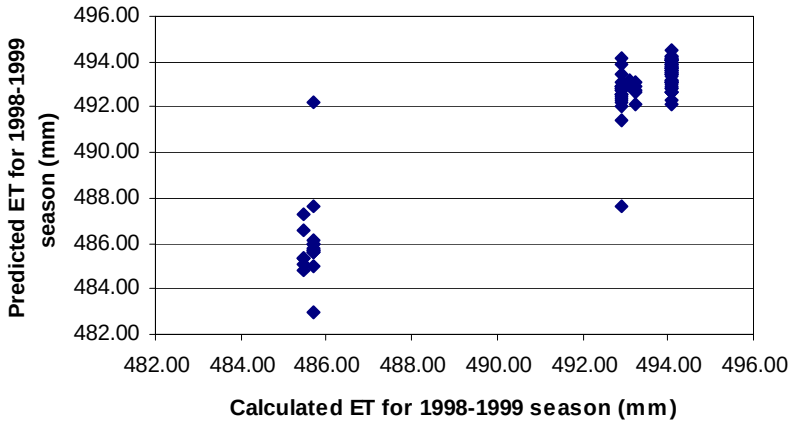

Figure 5-1 Interpolation comparison of 1998-1999 actual ET.

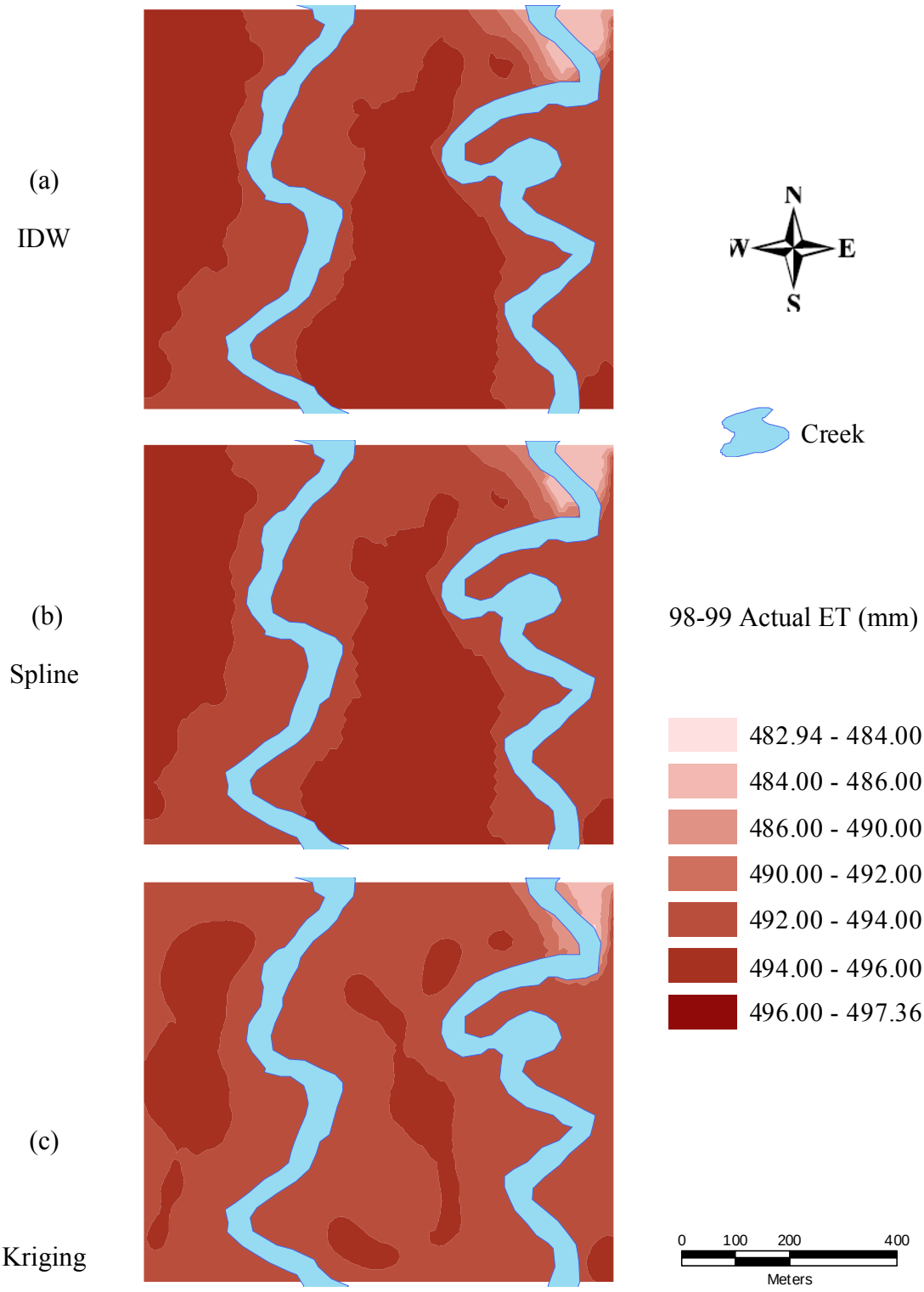

Figure 5-2 Interpolation comparison of actual ET for 1998-1999 growth season.

For further study correlation between ET and yield, the IDW method was chosen to interpolate actual ET data.

Results and Discussions

The interpolated ET was correlated to the yields for each growth season. The correlation coefficient (r) calculated for the entire field pixel data is shown in Table 5-13; The correlation coefficient (r) calculated only for soil samples locations is shown in Table 5-14.

Table 5-13 Correlation coefficients by year between yield and ET for the entire study field

	1996 yield	1997 yield	1998 yield	1999 yield	Average yield
1995-1996 ET	0.3395				
1996-1997 ET		0.3580			
1997-1998 ET			0.3143		
1998-1999 ET				0.1989	
Average ET					0.4500

Table 5-14 Correlation coefficients between yield and ET for the sample locations

	1996 yield	1997 yield	1998 yield	1999 yield	Average yield
1995-1996 ET	0.6534				
1996-1997 ET		0.5041			
1997-1998 ET			0.5858		
1998-1999 ET				0.3099	
Average ET					0.6991

From Table 5-13, we can see that the correlation coefficient between ET and yields ranges from 0.1989 to 0.3580; the correlation coefficient between average yield and average ET over four growth seasons is 0.4500 for the entire study field. Combining the weather information and total rainfall during the four growth seasons in Table 5-15, we can see that the lowest correlation coefficient happened in 1999, in which year the total rainfall was 1200 mm. The total of 1200 mm rainfall was more than adequate for wheat growth. And during this year, the differences in soil moisture due to different soil water holding capacities of different soils was not as significant as that in other years, because in this year, soil water content was adequate for crop growth because of timely and excess rainfall. Table 5-12 and Table 5-13 show that a correlation between ET and yields exists.

Table 5-15 Total precipitation for four growth seasons

Yield	Planting date	Harvest date	Total precipitation during growth season (mm)
1994	Sep. 14, 1993	Jun 20, 1994	
1996	Oct. 06, 1995	Jun. 14, 1996	122
1997	Oct. 02, 1996	Jun. 25, 1997	530.35
1998	Oct. 10, 1997	Jun. 09, 1998	510.54
1999	Oct. 14, 1998	Jul. 07, 1999	1049.02

We can see that the correlation coefficient between ET and yield is stronger in Table 5-14 than in Table 5-13, but has the same pattern as Table 5-13. These two tables demonstrate that correlation between yield and ET does exist. It is possible to increase the correlation by taking more soil samples to get more detailed soil information, and therefore to use variability of ET across a field to indicate the yield variability in order to study the weather effects on yield variability on a field scale. Another possible approach to increasing the correlation between yield and ET is to validate and modify the yield prediction equation using the weather and environment information after heading time during the growth season. Since the yield prediction equation was developed using the remote sensing NDVI at heading stage, this prediction equation did not account for the influences after heading stage and itself has a predicted error interval from the measured values.

CHAPTER 6

SUMMARY, CONCLUSIONS AND RECOMMENDATIONS

Summary

Wheat yields vary from year to year for specific sites as well as from site to site within a given year. The factors affecting the spatial and temporal variability of yield across a field are many: soil properties, such as soil classification, soil texture, organic matter content, and water holding capacity; soil fertilities, such as soil pH, nitrogen, phosphorus, potassium, and other nutrients; crop cultivars; topography, such as slope, aspect, and relief; and weather, such as rainfall and temperature. Most of these factors interact to influence the yield across a field. It is quite challenging to distinguish the variability controlled by the different factors. Because the factors controlling yield are dynamic, the specific factor that controls yield may change from year to year.

Attempts to study and explain within-field spatial yield variability began with fertility limitations and focused primarily on nitrogen, phosphorous, pH, and organic matter content. In recent years, the focus of research has shifted toward examining the effect on yield variability of topography or other site-specific soil properties that change with topography and affect patterns in soil moisture or soil drainage. Non-irrigated wheat, such as that in much of Oklahoma, generally uses most of the water that is available from precipitation during the growth season. In dry-land farming, topography and weather

interact to influence the conditions across a field.

The main objective of this research was to study the influence of weather and topography on the temporal and spatial variability of wheat yields in Oklahoma by examining the soil moisture distribution and storage and evapotranspiration (ET) variability that are induced by topographical changes, and evaluating their correlation with wheat yield variance across the field.

For this research, a 160-acre wheat field, privately owned by Jim Kent east of Nash, Grant County, Oklahoma, was selected as the study field. The legal description of this study field is T 25 N, R7W, Sec.7, and SE/4. There are two creeks across the study field. The one in the eastern part of the study field is called Sand Creek, the other, in the western part of the field is called Coldwater Creek. These two creeks divide the study field into three parts, east, middle and west. This field exhibits natural variability in topography and soil, and time series satellite images are available for this field. Spatial data are a fundamental component of this study in the spatial variability of wheat yield across a field. The spatial data required for this research include soil data, elevation data, weather, and actual ET data.

A stratified random sampling method was used to take soil samples in the study field. After thorough investigation of the study field, the whole study field was divided into 17 sub areas according to the observed soil differences. Sampling was conducted using a 25-mm diameter soil probe at two soil depths, 23cm and 23-46cm. In each sub area, at each soil depth, 2-6 random soil samples were taken and combined. Particle size distribution experiments were conducted to determine the soil texture classes according to the USDA soil classification and therefore to determine the soil water classes.

The weather data used for this research was obtained from the Medford Mesonet Station (lat: 36° 47' 31"N, long: 97° 44' 44" W, elev: 330m), which is 25.49 km from the study field. The daily variables used were maximum air temperature (C), minima air temperature (C), Mean air temperature (C), dew point temperature (C), pressure (Pa), precipitation (mm), solar radiation (W m^{-2}), and wind speed at a height of 2 m above ground (ms^{-1}).

Winter wheat was planted in the study field, in Grant County, Oklahoma from September 1993 to 1999, and wheat grain yield was monitored using satellite imagery. A time series of LANDSAT five Thematic Mapper (TM) scenes of north central Oklahoma, with radiometric and geometric corrections, spanning the period 1993 to 1999, were obtained from Earth Observation Satellites, Inc. (EOSAT). Images were georeferenced to US Geological Survey digital 7.5 min orthophoto quadrangle maps and then resampled to a Universal Transverse Mercator grid, with a 25 m pixel size, using the nearest neighbor algorithm. The TM scenes were chosen at the date when the satellite overpasses occurred at or near the heading stage of winter wheat in the area, middle April to early May. A winter wheat yield prediction equation developed and calibrated by Itenfisu et al. (1999) for north central Oklahoma was used in this research; this prediction equation was applied to compute wheat yield on a pixel-by-pixel basis with a pixel size of 25 m.

A Trimble GPS unit, Model 4000, whose horizontal accuracy is within 0.01 m, and vertical accuracy is within 0.02 m, was used to collect the detailed elevation data in the study field. Elevation measurements were taken on a semiregular grid with a distance from 2-8 m, depending on the complexity of terrain. Measurements on level areas in the study field were taken at larger distances, while marked depressions and elevations were

measured intensely. A total of 9210 elevation measurements were taken in the study field.

In order to study the relationship between soil, topography, and yields, it is necessary to use interpolation to convert soil and elevation data from point measured and calculated data to continuous surfaces so that the spatial patterns sampled by these estimates can be compared with and correlated to the spatial patterns of yield. Three methods, IDW, spline and kriging were used to interpolate each of these data sets. Interpolated results were compared and best-interpolated method for each data set was used to carry out the further study.

Topographical factors, aspect, slope and curvature were derived from the DEM using the elevations collected in the study field with the GPS unit. Their correlations with yields were examined.

A topography-related soil moisture index (TRSMI) was constructed from combining two topographic variables, slope and curvature, with one soil variable, available soil water content. TRSMI is a scalar index determined by summing assigned values for these three variables. TRSMI values may range from 0 to 40. For each stand, the values of slope and curvature were classified into 11 groups, and between 0 and 10 units were assigned for each group; available soil water content were classified into 21 groups, and between 0 and 20 units were assigned to each group. The correlations between yields and TRSMI were examined. To develop topography related soil moisture using a one-time measurement of elevation and soil data is important for (1) quickly and simply identifying yield losses due to water stress and predicting yield patterns earlier in the season, (2) estimating soil water interaction with other stressors such as weeds, pests,

and nutrients, (3) forecasting spatial yield patterns in similar years, and (4) supplying support and supplements for variable rate fertilizer application to improve site-specific management.

The actual ET data were calculated using weather data and soil data. ET was estimated by the commonly applied two-step approach: the atmospheric demand is quantified through the calculation of a "reference ET," and the surface characteristics are incorporated into a "crop coefficient." The product of these two parameters provides an estimate of the actual crop ET. The ASCE standardized reference evapotranspiration equation was used to calculate reference ET on a daily time step for the study field. The grass-based mean crop coefficients using the ASCE short crop developed at USDA-ARS lab in Bushland, TX, based on growth stage and growing degree days (GDD) for winter wheat was used to calculated crop evapotranspiration. A soil water balance model was developed to simulate soil moisture for each growth season on a daily basis. The mean crop coefficients were adjusted based on the soil wet effects obtained from the soil water modeling, and used to calculate actual ET. After actual daily ET was calculated, the seasonal ET for each growth season was calculated by summing up the daily ET. Seasonal ET data was converted from point-calculated data to continuous surfaces so that the spatial patterns sampled by these estimates can be compared with and correlated to the spatial patterns of yield. The IDW method was used to interpolate ET, with interpolation parameters set as power of 2, and searching neighbor of 5 to a grid-based surface; the grid size is 25 m. The correlation between seasonal ET and yields for each growth season was examined.

Conclusions

The examination of relationships between topographical factors, slope and curvature, soil property, and available soil water content for the entire study field showed that available soil water content has the highest correlation with yield among the factors listed above. This demonstrated that the amount of water soils can retain is an important factor in yield variability on a field scale. In dry years and years with adequate precipitation, the concave areas in the field had high yields, and the convex areas in the field had low yields. This is because that in these years, the concave areas accumulate runoff during rainfall events while the convex areas lose runoff. The accumulated runoff in concave areas infiltrates into the soil later for crop growth. In wet years, the pattern was reversed because more water than was needed accumulated in concave areas and decreased yields. The correlation pattern between the slope and yield calculated from NDVI, was similar to the correlation pattern between yields and the slope curvature, but not as strong.

The correlation coefficient between TRSMI and yields ranged from 0.079 to 0.2630. Although the correlation coefficient between TRSM and yield is not as high as expected, it does reveal some correlation between yield, topography, and soil.

Wheat yields were correlated to topographical factors, soil, and TRSMI in 92 sample locations. The patterns of correlation between yields and the slope, curvature, available soil water content, and TRSMI for these 92 sample locations were similar to those for the entire study field, but the correlations were stronger.

The seasonal ET for the four growth seasons was correlated to yield for the entire field. The correlation coefficient between ET and yield ranged from 0.1989 to 0.3580; the

correlation coefficient between average yield and average ET over four growth seasons is 0.4500 for the entire study field. The correlation coefficient in dry years and years with adequate precipitation is higher than that in wet years. The correlation coefficients between seasonal ET and yields for the 92 sampled locations were higher than those for the entire study filed, but had the similar patterns.

Recommendations

The objectives of this dissertation were accomplished as described in previous chapters and summarized and concluded in the earlier sections of this chapter. However, in continuing to address some of the issues, improvement could be made in the following areas:

1. Although the soil water content is largely governed by the soil texture, compaction, hydraulic conductivity characteristics, tillage history, soil genesis, the organic matter, layering, climate and other factors also affect soil water content. Thus, consideration of the factors which have affects on soil water content besides soil texture is needed and should be supported by more soil experiments.
2. In order to improve the correlation between soil, topography, and weather influences on wheat yield variability on a field scale, it is necessary to increase the number of soil samples taken in the study field.
3. The yield prediction equation was developed using the satellites images obtained at the heading stage of winter wheat. The environmental effects on wheat growth and yields after heading stages were not considered. And the yield prediction

equation itself has an error range from the measured yield. In order to improve the study of the wheat yields variability on a field scale, it is necessary to improve the prediction equation by validating it with more measured data.

References

Brock, F. V., K.C. Crawford, R. L Elliott, G. W. Cuperus, S. J. Stadler, H. L. Johnson, and M. D. Eilts. (1995). The Oklahoma Mesonet: A technical overview. Journal of Atmospheric Ocean. Technology, 12(1): 5-19.

Brunt, D. 1932. Notes on radiation in the atmosphere: I. *Quart. J. Roy. Meteor. Soc.*, 58:389-420.

Brunt, D. 1952. Physical and dynamical meteorology, 2nd ed., Univ. Press, Cambridge, 428 pp.

Burrough, P. A. and R. A. McDonnell, 1998. Principles of geographical information systems. Boston, Oxford University Press.

Burrough, P. A.. 1986. Principles of geographical information systems for land resources assessment. Oxford University Press, New York, p. 50.

Campbell, C. A., R. P. Zentner, and P. J. Johnson. 1988. Effect of crop rotation and fertilizer on the quantitative relationship between spring wheat yield and moisture use in southwestern Saskatchewan. Canadian Journal of Soil Science 68: 1-6.

Cassel, D. K., O. Wendroth, and D. R. Nielsen. 2000. Assessing spatial variability in an agricultural experiment station field: Opportunities arising from spatial dependence. Agron. J. 92: 706-714.

Ciha, A. J., 1984. Slope position and grain yield of soft white winter wheat. Agronomy Journal 76:193-196.

Daniels, R. B., J. W. Gilliam, D. K. Cassel, and L. A. Nelson. 1987. Quantifying the effects of past soil erosion on present soil productivity. Journal of Soil Water Conservancy 42: 183-187.

Elliott, R. L., F. V. Brock, M. L. Stone, and S. L. Harp. 1994. Configuration decisions for an automated weather station network. Applied Engineering in Agriculture, 10(1): 45-51.

EOSAT, 1993 Fast format document Version B, pp.1-3.

EOSAT, 1993 Fast format document Version B, pp.1-3.

Everett, M. W., and F. J. Pierce. 1996. Variability of corn yield and soil profiles nitrates in relation to site-specific N management. In Proc. of the 3rd international conference on precision agricultural, eds. P. C. Robert et al., 43-54. Madision, Wis.:ASA-CSSA-SSSA.

Fiez, T. E., B. C. Miller, and W. L. Pan. 1994. Winter wheat yield and grain Protein across varied landscape positions. Agronomy Journal 86: 1026-1032.

Gao J. 1997. Resolution and accuracy of terrain representation by grid DEMs at a micro-scale. International Journal of Geographical Information Science. 11(2), 199-212.

Garbrencht J., and L. W. Mart. 1996. Comment on "Digital elevation model grid size, landscape representation, and hydrologic simulations" by Weihua Zhang and David R. Montgomery. Water Resources Research. 32(5), 1461-1462.

Garbrencht J., and L. W. Martz. 2001. Digital elevation model issues in water resources modeling.

http://conservation.esri.com/library/userconf/proc99/proceed/papers/pap866/

Girma, Kefyalew, K.L. Martin, R.H. Anderson, D.B. Arnall, K.D. Brixey, M.A. Casillas, B. Chung, B.C. Dobey, S.K. Kamenidou, S.K. Kariuki, E.E. Katsalirou, J.C. Morris, J.Q. Moss, C.T. Rohla, B.J. Sudbury, B.S. Tubana, and W.R. Raun. 2005.

Mid-Season Prediction of Wheat Grain Yield Potential Using Plant, Soil, and Sensor Measurements. J. Plant Nutr.

Haan, C. T., B. J. Barfield, and J. C. Hayes. 1994. Design hydrology and sedimentology for small catchments. Academic Press, Inc. San Diego, California. P:38, 63, 64, 65,

Hairston, J. E., J. O. Sanford, F. E. Rhoton, and J, G. Miller. 1988. Effect of soil depth and erosion on yield in the Mississippi Blacklands. Soil Science Society of America Journal 52:1458-1463.

Halvorson, G. A., and Doll, E. C. 1991. Topographic effects on spring wheat yields and water use. Soil Sci. Soc. Am. J. 55: 1680-1685.

Halvorson, G. A., and Doll, E. C.. 1991. Topographic effects on spring wheat yields and water use. Soil Science Society of America Journal 55: 1680-1685.

Halvorson, G. A., and E. C. Doll. 1991. Topographic effects on spring wheat yield and water use. Soil Science Society of America Journal 55:1680-1685.

Hanna, A. Y., P.W. Harlan, and D. T. Lewis. 1982. Soil available water as influenced by landscape position and aspect. Agronomy Journal 74:999-1004.

Irmak, A., W. D. Batchelor, J. W. Jones, S. Irmak, J. O. Paz, H. W. Beck, M. Egeh. 2002. Realtionship between plant available soil water and yield for explaining soybean yield variability. Applied Engineering in Agriculture. 18(4): 471-482.

Itenfisu, D., R. L. Elliott, J. B. Solie, and E. G Krenzer, 1999. Assessing Wheat Yield Variability Using Satellite Remote Sensing; Proceedings of the Pecora 14/Land Satellite Information III ; Proceedings: , December 6-10, Denver, Colorado.

Itenfisu, D., R. L. Elliott, J. B. Solie, and E. G. Krenzer, 1999. Assessing wheat yield variability using satellite remote sensing; Proceedings of the Pecora 14/Land Satellite Information III ; Proceedings: , December 6-10, Denver, Colorado.

Itenfisu, D., R. L. Elliott, J. B. Solie, and E. G. Krenzer, 1999. Assessing Wheat Yield Variability Using Satellite Remote Sensing; Proceedings of the Pecora 14/Land Satellite Information III ; Proceedings: , December 6-10, Denver, Colorado.

Jensen M.E., Burman, R.D., and Allen, R.G. (1990). Evapotranspiration and irrigation water requirements. ASCE Manuals and Reports on Engineering Practice No. 70, American Society of Civil Engineers, New York, NY.

Jensen, M. E., R. D. Burman, and R. G. Allen, 1989. ASCE manuals and reports on engineering practice No. 70. Evapotranspiration and irrigation water requirements. P: 20, 21, 22, 47, 117, 118

Jensen, M. E., R. D. Burman, and R. G. Allen. 1989. ASCE manuals and reports on engineering practice No. 70. Evapotranspiration and irrigation water requirements. P: 20, 21.

Jones, A. J., L. N. Mielke, C. A. Bartles, and C. A. Miller. 1989. Relationship of landscape position and properties to crop production. Journal of Soil and Water Conservation 44:328-332.

Kravchenko, A., and D. G. Bukkock. 2000. Spatial variability: Correlation of corn and soybeans with topography and soil properties. Agronomy Journal 92:75-83.

Lukina, E.V., K.W. Freeman, K.J. Wynn, W.E. Thomason, R.W. Mullen, A.R. Klatt, G.V. Johnson, R.L. Elliott, M.L. Stone, J.B. Solie, and W.R. Raun. 2001.

Nitrogen fertilization optimization algorithm based on in-season estimates of yield and plant nitrogen uptake. J. Plant Nutr. 24:885-898.

Mark D. M. 1979. Phenomenon-based data structure and digital terrain modeling. Geo-processing 1: 27-36.

Markham, B. L. and J. L. Baker, 1987. Landsat MSS and TM post-calibration dynamic ranges, exoatmospheric reflectance and at-satellite temperatures. EOSAT Landsat Tech. Notes, 1, 3-8.

Michelle, P., M. J. Singer, and D. R. Nielsen. 1988. Spatial variability of wheat yields and soil properties on complex hills. Soil Science Society of America Journal 52:1133-1141.

Miller, P. M., M. J. Singer, and D. R. Nielsen. 1988. Spatial variability of wheat yields and soil properties on complex hills. Soil Science Society of America Journal 52:1133-1141.

Moore I. D., E. M. O'Loughlin, and G. Burch. 1988. A contour-based topographic model for hydrological and ecological applications. Earth Surface Process and Landforms 13, 305-320.

Moulin, A. P., D. W. Anderson, and M. Mellinger. 1994. Spatial variability of wheat yield, soil properties and erosion in hummocky terrain. Canadian Journal of Soil Science 74: 219-228.

Parker, A.. 1982, The topographic relative moisture index: an approach to soil-moisture assessment in mountain terrain. Physical Geography, 1982, 3(2): 160-168.

Peucker T. K., R. J. Fowler, J. J. Little, and D.M. Mark. 1978. The triangulated irregular network. Proceedings of the DTM Symposium. ASPRS (America Society for Photogrammetry and Remote Sensing) Fall Church, VA; 516-540.

Raun, W.R., G.V. Johnson, M.L. Stone, J.B. Solie, E.V. Lukina, W.E. Thomason and J.S. Schepers. 2001. In-season prediction of potential grain yield in winter wheat using canopy reflectance. Agron. J. 93:131-138.

Raun, W.R., J.B. Solie, G.V. Johnson, M.L. Stone, R.W. Whitney, H.L. Lees, H. Sembiring, and S.B. Phillips. 1998. Micro-variability in soil test, plant nutrient, and yield parameters in bermudagrass. Soil Science Society of America Journal 62: 683-690.

Raun, W.R., J.B. Solie, M.L. Stone, K.L. Martin, K.W. Freeman, R.W. Mullen, H. Zhang J.S. Schepers, and G.V. Johnson. 2004. Optical sensor based algorithm for crop nitrogen fertilization. Commun. Soil Sci. Plant Anal.

Raun, W.R., J.B. Solie, M.L. Stone, K.L. Martin, K.W. Freeman. And D.L. Zavodny. 2005. Automated calibration stamp technology for improved in-season nitrogen fertilization. Agron. J.

Rieger W.. 1998. A phenomenon-based approach to upslope contributing areas and depressions in DEMs. Hydrological Process 12, 857-872.

Sadler, E. J., P. J. Bauer, W. J. Busscher, and J. A. Millen. 2002. Site-specific analysis of a droughted corn crop: II. Water use and stress. Agronomy Journal 92: 403-410.

Simmons, F. W., D. K. Cassel, and R. B. Daniel. 1989. Landscape and soil property effects on corn grain yield response to tillage. Soil Science Society of America Journal 53: 534-539.

Sinai, G., D. Zaslavsky, and P. Golany. 1981. The effect of soil surface curvature on moisture and yield---- Beer Sheba observation. Soil Science 132:367-375.

Solie, J.B., W.R. Raun and M.L. Stone. 1999. Submeter spatial variability of selected soil and bermudagrass production variables. Soil Sci. Soc. Am. J. 63:1724-1733.

Solie, J.B., W.R. Raun, R.W. Whitney, M.L. Stone and J.D. Ringer. 1996. Optical sensor based field element size and sensing strategy for nitrogen application. Trans. ASAE 39(6):1983-1992.

Stone, M.L., J.B. Solie, W.R. Raun, R.W. Whitney, S.L. Taylor and J.D. Ringer. 1996a. Use of spectral radiance for correcting in-season fertilizer nitrogen deficiencies in winter wheat. Trans. ASAE 39(5):1623-1631.

Stone, M. L., J. B. Solie, R. W. Whitney, W. R. Raun and H. L. Lees. 1996b. Sensors for detection of nitrogen in winter wheat. SAE Technical paper series. SAE Paper No. 961757. SAE, Warrendale PA.

Timlin, D. J., Y. Pachepsky, V. A. Snyder, and R. B. Bryant. 1998. Spatial and temporal variability of corn grain yield on a hillslope. Soil Science Society of America Journal 62:762-773.

Walter, I.A., R.G. Allen, R.Elliott, B. Mecham, M.E. Jensen, D. Itenfisu, T.A. Howell, R. Snyder, P. Brown, S. Echings, T. Spofford, M. Hattendorf, R.H. Cuenca, J.L. Wright and D. Martin. 2000. ASCE's standardized reference evapotranspiration equation. Proceedings of the 4th National Irrigation Symposium, ASAE, St. Joseph, MI.

Wise S. 2000. Assessing the quality for hydrological application of digital elevation models derived from contours. Hydrological Process 14, 1909-1929.

Yang D., S. Herath, and K. Musiake. 2001. Spatial resolution sensitivity of catchment geomorphologic properties and the effect on hydrological simulation. Hydrological Processing. 15, 2085-2099.

Yang, C., C. L. Perterson, G. J. Shropshire, and T. Otawa. 1998. Spatial variability of field topography and wheat yield in the Palouse region of the Pacific Northwest. Transaction of the ASAE. 41, NO. 1: 17-29.

Zhang W., and D. R. Montgomery. 1994. Digital elevation model grid size, landscape representation, and hydrologic simulations. Water Resources Research. 30 (4), 1019-1028.

APPENDIX A

PREDICTED YIELD OF THE STUDY FIELD FOR 1993, 1994, 1996, 1997, 1998, 1999 FROM STATELLITE IMAGES

(Supplement to Chapter II, IV, V)

1993

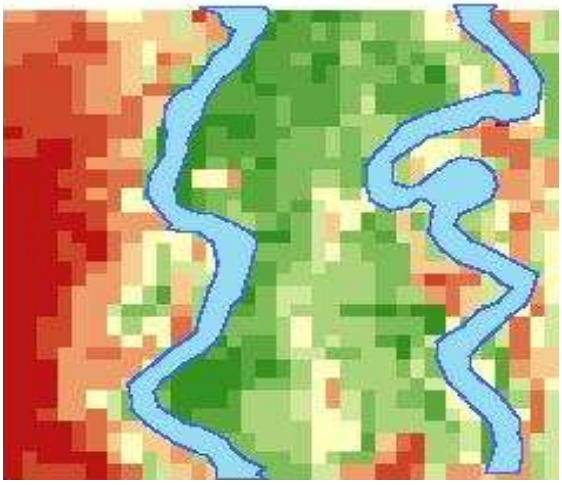

1994

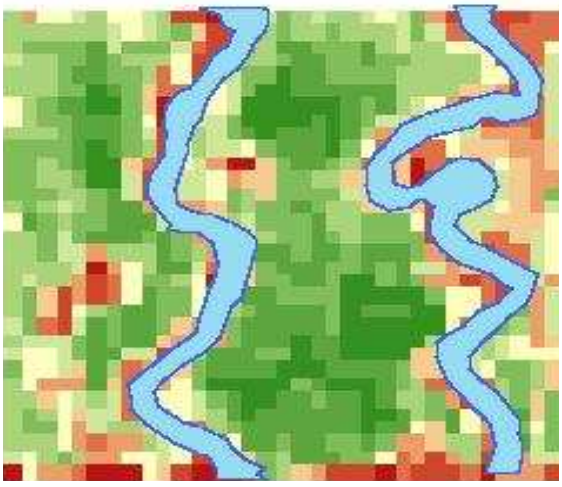

1996

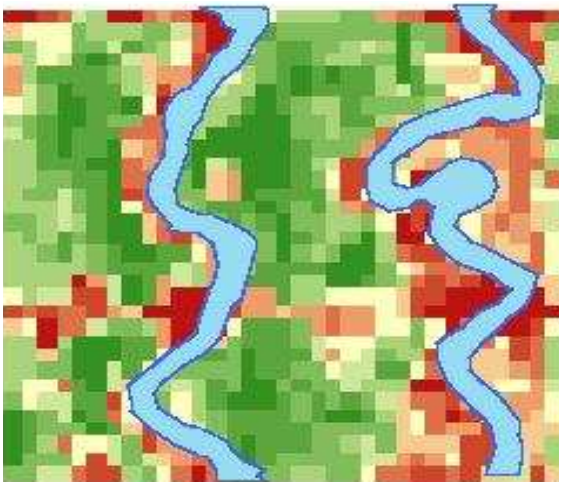

Creek

Yield (Kg/ha)

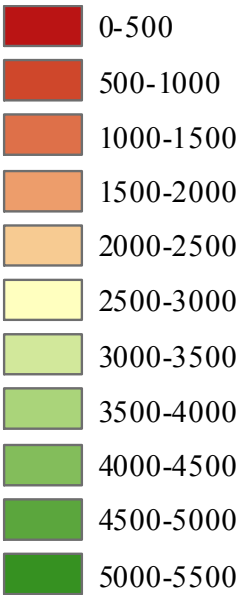

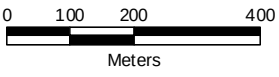

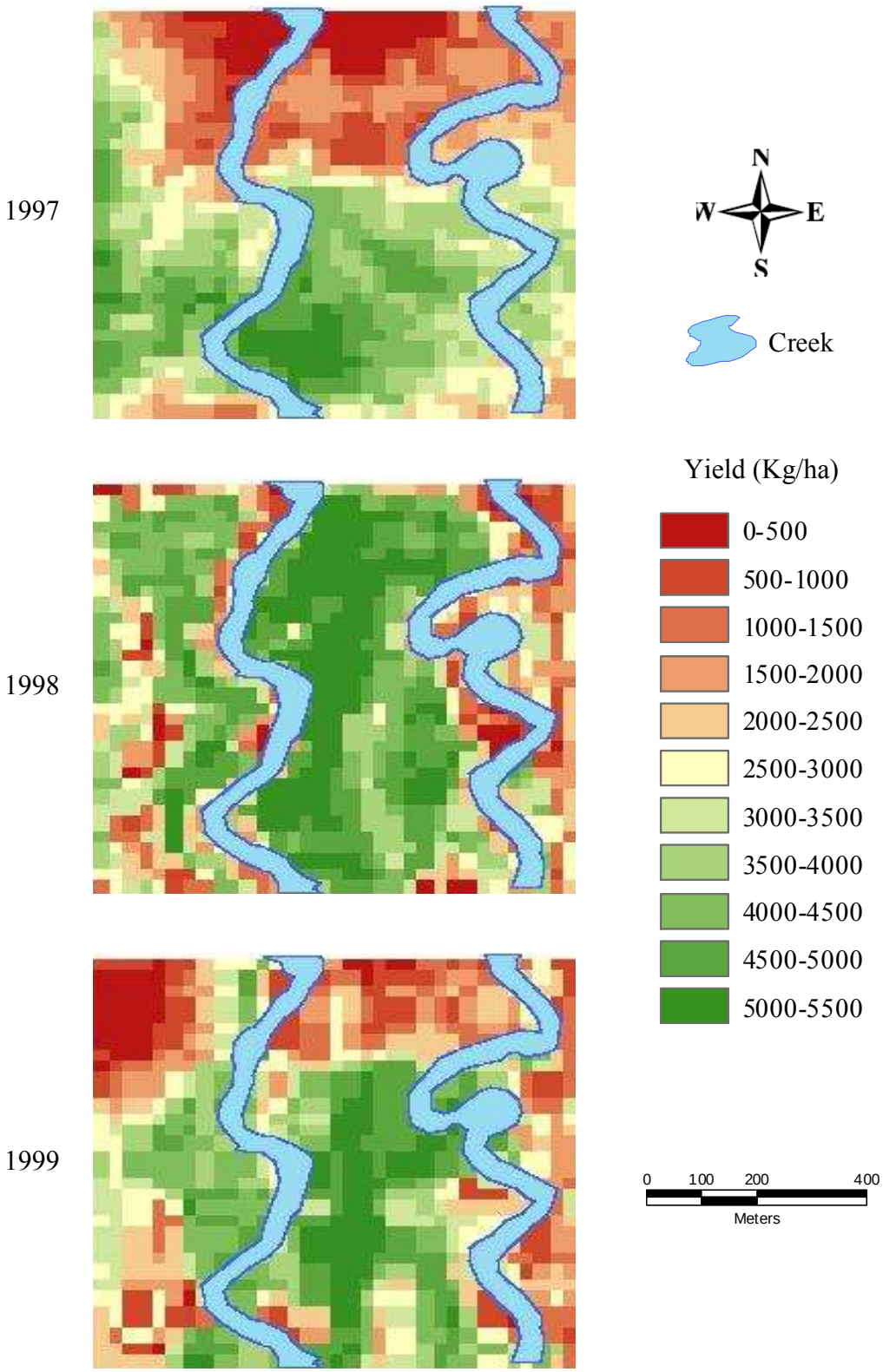

Figure A Predicted yield for the study field.

APPENDIX B

COMPARISON OF MEASURED AND INTERPOLATED AVAILABLE SOIL WATER CONTENT, ELEVATION AND ACTUAL ET FOR THE 1994-1995 GROWTH SEASON

(Supplement to Chapter III)

(a)

IDW

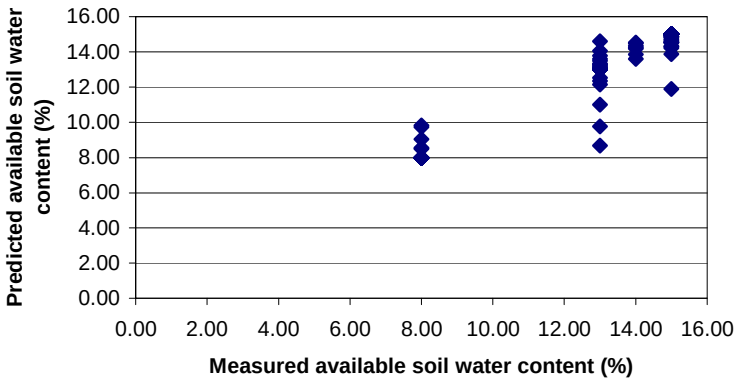

(b)

Spline

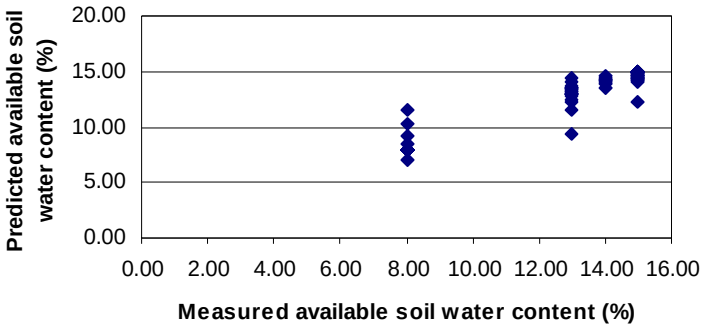

(c)

Kriging

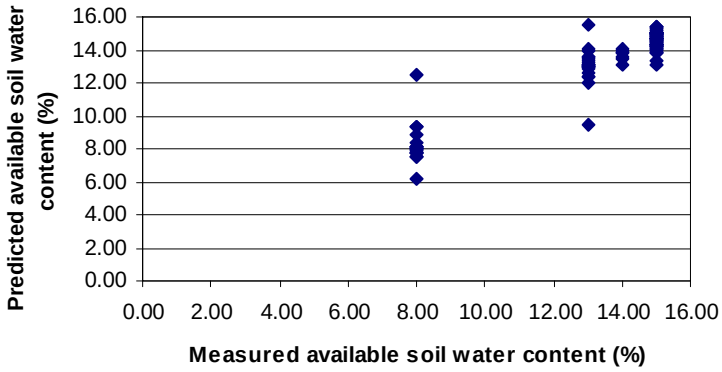

Figure B-1. Interpolation comparison of available soil water content

(a)

IDW

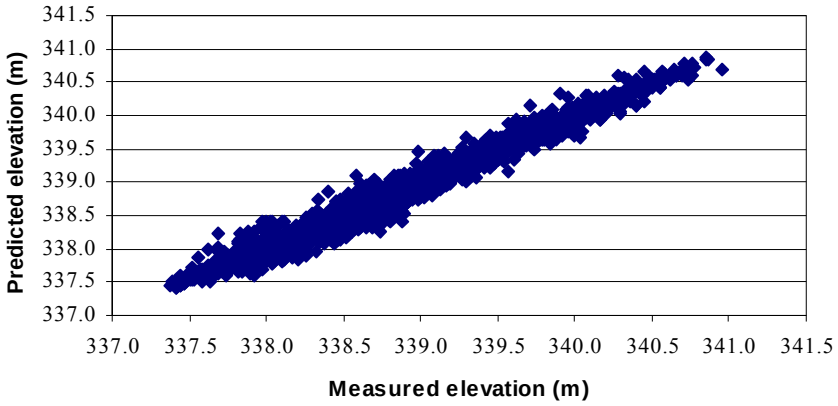

(b)

Spline

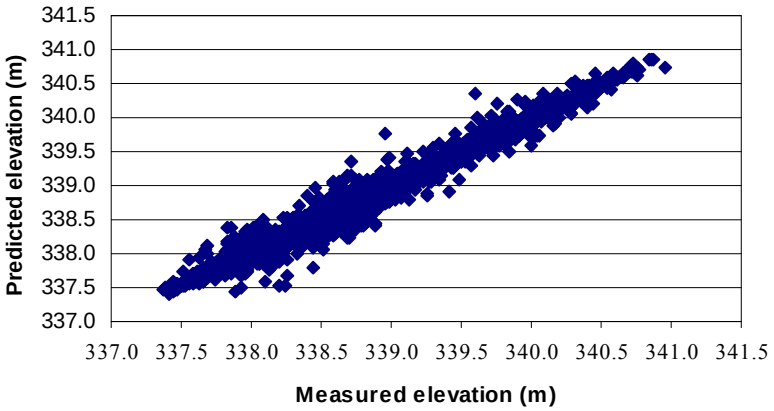

(c)

Kriging

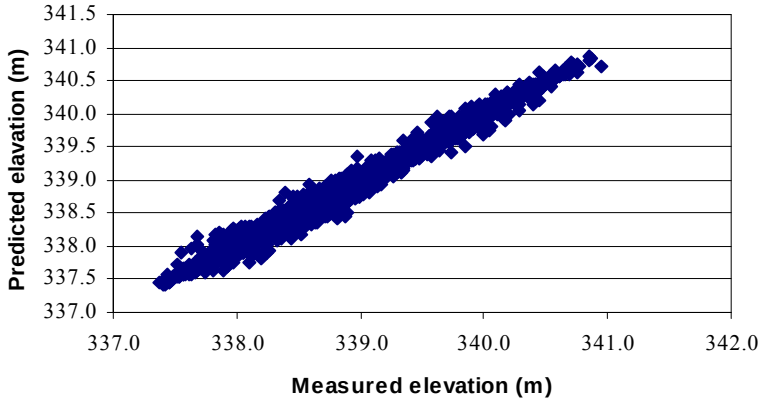

Figure B-2. Interpolation comparison of elevation.

(a)

IDW

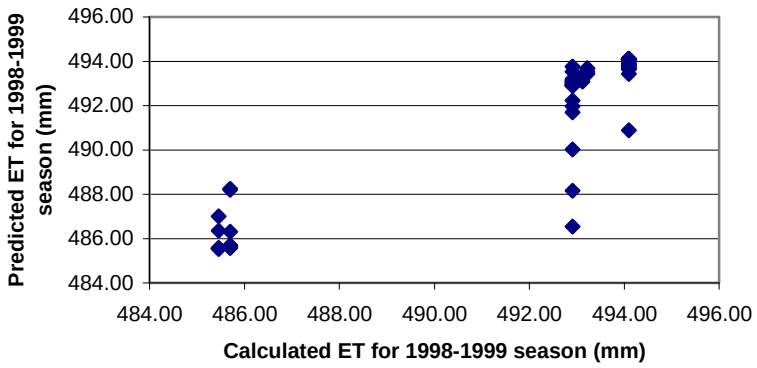

(b)

Spline

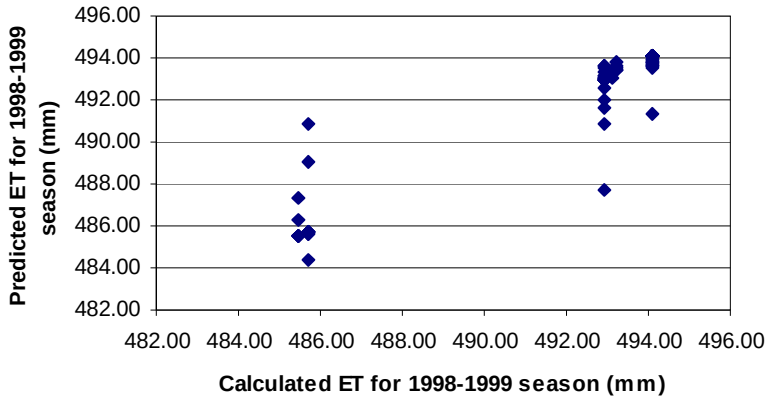

(c)

Kriging

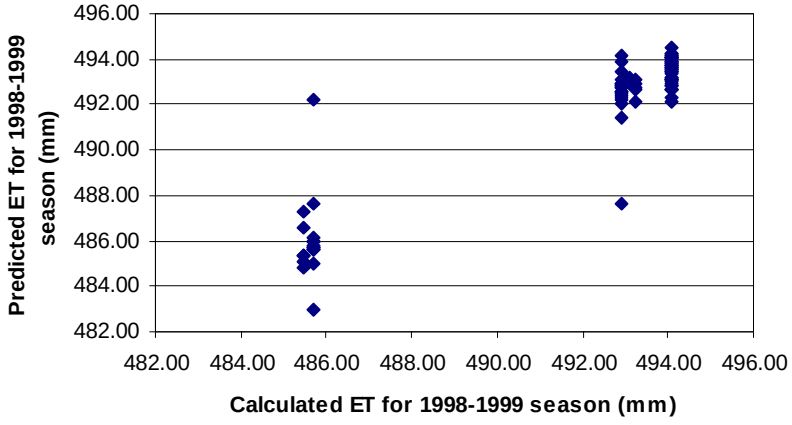

Figure B-3. Interpolation comparison of 1998-1999 actual ET.

APPENDIX C

COMAPRISON OF INTERPOLTION OF AVAILABEL SOIL WATER CONTENT, ELEVATION AND ACTAUL ET FOR THE 1998-1999 GROWTH SEASON USING IDW, SPLINE AND KRIGING

(Supplement to Chapter III)

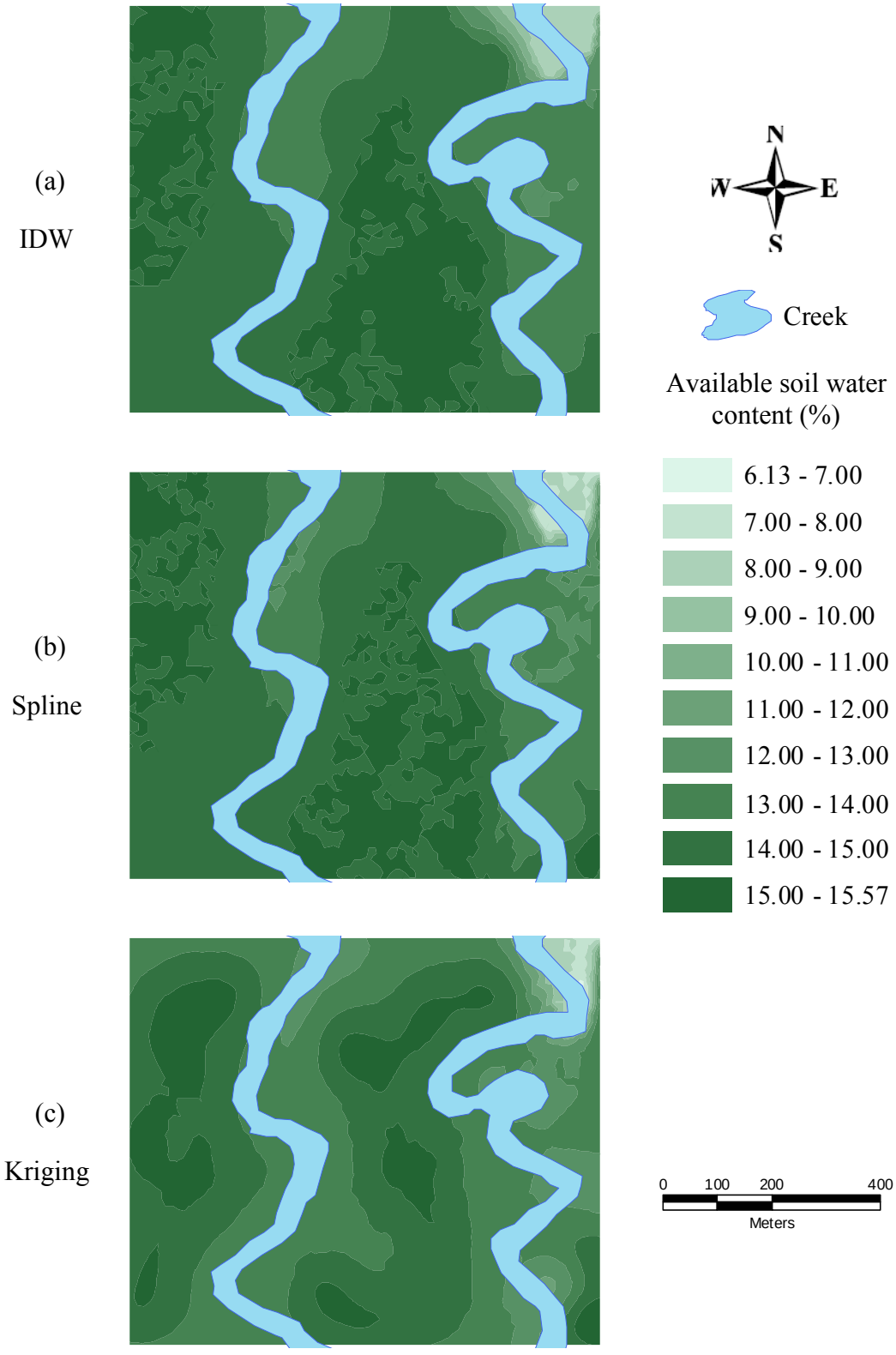

Figure C-1. Interpolation comparison of available soil water content.

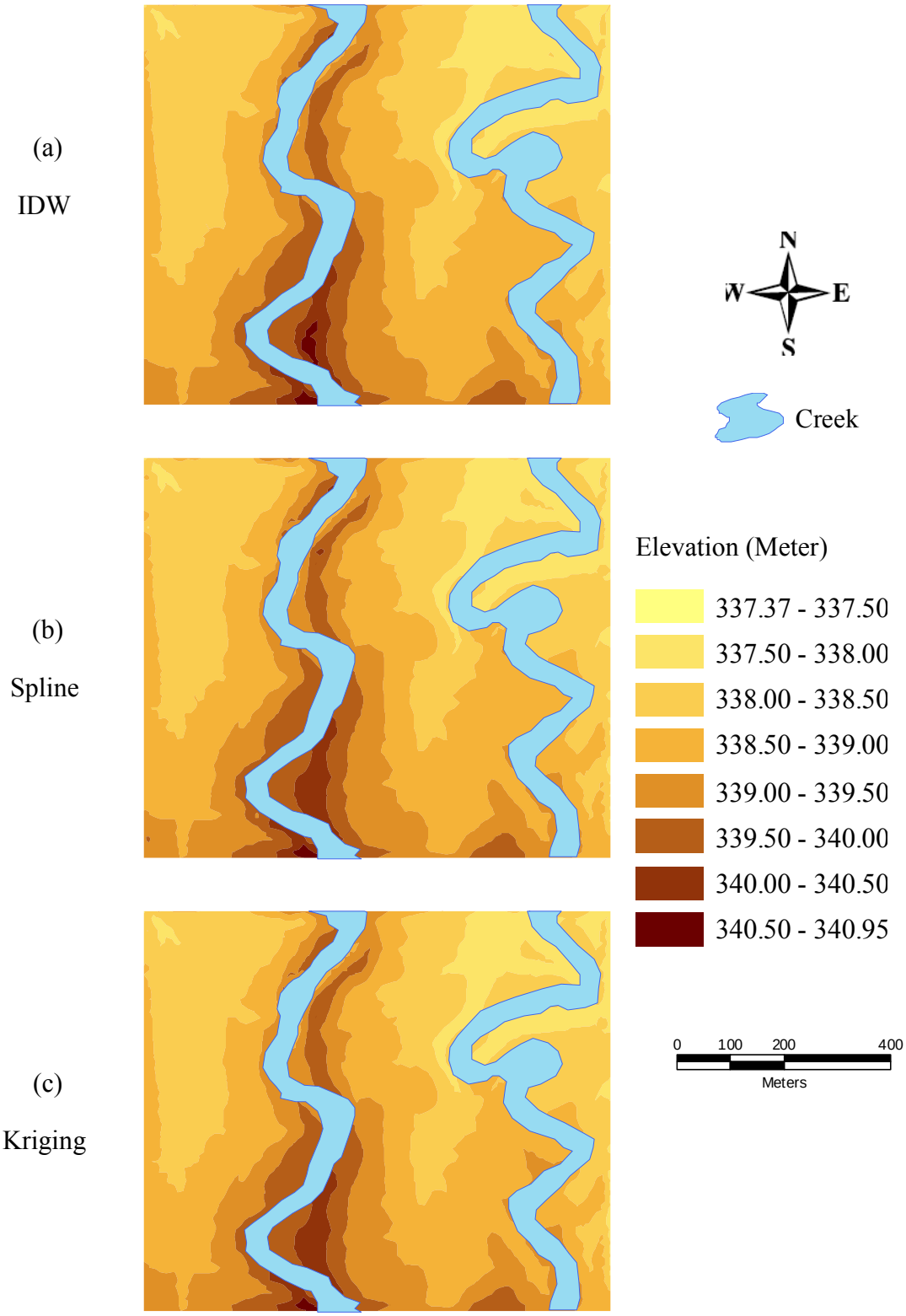

Figure C-2. Interpolation comparison of elevation.

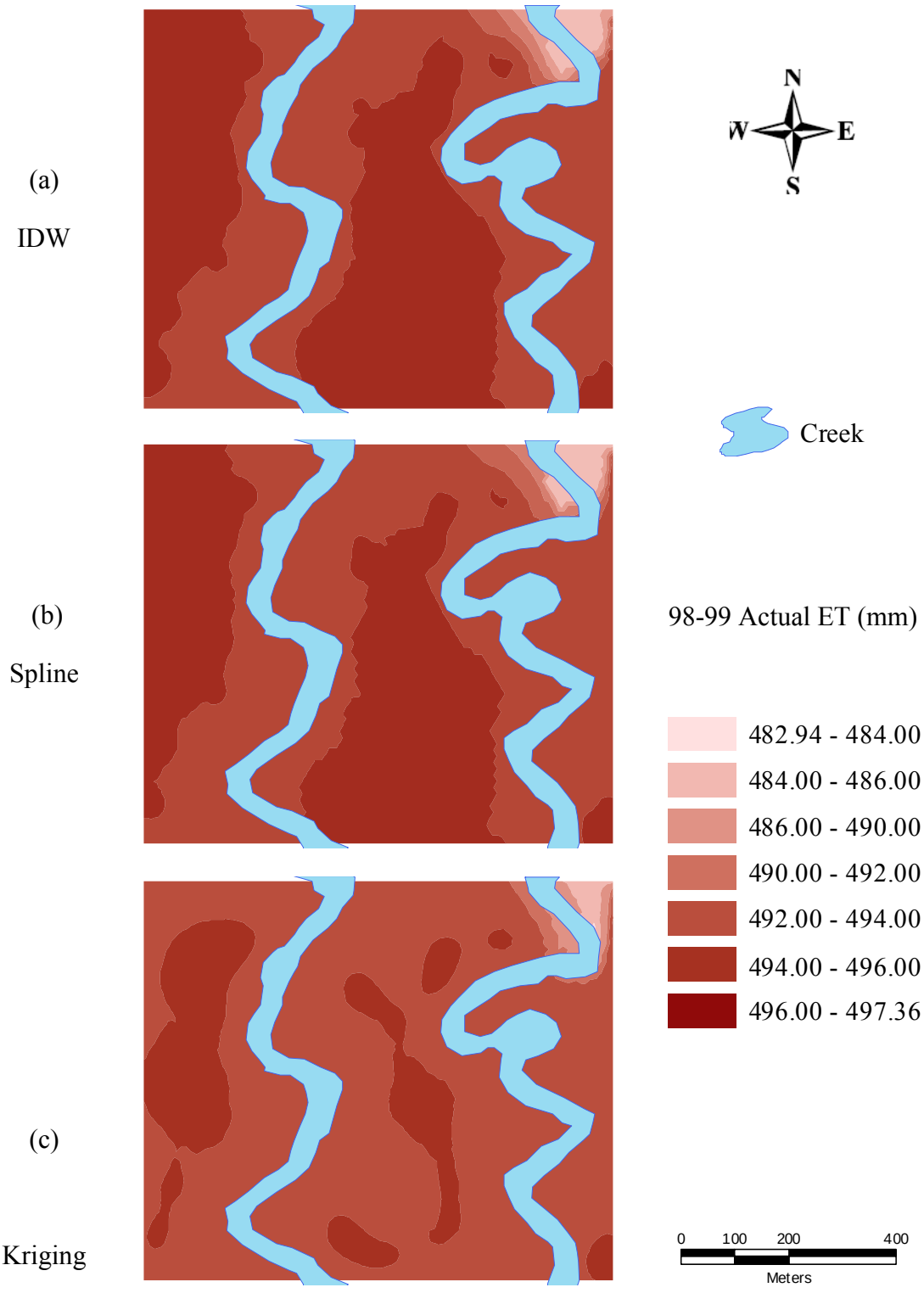

Figure C-3. Interpolation comparison of actual ET for 98-99 growth season.

APPENDIX D

INTERPOLATED SEASONAL ET OF THE STUDY FIELD FOR 1994-1995, 1995-1996, 1996-1997, 1997-1998, 1998-1999 GROWTH SEASONS.

(Supplement to Chapter III, V)

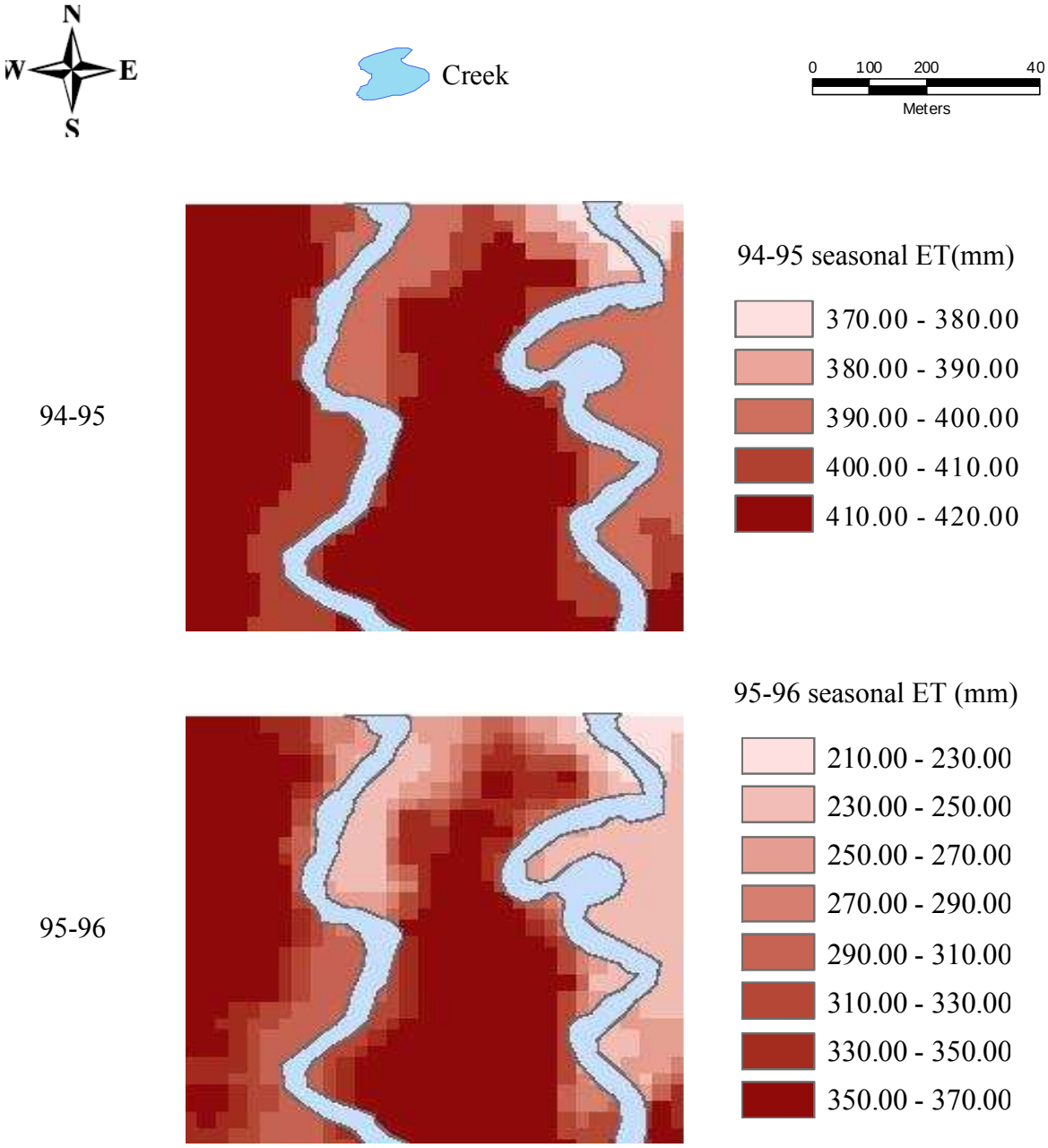
N
W
E
S
Creek
0 100 200 40
Meters
94-95
94-95 seasonal ET(mm)
370.00 - 380.00
380.00 - 390.00
390.00 - 400.00
400.00 - 410.00
410.00 - 420.00
95-96
95-96 seasonal ET (mm)
210.00 - 230.00
230.00 - 250.00
250.00 - 270.00
270.00 - 290.00
290.00 - 310.00
310.00 - 330.00
330.00 - 350.00
350.00 - 370.00

96-97

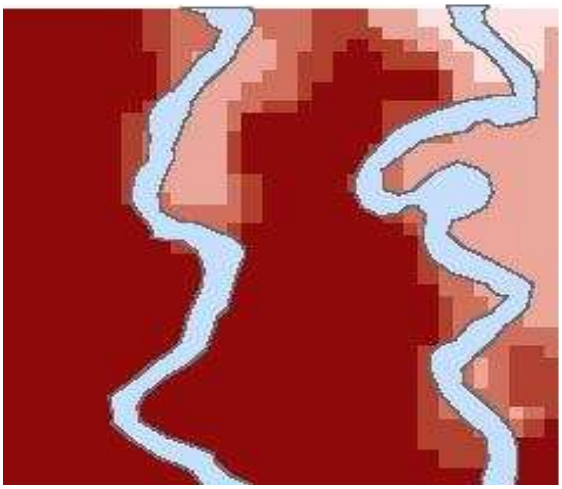

96-97 seasonal ET (mm)

540.00 - 555.00
550.00 - 560.00
560.00 - 570.00
570.00 - 580.00
580.00 - 590.00

97-98

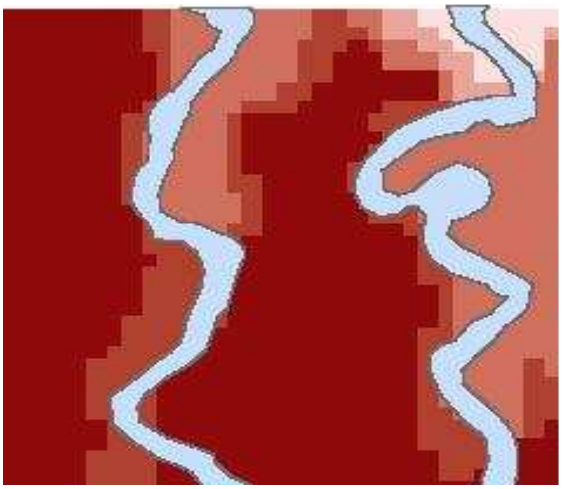

97-98 season ET (mm)

430.00 - 440.00
440.00 - 450.00
450.00 - 460.00
460.00 - 470.00
470.00 - 480.00

98-99

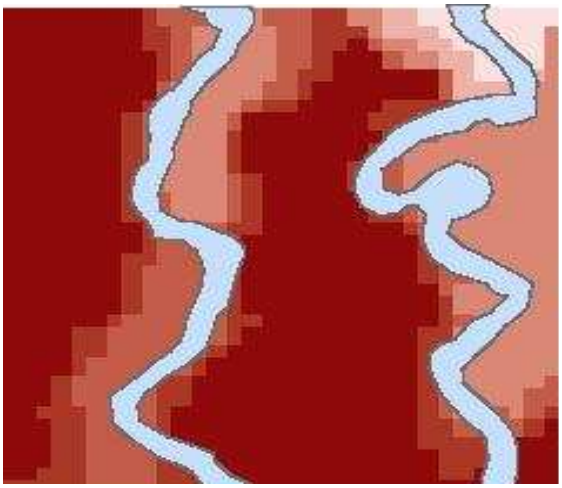

98-99 seasonal ET(mm)

484.00 - 486.00
486.00 - 488.00
488.00 - 490.00
490.00 - 492.00
492.00 - 494.00
494.00 - 496.00

Figure D Interpolated seasonal ET for the study field.

VITA

Xiaoxue Li

Candidate for the Degree of

Doctor of Philosophy

Thesis: WEATHER AND TOPOGRAPHIC INFLUENCES ON TEMPORAL AND SPATIAL VARIABILITY IN A WINTER WHEAT FIELD IN OKLAHOMA

Major Field: Biosystems Engineering

Biographical:

Personal Data: Born in Tianshui, Gansu, P. R. China, on January 23, 1971.

Education: Graduated from No. 1 High School, Tianshui, Gansu, P. R. China in July 1989; received Bachelor of Engineering in Water Resources Engineering from Gansu Agricultural University, Lanzhou, Gansu, P. R. China in June 1993; Received Master of Engineering in Irrigation and Drainage from Postgraduate School of North China Water Conservancy and Hydropower Institute, Beijing, P. R. China in April 1993; completed the requirements for the Doctor of Philosophy with a major in Biosystems Engineering at Oklahoma State University in May 2011.

Experience: Employed as an Assistant Professor by Postgraduate School of North China Water Conservancy and Hydropower Institute, Beijing, P. R. China in April 1993; employed by the Department of Biosystems and Agricultural Engineering as a Graduate Research Assistant, Oklahoma State University, September 1998 to March 2003; employed by Albert A. Webb Associates as a civil engineer from March 2003 to March 2009; employed by Lim & Nascimento Corp. (AECOM/LAN) from May 2009 to November 2009; employed by Coachella Valley Water District from November 2009 to present.

Name: Xiaoxue Li Date of Degree: May, 2011

Institution: Oklahoma State University Location: Stillwater, Oklahoma

Title of Study: WEATHER AND TOPOGRAPHICAL INFLUENCES ON SPATIAL AND TEMPORAL VARIBAILITY OF WINTER WHEAT YIELD IN OKLAHOMA

Pages in Study: 130 Candidate for the Degree of Doctor of Philosophy

Major Field: Biosystems Engineering

Scope and Method of Study: The main objective of this research was to study the influence of weather and topography on the temporal and spatial variability of wheat yields in Oklahoma by examining the soil moisture distribution and storage and evapotranspiration (ET) variability that are induced by topographical changes, and evaluating their correlation with wheat yield variance across the study field. A stratified random sampling method was used to take soil samples in the study field. Elevation data were collected with a GPS unit on a semiregular grid with a distance from 2-8 m. The weather data used for this research was obtained from the Medford Mesonet Station. The seasonal ET data were calculated using weather data and soil data. Topographical factors, aspect, slope and curvature were derived from the DEM using the elevations collected in the study field with the GPS unit. Their correlations with yields were examined. A topography-related soil moisture index (TRSMI) was constructed from combining two topographic variables, slope and curvature, with one soil variable, available soil water content. Its correlations with yields for each year were examined. The correlation between seasonal ET and yields for each growth season was examined.

Findings and Conclusions: The examination of relationships between topographical factors, slope and curvature, soil property, and available soil water content for the entire study field showed that available soil water content has the highest correlation with yield among the factors listed above. This demonstrated that the amount of water soils can retain is an important factor in yield variability on a field scale. The correlation coefficient between TRSMI and yields indicates that a positive correlation exists between yield and TRSM. The correlation coefficient between seasonal ET and yields in dry years and years with adequate precipitation is higher than that in wet years. The patterns of correlation coefficients between yields and the slope, curvature, available soil water content, TRSMI, and seasonal ET are for the sample locations are similar to those for the entire study field, but the correlations were stronger

ADVISER'S APPROVAL: _____